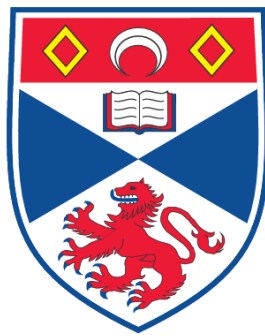


**THE FRONTAL SYSTEM OF THE ANTARCTIC CIRCUMPOLAR  
CURRENT : MARINE MAMMALS AS OCEAN EXPLORERS**

**Lars Boehme**

**A Thesis Submitted for the Degree of PhD  
at the  
University of St. Andrews**



**2008**

**Full metadata for this item is available in the St Andrews  
Digital Research Repository  
at:**

**<https://research-repository.st-andrews.ac.uk/>**

**Please use this identifier to cite or link to this item:**

**<http://hdl.handle.net/10023/687>**

**This item is protected by original copyright**

**This item is licensed under a  
Creative Commons License**

**The Frontal System of the  
Antarctic Circumpolar Current:  
Marine Mammals as Ocean Explorers.**

A thesis submitted to the University of St. Andrews  
for the degree of Doctor of Philosophy

Lars Boehme

School of Biology

NERC Sea Mammal Research Unit

University of St Andrews

July, 2008

"I hold ... that a man should strive to the uttermost for his life's set prize."

(Robert Browning, 1812-1889)

Robert Browning was Shackleton's favourite poet and this inscription can be found on the reverse side of Shackleton's grave marker in Grytviken, South Georgia.

## Declarations

- 1) I, Lars Boehme, hereby certify that this thesis, which is approximately 49000 words in length, has been written by me, that it is the record of work carried out by me and that it has not been previously submitted in any previous applications for a higher degree.
- 2) I was admitted as a research student in December 2004 and as a candidate for the degree of Doctor of Philosophy in December 2004; the higher study for which this is a record was carried out in the University of St Andrews between December 2004 and December 2007.

date ..... signature of candidate .....

- 3) I hereby certify that the candidate has fulfilled the conditions of the Resolution and Regulations appropriate for the degree of Doctor of Philosophy in the University of St Andrews and that the candidate is qualified to submit this thesis in application for that degree.

date ..... signature of supervisor .....

The following is an agreed request by candidate and supervisor regarding the electronic publication of this thesis:

Access to Printed copy and electronic publication of thesis through the University of St Andrews.

date ..... signature of candidate .....

date ..... signature of supervisor .....

# Abstract

In this thesis, I describe large-scale and small-scale features of the Antarctic Circumpolar Current (ACC) by merging conductivity-temperature-depth (CTD) data obtained by novel animal-borne sensors with data obtained by more conventional means. Twenty-one CTD-Satellite Relay Data Loggers (CTD-SRDLs) were attached to Southern elephant seals (*Mirounga leonina*) on South Georgia in 2004 and 2005. This was part of a larger international study (Southern Elephant Seals as Oceanographic Samplers; SEaOS), in which I played a major role in developing the oceanographic approach used to integrate physical data from a range of sources, and the means to link biological findings to oceanographic parameters.

The development of animal-borne oceanographic sensors and their potential place within an ocean observing system is reviewed initially. Then I describe the Series 9000 CTD-SRDL in detail, discussing its performance in the lab and during two field experiences with Southern elephant seals and Weddell seals (*Leptonychotes weddellii*).

Following this, a detailed study of the ACC frontal system in the South Atlantic is presented that uses merged Argo float data and CTD-SRDL data. The structure of the frontal field revealed by this unique dataset is examined, and unprecedented insight into its variability is obtained. Amongst the important findings is that, contrary to most climate models, our in situ data suggest a northward shift of the ACC east

---

of 40°W in 2004 and 2005 compared to previous work. Next, two CTD-SRDL sections are presented to identify the locations of the ACC fronts across Drake Passage, and an empirical relationship between upper ocean temperature and baroclinic mass transport is used to determine the transport through Drake Passage at the times of the sections. This technique is a powerful complement to more conventional means of data collection in this region, especially given the ability of the seals to conduct "sections" at times when ship-based fieldwork is logistically most challenging, i.e. in the winter time.

The CTD-SRDLs do not only record hydrographic data, but simultaneously record seal movements and diving behavior. This enables insight to be obtained on the behavioral and physiological responses of Southern elephant seals to spatial environmental variability throughout their circumpolar range. The resulting energetic consequences of these variations could help explain recently observed spatially varying population trends. With a stable population at South Georgia and declining populations at Kerguelen and Macquarie Island. This study also highlights the benefits to the sensor-carrying animals themselves by showing the usefulness of this approach in examining the sensitivity of top predators to global and regional-scale climate variability. More importantly, I conclude that, by implementing animal-borne sensors into ocean observing strategies, we not only gain information about global ocean circulation and enhance our understanding of climate and the corresponding heat and salt transports, but at the same time we increase our knowledge about ocean's top predators, their life history and their sensitivity to climate change.

## Acknowledgements

A PhD is truly a marathon event, and I would not have been able to complete this journey without the aid and support of countless people over the past three years. It was a pleasure for me to work with all the wonderful people in the Sea Mammal Research Unit.

First of all, I want to thank my supervisors. To Mike Fedak for being a great supervisor. His ideas and tremendous support had a major influence on this thesis. He spend a lot of time helping me, advising on everything related to my thesis. He also gave me the chance not only to visit several interesting conferences, but I has the wonderful opportunity to spend time on the fantastic island of South Georgia. I also thank him for being my landlord. Many thanks to Martin Biuw for being a supervisor, my biology teacher, a friend and for sharing an office with me. The clash of worlds in our office between biology and physics created an environment, which forced me to look beyond my own nose and culminated in chapter 5. He was also a great supervisor during the fieldwork on South Gerogia. I learned a lot during the time I spend with Mike and Martin and I am convinced that this knowledge will help me in the future.

To Sally Thorpe, who took me under her wings, when I joined the research cruise on the James Clark Ross in the first week of my PhD. She also has the best eyes to spot all the little details and typos in a manuscript. Finally to Mike Meredith, who managed to force my German non-persistency to focus, enabling me to pick up the thread in each new chapter. To all my supervisors, I don't think that I had a single conversation with either of you without feeling (at least a little) brighter afterwards.

Concerning my fieldwork, I'm particularly grateful to Simon Moss and Kimberley Bennet, who helped us tagging seals on South Georgia in 2005. But they not only helped during the work, I also really enjoyed spending several weeks with them on a

---

remote island in the Southern Ocean. I also thank Callan Duck and Ian Field, who helped during the fieldwork in 2004.

For advice on everything not related to my PhD, for making coffee (very weak tho) and for about 2000 discussions (I enjoyed all of them), I thank Dave Thompson. He was also a great help as a native English speaker, when I was lost in translations. Many thanks go to Bernie McConell, who always had good advice on telemetry and seamanship. In this context, I have to thank the whole SMRU instrumentation group and Valeport Ltd. for designing and building the CTD-SRDLs used for this thesis. I also have to thank Jason Matthiopoulos for a lot of good advice on several topics in this work. It is difficult not to forget someone that helped, in some way or another, honestly. Many people crossed my life and helped substantially, not only here in St Andrews. I liked the interdisciplinary work with all of them. Before forgetting someone, I just thank them all.

To the British Antarctic Survey I owe a great thank you for supporting me and the project.

This thesis is dedicated to my wife Anja Boehme and my sons Leif and Ole: without their support and encouragement, this work may not have been completed.

# Contents

<b>Abstract</b>	<b>1</b>
<b>1 General Introduction</b>	<b>10</b>
1.1 The Antarctic Circumpolar Current . . . . .	11
1.2 Animal-Borne Sensors . . . . .	15
1.3 The SEaOS Project . . . . .	20
1.4 PhD objectives . . . . .	22
<b>2 CTD-SRDLs for Real-Time Oceanographic Data</b>	<b>27</b>
2.1 Abstract . . . . .	28
2.2 Introduction . . . . .	29
2.3 Series 9000 CTD-Satellite Relay Data Loggers . . . . .	31
2.3.1 Design . . . . .	32
2.3.2 Sensors . . . . .	33
2.3.3 Data compression and transmission . . . . .	39
2.3.4 Remote data quality control . . . . .	44
2.3.5 Costs (as-of 1 June 2008) . . . . .	49
2.4 Field Experiences . . . . .	51
2.5 Summary and Conclusions . . . . .	54

<b>3</b>	<b>The ACC frontal system in the South Atlantic</b>	<b>58</b>
3.1	Abstract . . . . .	59
3.2	Introduction . . . . .	60
3.3	Data and Methods . . . . .	63
3.3.1	Hydrographic in situ Data . . . . .	63
3.3.2	Sea surface temperature . . . . .	73
3.3.3	Sea level anomaly . . . . .	73
3.4	Results . . . . .	74
3.4.1	Definition and Determination of Fronts . . . . .	74
3.4.2	Frontal positions . . . . .	80
3.4.3	SST and SLA . . . . .	87
3.5	Discussion . . . . .	91
3.5.1	The frontal positions . . . . .	91
3.5.2	A shift of the ACC . . . . .	93
3.5.3	Correlations between the surface and sub-surface expressions . . . . .	95
3.6	Summary and Conclusions . . . . .	97
<b>4</b>	<b>Monitoring Drake Passage with elephant seals</b>	<b>101</b>
4.1	Abstract . . . . .	102
4.2	Introduction . . . . .	103
4.3	Data . . . . .	106
4.3.1	Hydrographic data . . . . .	106
4.3.2	Absolute dynamic topography . . . . .	107
4.4	Results . . . . .	110
4.4.1	Frontal structures in Drake Passage . . . . .	110
4.4.2	Estimating transports from in situ temperature . . . . .	111
4.4.3	Estimating transports from density . . . . .	117

4.5	Discussion and Summary . . . . .	119
4.5.1	Frontal structures . . . . .	119
4.5.2	Transports . . . . .	122
<b>5</b>	<b>Behaviour of a top predator in relation to the environment</b>	<b>127</b>
5.1	Preface . . . . .	128
5.2	Abstract . . . . .	129
5.3	Introduction . . . . .	130
5.4	Results and Discussion . . . . .	133
5.4.1	Movements and Distribution . . . . .	134
5.4.2	Diurnal Variations in Diving . . . . .	137
5.4.3	Drift Rate and Relative Body Condition . . . . .	137
5.4.4	Physical Ocean Properties . . . . .	139
5.4.5	Global Snapshot of Elephant Seal Habitats . . . . .	141
5.4.6	Ecological Implications . . . . .	144
<b>6</b>	<b>Discussion</b>	<b>147</b>
6.1	Animal-borne sensors in oceanography . . . . .	148
6.1.1	Sensor accuracy . . . . .	149
6.1.2	Spatial and temporal coverage . . . . .	150
6.1.3	Ocean Observing System . . . . .	152
6.1.4	The future of animal-borne sensors in oceanography . . . . .	154
6.2	The frontal system of the ACC . . . . .	155
6.2.1	The variability of the ACC . . . . .	155
6.2.2	The branching of ACC fronts . . . . .	157
6.2.3	The future of monitoring the ACC . . . . .	160
6.3	Behaviour of marine animals in relation to their immediate environment	161
6.3.1	Marine mammal habitats in a changing environment . . . . .	164

**References**

**173**



# 1 General Introduction

Extracts of this chapter are published in  
Boehme, L., M. Biuw, M. Fedak, K. Nicholls, S. Thorpe, and M. Meredith, 2008:  
Animals as exploratory underwater vehicles. *Proceedings of the International  
Workshop on Autonomous Underwater Vehicle Science in Extreme Environments  
held at the Scott Polar Research Institute*, K.J. Collins and G. Griffiths, eds.,  
London: Society for Underwater Technology, 55–62.

## 1.1 The Antarctic Circumpolar Current

Nowadays it is well known that the atmosphere and ocean are one coupled physicochemical system, that through its interior circulation the ocean plays a major role in the distribution of the planet's heat content as well as of some gases like CO<sub>2</sub>, and that this coupling has a fundamental influence in climate. Formation of water masses, fluxes of salt, heat and moisture between atmosphere and ocean, and the unique buffering role that the ocean plays for the atmosphere, are factors that influence the climate on Earth over a wide spectrum of time scales. Therefore, if we want to understand climate and its changes we also have to understand the long-term processes in the ocean, including the thermohaline circulation and the corresponding heat and salt transports. The influence that the ocean has on climate has been a popular research topic over the last fifteen years (Broecker, 1991). A lot has been achieved during this time to understand the different mechanisms in which the ocean influences the climate of our planet but, due to the complexity of the processes involved, a lot still must be done. Indeed, the slow, long-term worldwide ocean circulation on centennial time scales and longer is complex and the term 'thermohaline circulation' by itself is not enough to describe all the processes involved. Some people prefer instead the term 'general circulation'. Strictly speaking, the thermohaline circulation is driven only by differences in temperature and salinity around the world (due to heterogeneous latitudinal solar radiation). The term 'general circulation' also includes other processes that influence the movement of water in the long-term: mixing and water mass formation, upwelling and downwelling, residual currents of Kelvin waves or of Rossby waves (e.g. planetary waves), and effects of the wind at the surface (wind drag) or in the deep ocean (e.g. Ekman pumping). This long term circulation, when considered in a global sense, is what the paleo community started to call the 'Great Ocean Conveyor Belt' (Broecker, 1991), an expression that has been widely accepted

by the researchers trying to connect ocean processes with climate.

Within the global ocean circulation, the seas around Antarctica exhibit some unusual properties. In the mid-latitudes, it is possible to balance all flow geostrophically (a balance between Coriolis force and horizontal pressure gradient) across the permanent thermocline, thus limiting the strong ocean currents to the surface layer. In the Southern Ocean, however, temperature differences between the sea surface and the deep sea are generally less than  $5^{\circ}\text{C}$ , and even below  $1^{\circ}\text{C}$  in some places close to the Antarctic continent. This lack of a permanent thermocline results in low density variations with depth, and as a consequence the pressure gradient force is evenly distributed over the entire water column: thus currents are not restricted to the upper few hundred metres of the ocean (Pickard and Emery, 1990; Tomczak and Godfrey, 1994). Another aspect that makes the Southern Ocean unique is the unlimited communication with all other oceans (Fig. 1.1). The Southern Ocean links the Atlantic, Indian and Pacific Oceans, and their hydrography cannot be understood without insight into the dynamics of Southern Ocean. This provides us with another reason why the Southern Ocean is of global relevance.

The water masses that meet in the Southern Ocean are generally mixed and redistributed by the Antarctic Circumpolar Current (ACC). Deep waters from the North Atlantic are upwelled at the Antarctic Divergence at the southern boundary of the ACC following the inclined isopycnals. During this process they mix with Circumpolar Deep Water (CDW) and, on reaching the surface flow, are diverted northward by Ekman transport (Tomczak and Godfrey, 1994). This newly formed water mass travels north across the ACC until it reaches the Antarctic Convergence. Here, it mixes with Subantarctic Water from the north. It is then subducted to mid-depth, becoming Antarctic Intermediate Water (AAIW), while the ACC carries the water further eastward (Fig. 1.2). The AAIW is then ejected into the Atlantic, Indian and

Pacific Oceans. Thus, the ACC is a crucial component of the ‘Great Ocean Conveyor Belt’.

The ACC is arguably the ‘mightiest current in the oceans’ (Pickard and Emery, 1990), transporting more water than any other current. The ACC extends from the sea surface to depths of 2000-4000 m and can be in excess of 2000 km wide (Tomczak and Godfrey, 1994). Although the eastward speed is generally low (around 10 cm/s in regions between the fronts), the ACC transports more than 100 Sv ( $1\text{Sv} = 1 \times 10^6\text{m}^3/\text{s}$ ) due to its tremendous cross-sectional area (Whitworth, 1983; Whitworth and Peterson, 1985; Cunningham et al., 2003). Historically, the ACC has been referred to as the ‘West Wind Drift’, because its flow is driven by strong, nearly zonal (west-east direction), westerly winds.

Observations show that south of the sub-tropics temperature and salinity do not vary uniformly from north to south; there exists a narrow band (100–200 km) around Antarctica where average Sea Surface Temperature (SST) changes from about 12° C to 7° C and salinity decreases from greater than 34.9 to 34.5 or less (Orsi et al., 1995). This narrow band is called the Subtropical Front (STF) and is usually found between 35° S and 45° S (Fig. 1.1). Four fronts lie south of the STF, namely (from north to south): the Subantarctic Front (SAF), the Polar Front (PF), the Southern ACC Front (SACCF) and the Southern Boundary (SB) of the ACC (Orsi et al., 1995; Belkin and Gordon, 1996). These fronts are clearly indicated in synoptic vertical sections by their large horizontal property gradients and pronounced isopycnal tilt throughout the deep water column. It has become accepted terminology to call the region between STF and SAF the Subantarctic Zone (SAZ), the region between SAF and PF the Polar Frontal Zone (PFZ) and the region between PF and SACCF the Antarctic Zone (Fig. 1.2). A fourth zone, including the Continental Zone and the westward flowing Antarctic Coastal (or Polar) Current, are located even further poleward, between the SB and

the Antarctic continent. This zone is characterized hydrographically by a water mass of uniform temperature and low salinity in the upper 500 m. SST poleward of  $65^{\circ}$  S is about  $-1.0^{\circ}$  C (Deacon, 1984; Orsi et al., 1995).

Using historical data, Orsi et al. (1995) and Belkin and Gordon (1996) mapped the circumpolar distribution of these Southern Ocean fronts using a variety of definitions based on water mass properties (see Orsi et al., 1995; Belkin and Gordon, 1996, for useful summaries of these definitions). However, the frontal properties are not uniform in all sectors of the Southern Ocean. The variations in frontal structure from region to region and the multiplicity of definitions used by various authors have led to some confusion in identifying particular fronts. In addition, many areas have remained relatively poorly sampled and in only a very few locations have sufficient repeat measurements been made to permit the variability of the fronts to be assessed. Only a few studies were able to collect in situ data with a sufficient temporal resolution to investigate the frontal variability using the subsurface expressions (Sokolov and Rintoul, 2002; Thorpe et al., 2002; Sokolov et al., 2006). None of these studies describe the three major fronts of the ACC (SAF, PF and SACCF) simultaneously with good spatial and temporal mesoscale coverage, which means spatial scales of 10 – 100 km and temporal scales of 10 – 100 days. These studies were based on ship-based measurements and benefited from their high accuracy and depth-resolving capability, but such data are scarce in the Southern Ocean as a whole and are biased on the summer season due to inherent logistic difficulties. The same applies to the estimated net transports of the ACC. Today it is known that the circumpolar transport of the ACC varies on time scales from days to years and longer (Hughes et al., 2003; Meredith et al., 2004). Meredith and Hughes (2005) showed that sampling intervals very much shorter than 10 days are needed to produce un-aliased estimates of the ACC transport.

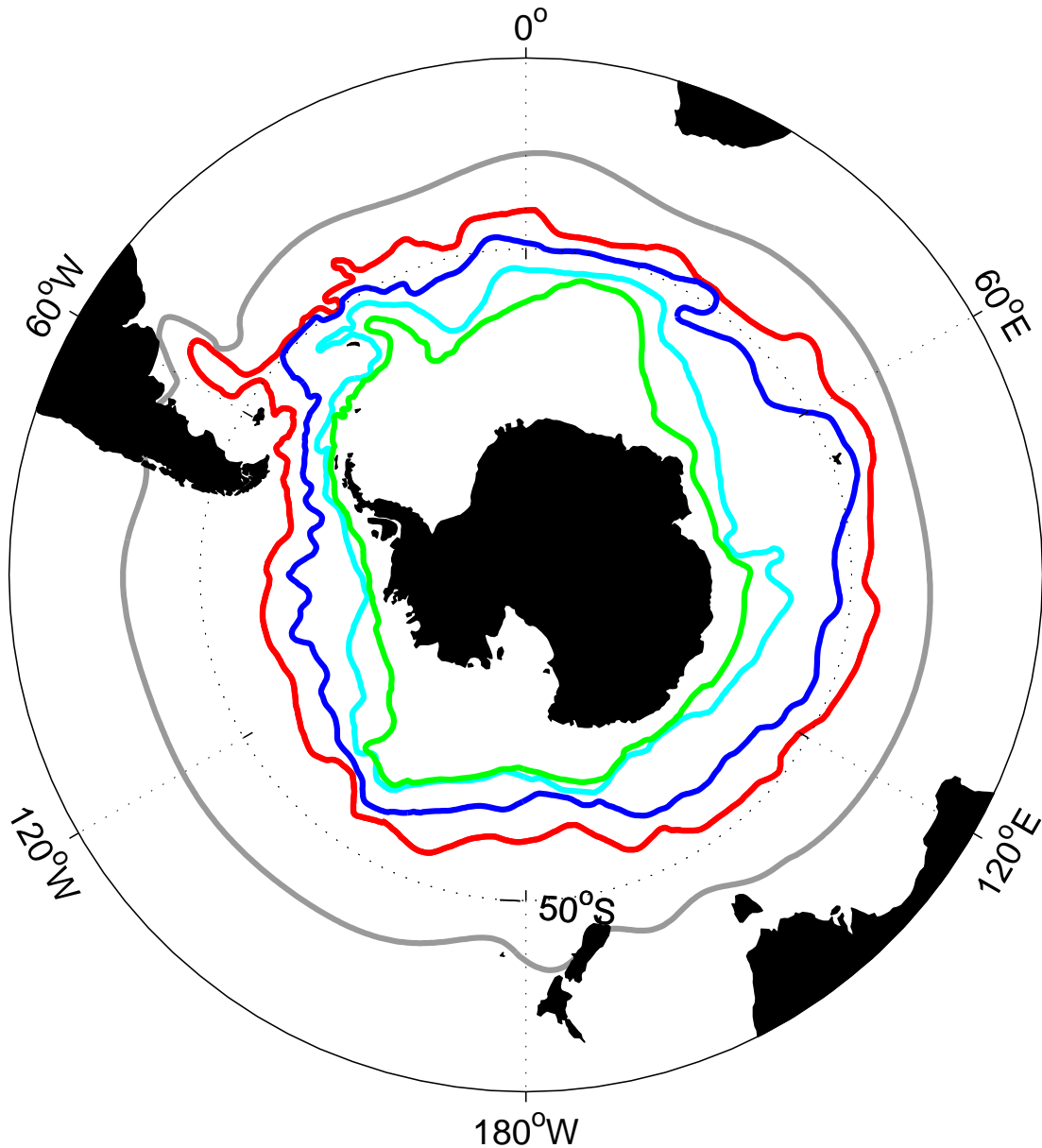


**Figure 1.1:** Fronts of the Antarctic Circumpolar Current in the Southern Ocean. From north to south: Subtropical Front (grey), Subantarctic Front (red), the Polar Front (blue), the Southern ACC Front (cyan) and the Southern Boundary of the ACC (green). The Subtropical Front is extracted from 50 km SST NOAA-16 global analysis data from 21-25 May 2005, whilst the other fronts are from Orsi et al. (1995).

## 1.2 Animal-Borne Sensors

The importance of monitoring these ocean processes (e.g. transport) for climate forecasting is increasingly being recognized (Gould et al., 2004; Guinehut et al., 2004)

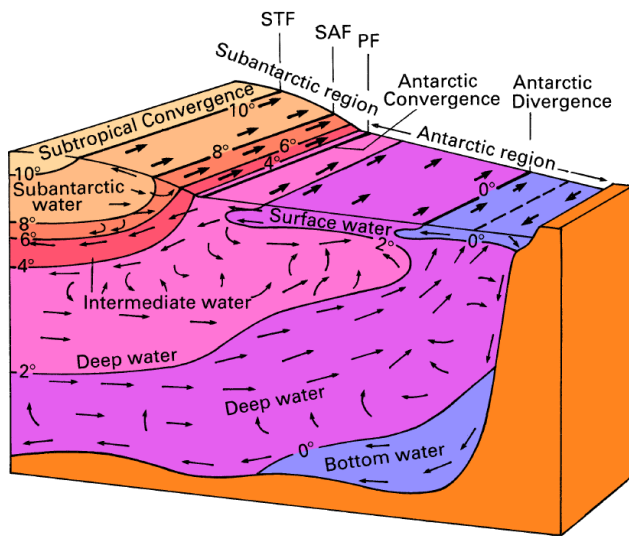


**Figure 1.2:** Block diagram of the circulation, temperature distribution and fronts of the Southern Ocean from Tomczak and Godfrey (1994). STF: Subtropical Front, SAF: Subantarctic Front, PF: Polar Front.

and innovative remote samplers such as moorings, buoys, floats and gliders are being developed, each of which can return data in near real-time. Ultimately, programs such as the Global Ocean Observation System (GOOS) will enable the assimilation of such data into ocean circulation models, with the intention of accurately representing and predicting climate variability on seasonal and longer timescales (Bell et al., 2005; MERSEA, 2004). Although these techniques have an enormous potential for broad-scale ocean observations of the order of several hundreds of kilometers, they do not provide a complete observational strategy. Even today, profound investigations of the polar oceans and their dynamics continue to be hampered by lack of in situ observations. Satellite remote sensing can only observe the uppermost few millimetres of the oceans and is hampered by sea ice; the ocean beneath remains almost entirely unobserved. The coverage of profiling floats in the Southern Ocean is more sparse than elsewhere, and sea ice prohibits the surfacing of floats to transmit their data, although ice-capable autonomous floats are being developed (Klatt et al., 2007). Existing observations are still heavily biased towards summer and to open water. Marine mammals, however, can help to overcome these limitations and provide a complementary high resolution data source.

The idea of tagging marine mammals to find out about their lives is not a new one. Until recently, however, no one had developed the technology to allow concurrent collection of high quality CTD information. In 1940 Per Scholander, inspired by a description written by Lord Kelvin in the 19th Century, developed a mechanical depth gauge to record the diving depths of whales. But these early devices were bulky and had to be recovered in order to retrieve the measurements. Such recovery was not always possible and, even when it was, data were only available some time after measurements were made. An alternative, which is possible today, is to add transmitters to these measuring devices. This enables results to be received, almost in real-time, even if a device is ultimately lost. Nowadays, the technological developments, miniaturization and reductions in power requirements, combined with increases in computing power, have made it possible to broaden the spectrum of measurements and to program complex measurement and sampling operations into very small packages.

The development and deployment of logging and telemetry equipment on marine animals to describe their behaviour has provided a wealth of data. Scientists can now monitor the migration patterns and diving depths of many species. But understanding the context and implications of their behaviour requires a general description of the physical environment that animals encounter. However, data on the oceanographic conditions in areas through which the animals move is often incomplete or lacking. These areas are either poorly covered by more traditional means, or information on a finer spatial or temporal scale is needed than conventional sampling strategies or even oceanographic models can provide.

This gap between what we would like to know and the limited information available, both about the ocean and the animals that depend on it, motivated the Sea Mammal Research Unit Instrumentation Group of the University of St Andrews to



**Figure 1.3:** Southern elephant seal tagged with miniature SRDL-CTD.

supply more environmental data by including oceanographic sensors on the generally available behavioural tags. This idea of using marine animals as sampling platforms has matured among both biologists and oceanographers alike over the past few years and its implementation has grown out of its infancy (Fig. 1.3).

Enlisting marine animals as oceanographic sampling platforms is not a new idea. The earliest published reference to this approach is from 1970 (Evans, 1970). But until recently no one had ever developed the technology to allow collection of high quality CTD information. Nowadays these instruments have the potential to collect information about the oceans that is not only relevant to the study of physical structure of the oceans but also for studying the ecology of animals carrying the instruments (Lydersen et al., 2002; Hooker and Boyd, 2003; Lydersen et al., 2004; Charrassin et al., 2004; Sokolov et al., 2006). These animal-born sensors demonstrated convincingly that they can record hydrographic data at high frequency and in near real-time from remote, relatively inaccessible parts of the ocean (Lydersen et al., 2002, 2004).

However, animal-borne sensors do not sample randomly; nor do they deliver the pre-set transect coverage that can be accomplished with ships, gliders or AUVs. Thus, the exact locations of data collection cannot be pre-determined. However, today we

have enough information on many species to predict where they will go within reasonable limits on a regional scale ( $\pm 500$  km). Appropriate choice of study species can therefore enable us to pre-define the timing and spatial extent of sampling, including depths, and we can predict the likely number of hydrographic profiles that will be gathered. Unlike profiling Argo floats, animals often move relatively rapidly in a directed fashion and can deliver transects of nearly contemporaneous data (Chapter 4). Their tracks often cut across frontal regions as they travel between breeding, foraging and resting locations. They can direct sampling effort to particularly interesting and productive regions as they adaptively sample their environment based on previous experience. This also has the added benefit that individuals are likely to retrace previous tracks, and can therefore provide repeat sections. Some species penetrate deep into polar regions in ice-covered areas where cloud cover can limit the applicability of remote sensing, and where most profiling floats and ships cannot operate. Despite the necessary limitations imposed by small size, power restrictions and limited Satellite bandwidth, the specific characteristics mentioned above make animal-borne sensors advantageous in many instances, especially when used in a complementary way with other approaches. In addition, the ‘adaptive’ nature of the way animals sample their environment makes it necessary to incorporate data from them into broader, more general and systematic coverages provided by remote sensing, ship-borne data collection and models. The animal approach will always be most valuable when used in conjunction with these more conventional approaches, just as data from drifting buoys, ships of opportunity etc. are best in a systematic context.

## 1.3 The SEaOS Project

One approach developed to fill the present data gap in the Southern Ocean was the international SEaOS program (Southern Elephant seals as Oceanographic Samplers<sup>1</sup>). This interdisciplinary program was aimed at increasing our understanding of how Southern elephant seals interact with their physical environment and also at demonstrating and implementing this cost-effective means of gathering routine observations of hydrographic data from remote environments. CTD-Satellite Relay Data Loggers (CTD-SRDLs), custom-built by the Sea Mammal Research Unit, St Andrews, UK and Valeport Ltd., Devon, UK, were fixed harmlessly to seals' fur after the elephant seals completed their annual moult in January and February and were finally lost when the animals moulted again the following season (Fig. 1.3). During the animals' migration, the CTD-SRDLs report vertical profiles of salinity, temperature, and pressure to a depth of up to 2000 m. During 2004 to 2006, about 85 CTD-SRDLs were deployed on Southern elephant seals in late summer at key breeding and moulting sites around the Southern Ocean: South Georgia, Kerguelen, Macquarie Island and the South Shetland Islands. Seal migrations covered all longitudinal sectors of the Southern Ocean as well as its entire latitudinal range, from the Subtropical Front in the north via the ACC to polar continental waters along the Antarctic coast. Many seals spent substantial amounts of time within the winter pack ice in areas difficult or impossible to sample using other means.

SEaOS has provided over 22,000 CTD profiles at a rate of about 2 profiles/day and an average depth of about 560 m, representing a combination of transect-type sections with a spatial resolution of less than 34 km along the migratory routes of the seals, and detailed longitudinal mooring-like data from focussed feeding areas (Fig. 1.4). This dataset has greatly increased the coverage in regions even where historical

---

<sup>1</sup><http://biology.st-andrews.ac.uk/seaos/index.html>

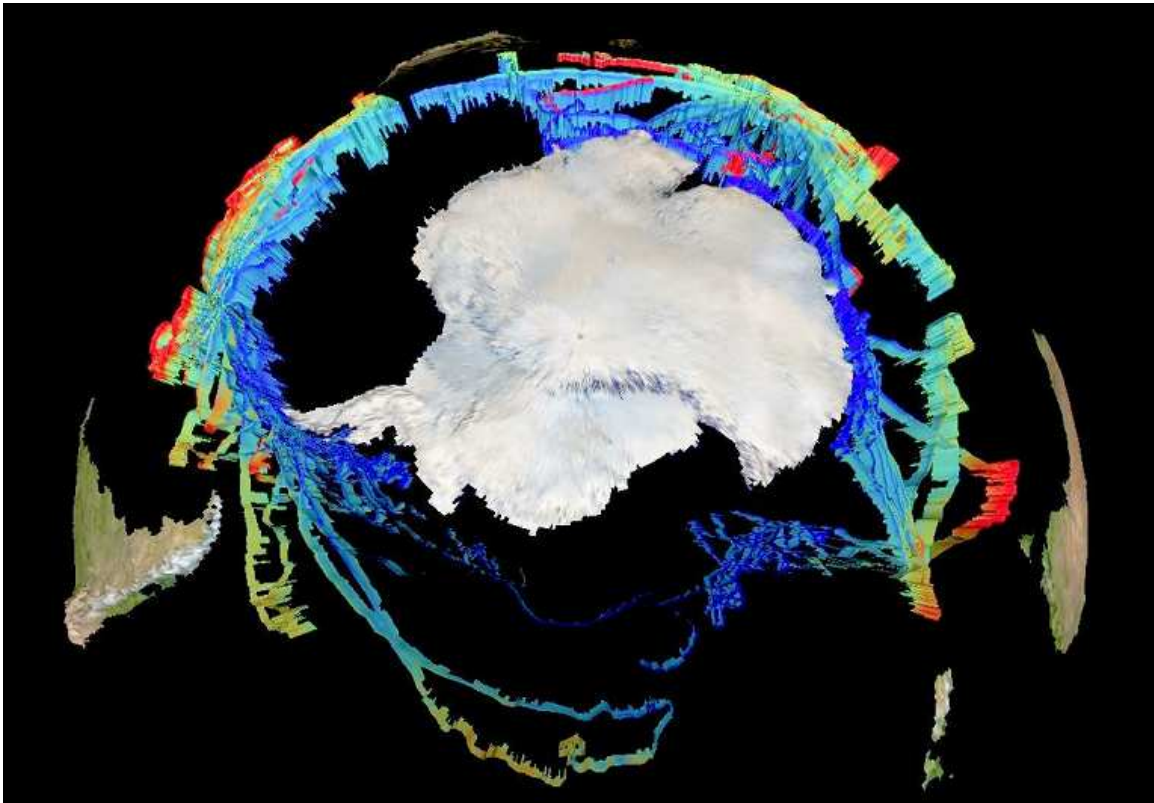


**Figure 1.4:** All temperature sections along seals' migration obtained during the SEaOS project.

hydrographic data are available and where Argo floats have been sampling intensively over the past years.

But the greatest contribution of these new sampling platforms is the substantial increase in the number of CTD profiles from areas that have previously been virtually un-sampled, especially during the winter months. This contribution is clearly seen below  $60^{\circ}$  S (Fig. 1.5), where during its three years of operation SEaOS provided more than three times the total number historical profiles previously available from these latitudes.

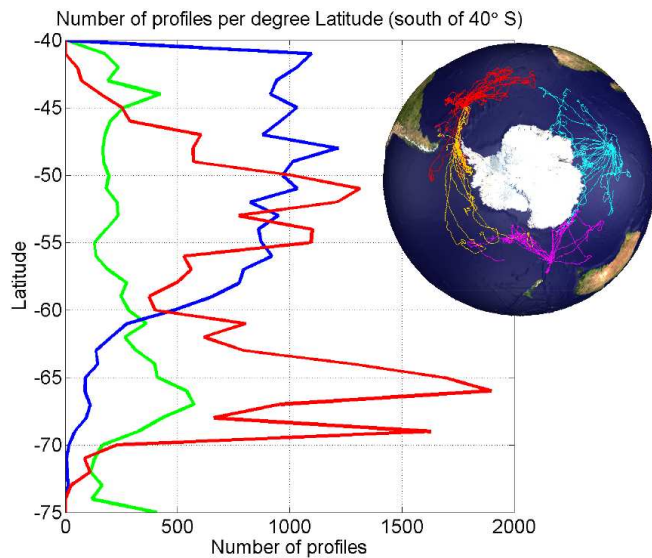


**Figure 1.5:** Accumulated number of CTD profiles per degree latitude in the Southern Ocean (Southern Ocean Database in green with 10513 profiles, 547 Argo floats in blue with 19463 profiles and 64 SEaOS animal tags in red with 22230 profiles) and positions of SEaOS operations (little insert at top right).

## 1.4 PhD objectives

The overall thrust of this PhD is to describe large-scale and small-scale features of the Antarctic Circumpolar Current (ACC) by merging conductivity-temperature-depth data obtained by novel animal-borne sensors with data obtained by more conventional means. As described above, the Southern Ocean is a highly variable environment, but lack of in situ data has prohibited investigations of the dynamic fields on high temporal and spatial scales. This work represents the largest effort to date to study the ACC with unprecedented temporal and spatial resolution using mainly in situ data. It gives not only new insights into the Southern Ocean but, at the same time, shows the extremely valuable complement to other approaches.

Analyses in chapters 3 and 4 are based on a subset of the dataset collected during the SEaOS project between 2004 and 2006 obtained from twenty-one CTD-Satellite Relay Data Loggers (CTD-SRDLs) attached to Southern elephant seals on South Georgia in 2004 and 2005. This dataset is obviously the fruit of extensive collaborative work, but I personally participated in the fieldwork in 2005 just after being in charge of validating

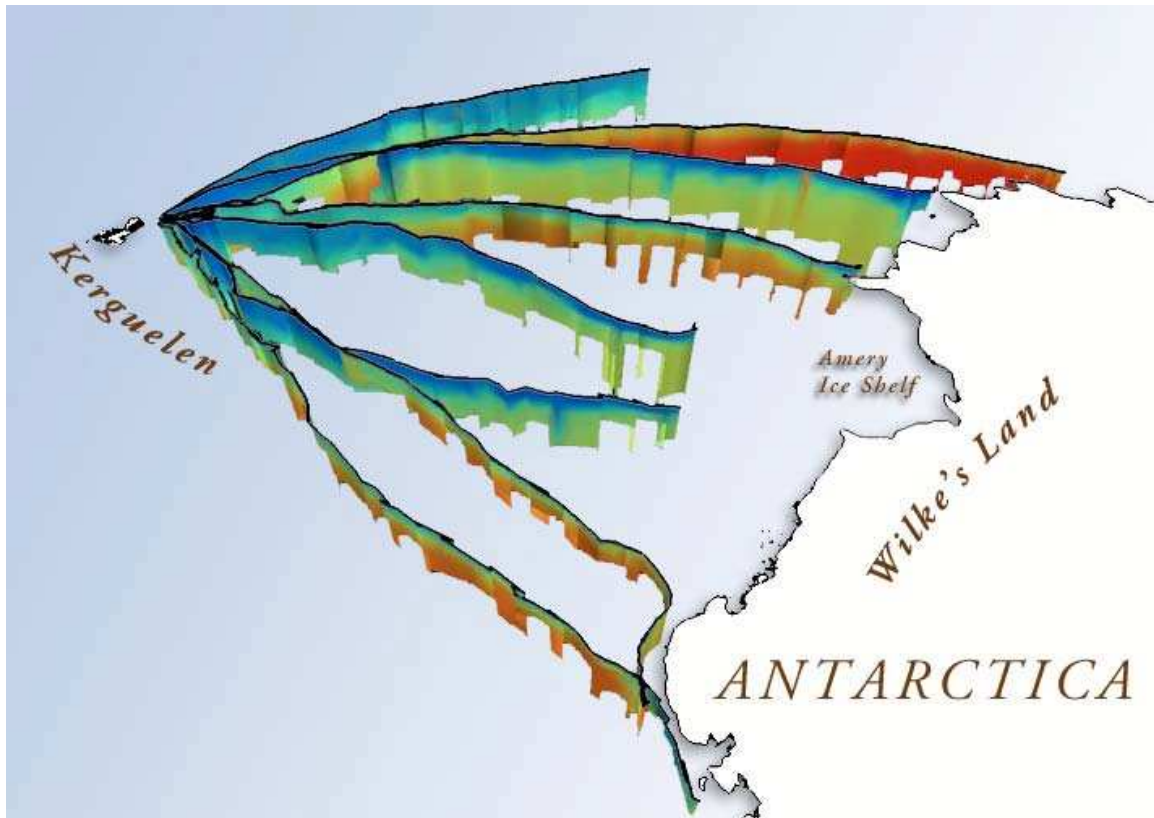


**Figure 1.6:** 8 hydrographic sections recorded simultaneously by Southern elephant seals in 2004.

the CTD-SRDLs against ship-based measurements on board the RRS James Clark Ross in December 2004 and January 2005 in the Scotia Sea.

The following topics were considered to have a high priority for this PhD thesis:

- Develop the data processing techniques to ensure high data quality from SRDLs.
- Investigate the large-scale pattern of the major ACC fronts in the Southern Ocean around South Georgia.
- Investigate the shorter term variability of the ACC fronts.
- Investigate the three main fronts of the ACC and their hydrographic properties.

- Develop the oceanographic approach used to integrate physical data from a range of sources, and the means to link biological findings to oceanographic parameters.

Most of the following chapters have been submitted for publication. I therefore present the chapters in that format.

In chapter 2, I describe the Series 9000 CTD-Satellite Relay Data Logger (CTD-SRDL) in detail, discussing their performance in the lab and during two field experiences on Southern elephant seals and Weddell seals. I also show the data processing techniques used to ensure high data quality.

In chapter 3, I present a detailed study of the ACC frontal system in the South Atlantic conducted by merging Argo float data and data obtained by CTD-SRDLs. The structure and variability of the frontal field revealed by this unique dataset is greater than had previously been appreciated. I discuss this elevated variability. In addition, contrary to most climate models, the in situ data suggest a northward shift of the ACC east of 40°W in 2004 and 2005 compared to previous work.

In chapter 4, two CTD-SRDL sections across Drake Passage in June 2004 and April 2005 are presented to identify the locations of the ACC fronts. Empirical relationships between upper ocean temperature and baroclinic mass transport are used to determine the transport through Drake Passage at the times of the sections. These transports are compared with estimates derived by other techniques, and the usefulness of seal-derived sections when added to other means of monitoring Drake Passage is highlighted.

The CTD-SRDLs do not only record hydrographic data but simultaneously record seal movements and diving behaviour. Chapter 5 reports the joint effort to analyse the behavioural and physiological responses of Southern elephant seals to spatial environmental variability throughout their circumpolar range. This work involved other

scientists, particularly on the biological side, but I gave the primary physical input, as explained in the preface to that chapter. The results are quite astonishing, showing that the resulting energetic consequences of physical variations in the environment could help explain recently observed population trends. This study also highlights the potential benefits to the sensor-carrying animals themselves by showing the usefulness of this approach in examining the sensitivity of top predators to global and regional-scale climate variability.

Finally, I conclude in the discussion that, by implementing animal-borne sensors into ocean observing strategies, we not only gain information about the global ocean circulation and enhance our understanding of climate and the corresponding heat and salt transports, but at the same time we increase our knowledge about ocean top predators, their life history and their sensitivity to climate change.



## **2 Animal-Borne CTD-Satellite Relay Data Loggers for Real-Time Oceanographic Data Collection**

Manuscript in preparation for  
*Journal of Atmospheric and Oceanic Technology*

## 2.1 Abstract

The increasing need for continuous monitoring of the world oceans has stimulated the development of a range of autonomous sampling platforms. One novel addition to these approaches is a small, relatively inexpensive data-relaying device that can be deployed on marine mammals to provide vertical oceanographic profiles throughout the upper 2000 m. When an animal dives, the CTD-Satellite Relay Data Logger (CTD-SRDL) records temperature, salinity and pressure and, once the animal returns to the surface, these data are relayed in compressed form via the Argos satellite system. Here I present two studies highlighting how CTD-SRDLs can provide both broad-scale sections covering entire ocean basins, and smaller scale, high-resolution datasets. In 2004 and 2005, CTD-SRDLs were deployed on 21 Southern elephant seals (*Mirounga leonina*) at South Georgia, providing 1-2 profiles per day ( $\sim$  every 34 km) during their winter migrations. These migrations covered the entire South Atlantic, from the Subtropical Front to the Antarctic coastline. In February 2007, instruments were deployed on four Weddell seals (*Leptonychotes weddellii*) just south of the shelf break in the southeastern Weddell Sea. The instruments are delivering 4-5 CTD profiles per day from beneath the pack ice, mainly over the continental shelf, and have yielded a view of the hydrography of this important, yet difficult-to-access region, unprecedented in both temporal and spatial resolution. The two case studies show that with careful selection of species, gender and age of the animals, as well as the geographic location and time of tagging, it is possible to undertake focused, highly cost-effective oceanographic studies in regions that might be difficult, and therefore expensive, if not impossible to access in any other way.

## 2.2 Introduction

One of the greatest impediments to our understanding of ocean processes is a lack of data from remote regions. The result is that we cannot detect all of the changes in the oceanic environment that may have an influence on climate change. Furthermore we are not even able to validate comprehensive models of global climate change. Understanding ocean's role in the climate system, and the impacts of human activities on the oceans, requires a regularly recorded global dataset of the time-varying storage of heat and freshwater, as well as their lateral fluxes and air-sea exchanges. While the heat budget reveals how the ocean absorbs heat, the freshwater budget shows variability in precipitation and evaporation through salinity anomalies. This and their lateral transport must be measured by an comprehensive observing system (Roemmich et al., 2004) in order for detecting changes in the ocean.

The Global Ocean Observing System (GOOS) is designed to fulfill these needs and required the creation of special profiling floats to observe the temperature and salinity of the world's oceans down to 2000 m depth. The broad-scale global array of profiling floats, known as Argo, has already grown to be a major component of GOOS. Deployments began in 2000 and, by the second half of 2007, 3000 floats were distributed over the global oceans at an average 3-degree spacing. This array will provide 100,000 hydrographic profiles and velocity measurements per year (Gould et al., 2004).

The Argo array is designed for broad-scale ocean sampling at spatial intervals of hundreds of kilometers, greater than the size of eddies and boundary currents (Roemmich et al., 2004). Although the profiling float has enormous potential for these broad-scale ocean observations, it does not provide a complete observational strategy. It is essential that parallel advances are made in the measurement of air-sea exchanges and small-scale sampling for estimation of lateral fluxes. It is necessary to sample

at higher spatial resolution in a line-sampling mode, resolving eddies and boundary currents for flux calculations, and to sample from ocean boundary to ocean boundary for flux integration. Research vessels lend themselves to the line-sampling mode, as per the ocean heat transport estimates from the World Ocean Circulation Experiment (e.g. Ganachaud and Wunsch, 2000).

In this chapter I present a complement to the existing observing systems. Autonomous CTD-Satellite Relay Data Loggers (CTD-SRDLs) can be attached to marine animals and report vertical profiles of salinity, temperature and pressure to depth of 2000 m and will help to populate remote and previously data-sparse regions e.g. of the southern hemisphere. These instruments have the potential to collect information about the oceans that is not only relevant to the study of physical structure of the oceans (Lydersen et al., 2002, Ch. 4) but which is useful for studying the ecology of the carrying animals (Lydersen et al., 2002; Hooker and Boyd, 2003; Lydersen et al., 2004; Charrassin et al., 2004, Ch. 5).

While these measurements are not regular in terms of spatial and temporal coverage (compared, for example, to satellite measurements of oceanographic fields), these studies provide valuable in situ information about the subsurface structure of the ocean. The use of oceanic predators for remote data collection, although suffering from the inability to predetermine the locations of sample collection, is likely to benefit from the ability of such predators to select foraging areas. Sampling will not be uniform, but in many cases, predators are 'adaptive samplers', targeting foraging areas which are likely to coincide with the regions of most interest to biological and physical oceanographers (Guinet et al., 2001, Ch. 4). With careful selection of species, gender and age of the animals, as well as the geographic location and time of tagging, it is even possible to undertake focused, highly cost-effective oceanographic studies in regions that might be difficult, and therefore expensive to access in any other way.

Accurate satellite positioning of diving marine animals, relatively high-accuracy sensors, and the potential to collect large numbers of profiles cost-effectively make these studies particularly important in regions where traditional oceanographic measurements are scarce (Ch. 5). Depending on the CTD-SRDL configuration, it is possible to sample and transmit hydrographic profiles on a daily basis. The CTD-SRDL is therefore intrinsically an eddy-resolving linemode device, rather than a broad-scale one. The natural niche for CTD-SRDLs in the observing system is in complementary measurements of boundary currents and fronts and of property fluxes across lines, as well as coverage of undersampled ocean basins. They are thus likely to be a powerful complement to profiling floats, rather than a replacement for them.

This chapter describes the design of the CTD-SRDL and its performance characteristics. I explain the calibration and data accuracy, which is followed by two case studies that show the effect of choosing a particular species depending on the focus of oceanographic study. Finally, I summarise the results and discuss them further.

## 2.3 Series 9000 CTD-Satellite Relay Data Loggers

The series 9000 CTD-SRDL (Fig.2.1) is designed and built at the NERC Sea Mammal Research Unit (SMRU), St Andrews, UK and the CTD sensor head is built and calibrated at Valeport Ltd, Devon, UK. Data from various sensors are collected when user-specified conditions of time and depth are met. Sampling algorithms onboard the tag detect the deepest point of a dive, and then begin rapidly sampling temperature, conductivity and depth until the surface is reached. From these detailed, high resolution data, a sub-set of depth points with corresponding temperatures and conductivities are selected for transmission. Detailed data from wet/dry and pressure sensors (Fig. 2.1) are collected and used to form detailed individual dive and haulout records along with synoptic summary records of animal behaviour. Data are then

stored in an internal memory and transmitted at the surface via the Argos satellite system. The limited Argos data channel does not allow all records to be transmitted. Therefore a pseudo-random method to schedule the transmission of an unbiased sample of stored records is used. If by chance the CTD-SRDLs are recovered at a later stage, all data collected for transmission, whether or not it was successfully relayed, can be downloaded. Within this chapter, I focus on the design of the CTD-SRDL and its oceanographic sensors.

### 2.3.1 Design

Potential effects on an animal's normal behavior must be considered whenever an animal is instrumented. While the 'rule of thumb' for complete instruments dictates that they weigh no more than 3-5% of the animal's total body weight (Cochran, 1980), subsequent studies have shown the importance of species-specific considerations (Aldrige and Brigham, 1988). Aldrige and Brigham (1988) showed that adverse impacts from the weight of instruments should be examined not only for each species but also for size variations within each species if no such data from closely related species exist. The CTD-SRDL is designed to minimize any effects on an animal, i.e. shaped to minimize the drag. The outside dimensions are 11.0 *cm* length, 7.2 *cm* width and 5.4 *cm* height (Fig.2.1). The antenna length is 17 *cm*. The volume is about 254 *cm*<sup>3</sup> with a mass of  $545 \pm 5$  *g* in air and  $255 \pm 5$  *g* in sea water. The cross-sectional area is about 34 *cm*<sup>2</sup>. Referring to the 'rule of thumb' for the animal's total body weight, an instrumented animal should have at least a mass of 16 – 18 *kg*.

CTD-SRDLs were deployed on harbour seals, grey seals, hooded seals, harp seals, ringed seals, bearded seals, Northern elephant seals, California sea lions, Southern elephant seals, Weddell seals, crabeater seals and leatherback turtles. Due to animal behaviour, CTD-SRDLs needs sometimes to be attached to the head of an animal

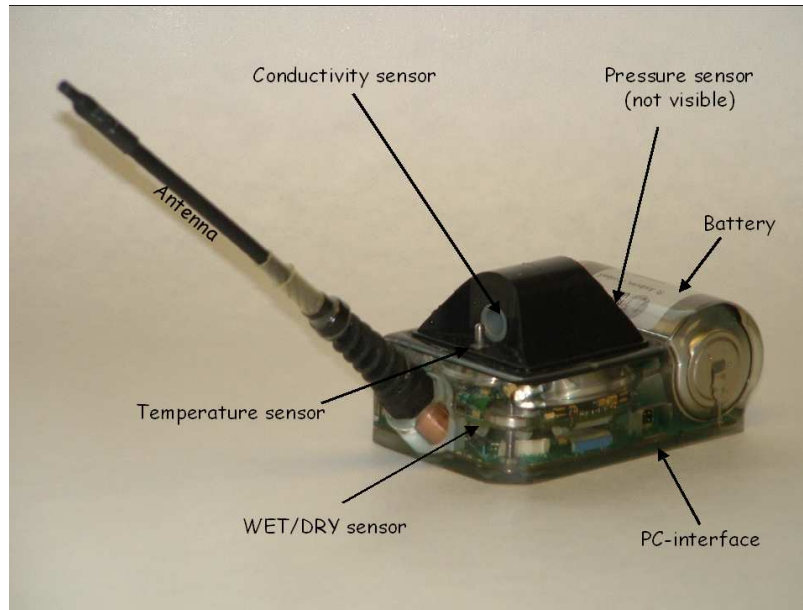


**Figure 2.1:** Picture of a CTD-Satellite Relay Data Logger (CTD-SRDL).

to increase the surface time or even make a transmission possible. In this case, the weight of the CTD-SRDL is of greater importance, because the head needs to be accelerated in order to catch prey. The practical experience with CTD-SRDLs and data loggers with similar size and weight showed no harm on various animals. Analyses on adult female southern elephant seals (250 – 800 *kg*) on Macquarie Island showed no measurable effect. Females carrying tags put on just as much weight over winter (and summer) as those not carrying tags (Hindell, pers. comm.). Another example is the male Southern elephant seal *Rudolph*, who was tagged in 2004 and 2005 on South Georgia gaining 147 *kg* in weight during the first year while carrying a CTD-SRDL.

### 2.3.2 Sensors

The design requirement to the CTD sensor head is to use almost no power, be virtually indestructible, and yet be minimised in size and weight. This requires small, non-pumped sensors that are less accurate when compared to larger pumped CTD

systems. The question was to determine the necessary accuracy of the oceanographic sensors to be useful for oceanography. Recent studies show that mid-depth Southern Ocean temperatures have warmed by as much as  $0.17^{\circ}\text{C}$  since the 1950's (Gille, 2002), but long-term changes in the ocean temperature are usually of the order of  $0.01^{\circ}\text{C}$  per decade (Fukasawa et al., 2004; Zenk et al., 2003). To detect such changes, high accuracy measurements are necessary. Less accurate data can be found in remote sensing. The sea surface temperature (SST) is covered by remote sensing satellites with a standard deviation of  $0.1^{\circ}\text{C}$  to  $0.5^{\circ}\text{C}$  and a spatial resolution between 50 km and 1 km (McClain et al., 1985; Reynolds et al., 2005). However, CTD-SRDLs deliver vertical profiles similar to expendable bathythermographs (XBTs), which are traditionally used to provide an ocean temperature versus depth profile with an accuracy of  $\pm 0.02^{\circ}\text{C}$  to  $\pm 0.1^{\circ}\text{C}$  (Lockheed Martin Sippican, Inc., 2005; Boyd and Linzell, 1993). So, in order for any SRDL data to be of particular use to the oceanographic community for long-term change purposes, proven accuracies of  $\pm 0.02$  for salinity and  $\pm 0.02^{\circ}\text{C}$  for temperature are necessary. While these sensor accuracies in themselves are quite easily achievable, they are substantially harder to attain in combination with the other requirements.

The pressure sensor is incorporated in the CTD head of the CTD-SRDL (Fig.2.1). This sensor consists of a Keller series 7 piezoresistive pressure transducer (Keller AG, CH) with a diameter of  $15\text{ mm}$ . A high-sensitivity piezoresistive silicon chip is used for pressure sensing. The chip is protected from ambient influences by a stainless steel housing sealed with a concentrically corrugated diaphragm. The housing is filled with silicone oil for the transfer of the pressure from the diaphragm to the sensing component. All metal parts in contact with the pressure media are made of stainless steel (316L). The fully welded housing is vacuum-tight. The pressure range given by the manufacturer is up to  $2000\text{ dbar}$  with an accuracy of about 1% of the full scale reading. However, comparisons with a SeaBird Electronics (SBE) 911plus CTD

SRDL ID	Maximum Error in Temperature [mK]	Maximum Error in Conductivity [ $10^{-3}$ mS/cm]	Maximum Error in Pressure[dbar]
10857	0	4	0.214
10859	2	1	0.180
10851	3	6	0.616
10854	2	3	0.861
10849	1	9	0.415
10847	2	2	0.491
10853	1	8	0.071
10850	2	9	0.575
10861	3	5	0.405
10848	2	2	0.612
Mean	1.800	4.900	0.444
Std	0.919	2.998	0.239
Max	3.000	9.000	0.861

**Table 2.1:** Summary of calibration checks done at Valeport Ltd, Devon, UK. 10 CTD-SRDLs were calibrated and then re-tested against one known temperature and salinity and against a range of pressure from 0 dbar to 2000 dbar in December 2007.

showed an accuracy of better than 1% of the actual reading, i.e. better than 5 dbar at the full scale reading, while checks in the calibration lab at Valeport Ltd showed errors in the pressure reading of less than 1 dbar over the full range (Tab. 2.1).

The CTD head of the CTD-SRDL is equipped with a Platinum Resistance Temperature Detector (PRT). The PRT works on the principle of resistance through a fine platinum wire as a function of temperature. The most common type (PT100) has a resistance of 100 *ohms* at 0° C and 138.4 *ohms* at 100° C. The probe is housed in a metal tube in front of the conductivity sensor (Fig.2.1). The PRT is calibrated by Valeport Ltd. to an accuracy better than  $\pm 0.005^\circ\text{C}$ , however post-calibration checks done by Valeport Ltd. (Tab. 2.1) and recalibrations at the calibration lab at the Naval Postgraduate School in Monterey, CA, USA (Fig.2.2) made by me showed that the temperature readings are in general better than  $\pm 0.002^\circ\text{C}$  (Fig.2.3).



**Figure 2.2:** Calibration of SRDLs in the calibration lab at the Naval Postgraduate School in Monterey

An inductive method was selected over an electrode cell to measure the conductivity of the sea water. This and the titanium and ceramic construction give improved durability. Valeport Ltd. also developed a new digital measurement technique for the inductive sensor, resulting in a highly accurate sensor with much lower power consumption than traditional methods, and with much shorter sampling duration. One known feature of some inductive cells is that they compress minutely under pressure. This could result in a significant effect on the necessary small bore of inductive cell on the CTD-SRDL. An inaccuracy of about  $1\mu m$  in the bore would throw the sensor out of specification. Again, use of high strength ceramics in the construction mean that even at 2000 dbar pressure, the conductivity cell retains its shape. The conductivity sensor is calibrated by Valeport Ltd. to an accuracy better than  $\pm 0.01 mS/cm$ . Post-calibration checks at Valeport Ltd. showed accuracies of about  $\pm 0.005 mS/cm$  (Tab. 2.1) and recalibrations performed by me at the calibration lab at the Naval Postgraduate School in Monterey showed that the conductivity readings are in general better than  $\pm 0.003 mS/cm$  (Fig.2.3).

One disadvantage of a single bore inductive cell is the increased risk of interference of the external field of the sensor. I tested the CTD-SRDLs in different configurations to estimate the possible effects on the salinity measurements (Fig.2.4). During the first test I moved the CTD-SRDL towards the calibration tank wall (non-conductive). The

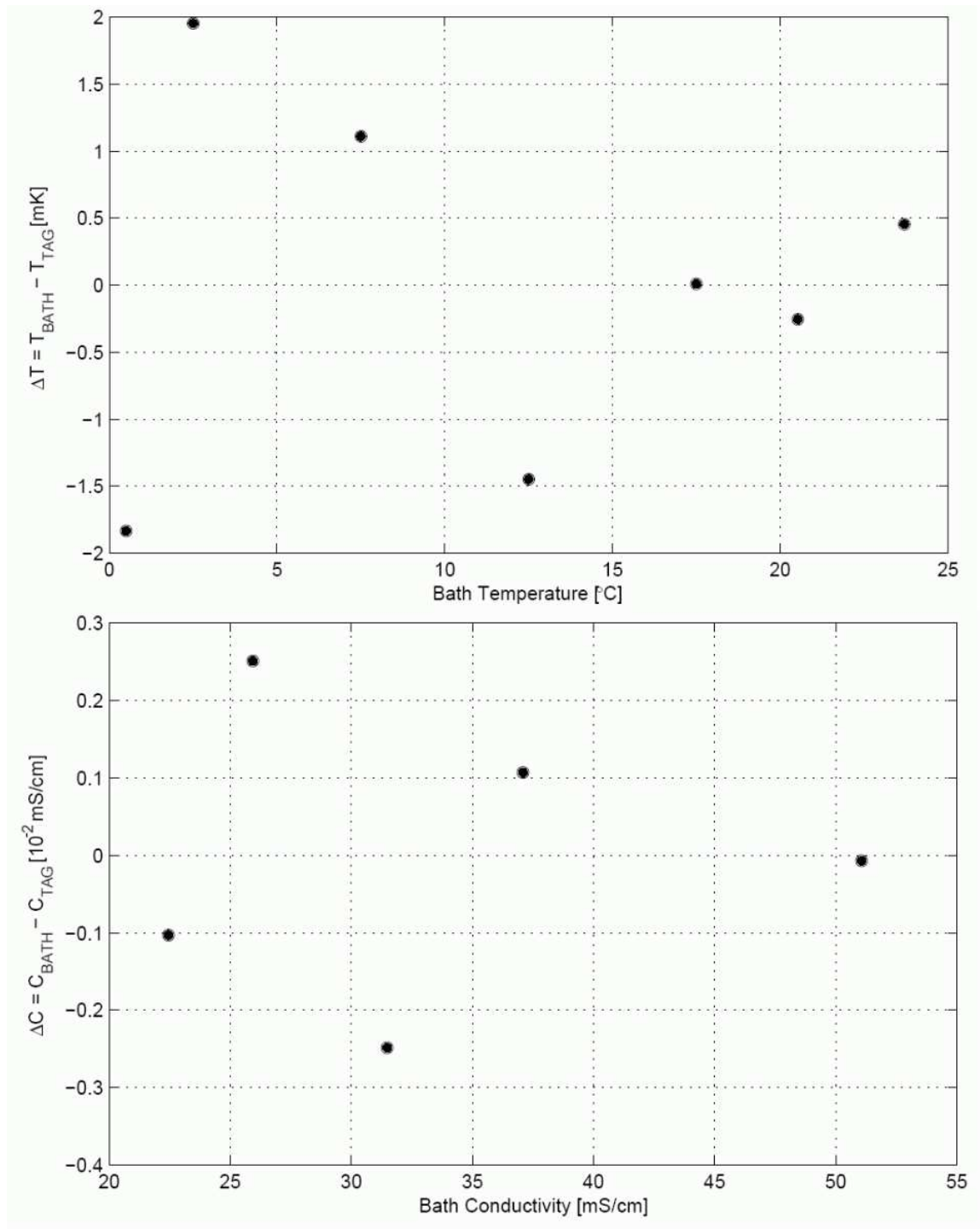


**Figure 2.3:** Comparison between the controlled temperature and conductivity baths and the CTD-SRDL measurements.

bottom of the CTD-SRDL was facing the wall. As I reduced the distance between the tank wall and the bottom of the CTD-SRDL an effect on the salinity readings is obvious at a distance below 10 cm (Fig.2.4). When the bottom of the CTD-SRDL was in contact with the tank wall the salinity readings were up to 0.075 too low. I also turned the CTD-SRDL in the tank, e.g that the side of it was in contact with the wall. The effect on the salinity measurements is greatest, when the inductive cell is in direct contact with the interference and the errors can be as big as 0.5 (Fig.2.4). Interesting is the fact that in on a second test the effect on salinity, when the bottom of the CTD-SRDL was touching the tank wall was around 0.01, much less than in the first test (Fig.2.4). Sometimes SRDLs are attached to a plate, which is already attached to the animal's fur, with cable ties. These configurations were also tested in the bath. I didn't use the plate, but put cable ties around the CTD-SRDL in front and behind the conductive cell. These cable ties have an effect on the conductivity reading and should be avoided in the future to minimise any possible offset in conductivity (Fig.2.4). Nevertheless, these tests suggest that the animal's head will have an effect on the conductivity measurements during a deployment and the data need to be corrected accordingly. The calibrations and checks by Valeport Ltd. and the recalibrations done by me show that the accuracies of the temperature and the derived salinity before deployment are better than the set requirements.

Some CTD-SRDLs were also checked against ship-based CTDs. Figure 2.5 shows differences between a ship-based CTD (SBE 911) and a CTD-SRDL, which was attached to the frame of the ship-based instrument. Only data measured in a homogeneous layer were used to compare both instruments. The differences in temperature are less than 5 mK and the resolution of the temperature data is obvious. The salinity data recorded by the CTD-SRDL is also within 0.005 of the measurements taken by the SBE 911 (Fig. 2.5). Such direct comparisons between ship-based CTDs and CTD-SRDLs were performed for some of the CTD-SRDLs before deployment.

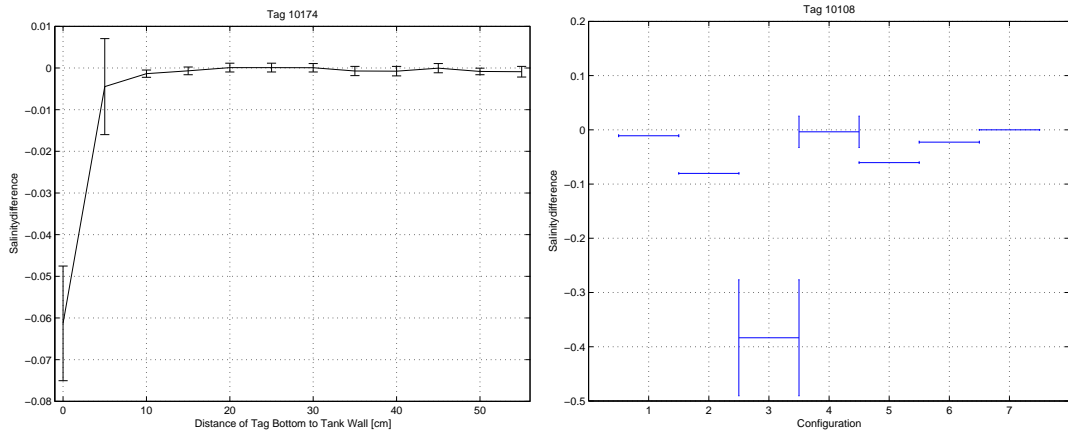


**Figure 2.4:** External field effect on salinity measurements. *Left:* Difference between the CTD-SRDL measurement and the bath salinity. An SRDL was moved towards a wall of the calibration tank. The bottom of the SRDL was facing the wall. *Right:* The effect on salinity and the error using different configurations: bottom at wall(1), side at wall (2), conductivity cell at wall (3), random movement (4), different cable tie configurations (5&6), nothing (7).

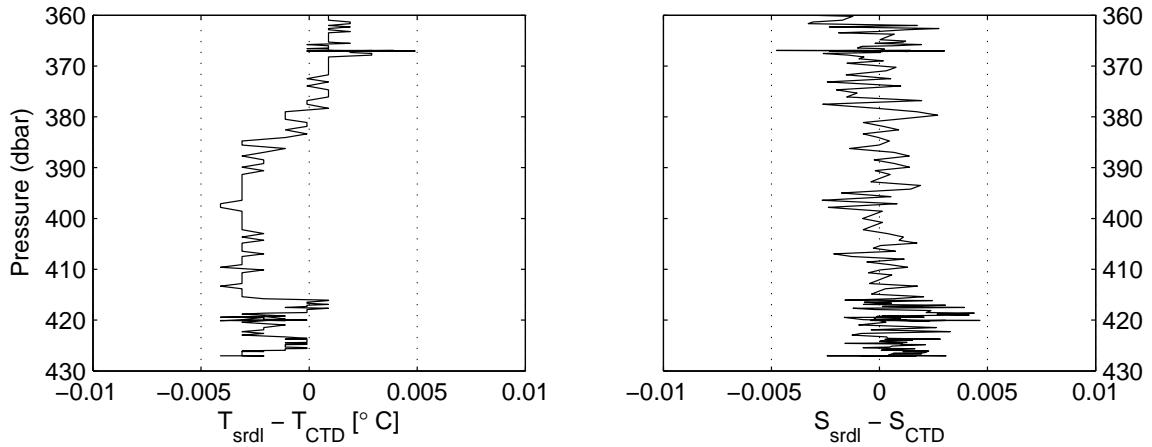


**Figure 2.5:** Differences in temperature (left) and salinity (right) of a CTD-SDRL and a ship-based CTD. The CTD-SRDL was attached to the frame of the ship-based instrument. Only measurements taken in a homogeneous water mass are used.

### 2.3.3 Data compression and transmission

Many marine mammals travel on a global scale, thus tracking of the animal with ships or aircraft is often not practicable. One better option is to relay the information using the Argos satellite system (Argos, 1996), which has been used successfully for sending data from oceanographic and weather buoys. Animal telemetry is providing a

rapidly increasing fraction of Argos bandwidth. The system has some drawbacks for telemetry from marine mammals. Transmitters that are certified to communicate with Argos must conform to very strict frequency tolerances. Individual messages (termed "uplinks") may be up to 960 msec in duration and it takes 2 or more complete uplinks for the system to compute a location. The accuracy of these locations depends on the number of uplinks received, the temporal pattern of these receptions and the position of the satellite relative to the transmitter. Uplinks may contain a maximum of 256 bits (32 bytes) per message in a rigid format and Argos sets a minimum interval of 40 sec between transmissions (Argos, 1989). However, Argos limits the usable number of bits to 228, because 28 bits are now used for the PTT (Platform Transmitter Terminal) number.

These restrictions, combined with the fact that animals are only briefly and infrequently at the surface (for example, 10% of the time in two minute segments for elephant seals), places unusually tight limits on bandwidth. These and those limitations caused by energy constraints both demand complex data collection software and extreme data compression, which in turn demand a sophisticated data collection platform. This bandwidth restriction is compounded by the fact that satellites are not always visible. However, the data transmission restrictions resulting from energy constraints and Argos restrictions do not interact in an additive way and steps taken to get around Argos limitations also serve to help avoid energy constraints. Detailed description of the collection and compression of behavioral data is given in Fedak et al. (2002); here, I concentrate on the hydrographic data compression. The setup of the compression method of the CTD data is determined by the user and can be changed at any time before the deployment. Here, however, I describe the standard program, which is used in most cases and is the default setup.

The tags begin sampling at the deepest point of a dive, detected by analysing

the trend provided by the pressure sensor every 4 seconds. If this depth exceeds a pre-set value in a 6 hour period, the tag switches to ‘sampling-mode’. On the ascent, the tag then begins sampling temperature (T), conductivity (C) and pressure (P) every second until the surface is reached. From these detailed, high-resolution data, salinity (S) is calculated. Finally, a set of four 256 bits Argos messages are produced. One message contains a detailed dive summary. Another message comprises of information about the cruise/haul-out pattern in the 6-hour period, while the CTD data is compressed into two other messages. Only 15 representative depth points with corresponding temperature and salinity values are selected for transmission using a combination of 8 predefined depths and 7 ‘inflection points’, which are chosen via a ‘broken stick’ point selection algorithm (Fedak et al., 2002). The first message contains 7 fixed depth T/S pairs. The second message contains 7 broken-stick and 1 fixed depth T/S pairs.

The fixed depth points are chosen, depending on the deepest point of the dive. One broken-stick point will be the one closest to the surface and one will be at the deepest point of the dive. Then the fixed depths points are chosen based on table 2.2. The remaining five points will be selected between the fixed depth points based on the broken stick method.

The standard software has a temperature range from  $-2^{\circ}\text{C}$  to  $30^{\circ}\text{C}$  with a resolution of 0.10% of the temperature range of the specific profile, i.e. if the maximum and minimum temperatures within one profile are less than  $10.24^{\circ}\text{C}$  apart, then the resolution will be better than  $0.01^{\circ}\text{C}$ . Only the minimum and maximum temperatures are transmitted as full values while all intermediate values are associated to one of 10 bits, hence the resolution depends on the temperature range. This means, this temperature setup will be better than the required accuracy in most of the high latitude oceans. The salinity range is 8.19, typically between 29 and 37 to be applicable

Pressure	Fixed depths used									
10 dbar	X	X	X	X	X	X	X	X	X	
14 dbar	X									
20 dbar	X	X	X	X	X	X	X	(X)	(X)	
26 dbar	X									
30 dbar	X	X	X	X	(X)					
36 dbar	(X)									
40 dbar	X	X	X							
50 dbar	X	X	X	X	X	X	X	X	X	X
60 dbar		X	(X)							
80 dbar		(X)		(X)						
100 dbar		X	X	X	X	X	X	X	X	X
150 dbar			X	X	X	(X)				
200 dbar				X	X	X	X	X	X	X
300 dbar					X	X	X	X	X	(X)
400 dbar						X	(X)			
500 dbar							X	X	X	X
750 dbar								X	X	X
1000 dbar									X	X
1500 dbar										X

**Table 2.2:** Fixed depth points transmitted depending on dive depth. All points are transmitted within one Argos message, except the one in brackets, which will be send together with the broken-stick depths.

in most of the world oceans. The resolution of the transmitted data points is about 0.39% of the salinity range of that specific profile, i.e. if the salinity range within the profile is less than 2.56, a resolution of better than 0.01 is achieved (8 bit resolution).

As mentioned above, one day is divided into four 6 hours periods in which one full CTD profile is recorded. This setting is chosen to ensure that the batteries last long enough to perform 4 CTD profiles a day assuming 12 months deployment with an

average diving depth of 1000 m.

The compressed hydrographic and behavioural data is then transmitted during each surfacing of the seal. Data of more than 115000 messages of 69 tags deployed during 2004 and 2005 were analysed (Fig. 2.6). The CTD-SRDL antenna is oriented so as to be out of the water when the seal is at the surface. The minimum interval between two successive messages is 40 sec. However, sometimes the CTD-SRDL is underwater, because of waves or the animal's movements, so that the next transmission can be delayed. The average surfacing time of an elephant seal is about 130 sec, which would allow the CTD-SRDL to send 3 messages. Unfortunately, Argos satellites are not always available and the low power of the transmitter together with the small antenna result in messages not received by the Argos satellite system. Nevertheless, for more than 75% of all surfacings 2-3 messages are received (Fig. 2.6) and 2 CTD profiles are decoded per day. A third of this data might have only the seven points of the first message. The limited surface time also reduces the possibilities of a position fix by the Argos system. To calculate a position fix the Argos system needs at least 4 received messages (Argos, 1996). Only for less than 25% of all surfacings are four or more messages transmitted and a position obtained (Fig. 2.6). Consequently, positions for some profiles are determined using delayed-mode auxiliary location processing, typically by removing locations requiring unrealistic swimming speed for a given species. Further information on post-processing such data is given in e.g. McConnell et al. (1992). In general, the accuracy of the position for each CTD-SRDL profile is of the order of 2 km. Research ships can hold their position within a couple of metres due to their dynamic positioning system, but ship-based CTDs can be captured by ocean currents and drift hundreds of metres away from the ship position, when lowered to great depths. Therefore, the position of a CTD-SRDL profile is not considerably less accurate than a ship-based CTD.

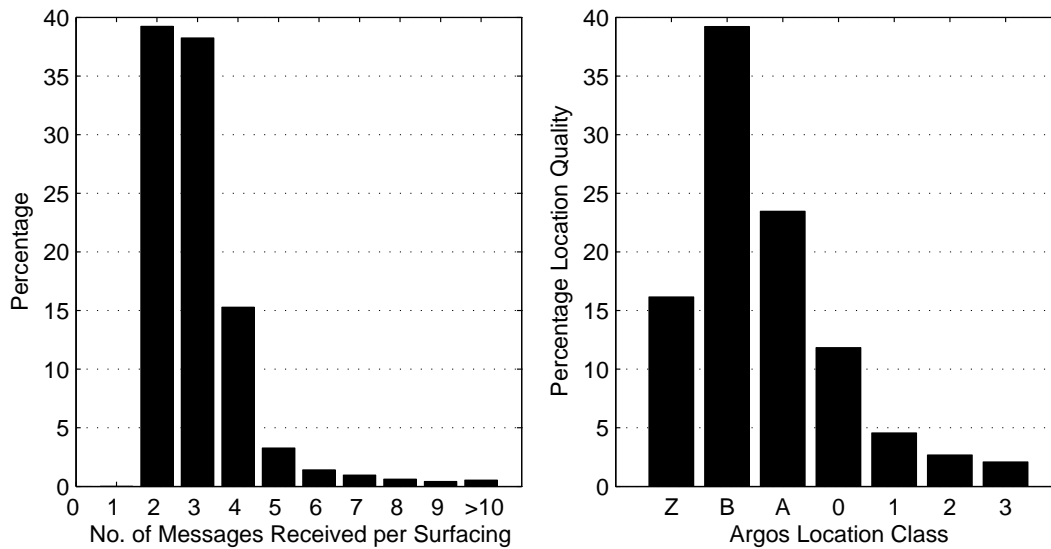


**Figure 2.6:** Percentage of numbers of Argos messages received for each surfacing (left) and the Argos location class for each calculated position (right). The position accuracy is: 3 ( $< 250m$ ), 2 ( $< 500m$ ), 1 ( $< 1500m$ ), 0 ( $> 1500m$ ), A (three messages received), B (two messages received), Z (no position fix). Data are from 69 CTD-SRDLs south of  $40^\circ$  S

### 2.3.4 Remote data quality control

In order to properly quantify possible sensor drifts with high accuracy, recovery of the CTD-SRDL and recalibration of its sensors would be necessary. However, this is not only too expensive on a routine basis, it also is often impossible (i.e. if a seal dies). So, usually only pre-deployment calibrations are available. Nevertheless, some investigators have recovered SRDLs and recalibrated them. But since a recalibration is generally not possible, CTD-SRDL data have to be checked in an indirect way, such as comparisons with climatology or shipboard high-resolution CTDs. Every water mass has its typical range of temperatures and salinities, which is a measure of its natural variability. To compare the relationships of potential temperature ( $\Theta$ ) and salinity measured by a CTD-SRDLs to that of calibrated measurements, a small temperature range will result in small uncertainties of a possible offset. But the variability of the surface water properties is often much too high to use for any kind of data quality check. Below the surface layer this natural variability will decrease by one order of

magnitude making comparisons more plausible. These comparisons are usually made on deep isotherms assuming that temperature and salinity on such isotherms are steady and uniform (Bacon et al., 2001).

Between 1st and 2nd of October 2004 the southern elephant seal *Rudolph* performed 8 dives close to  $52^{\circ}$  S and  $53.5^{\circ}$  W to depths up to 1000 dbar (Fig. 2.7). Within a 80 km by 60 km box around these profiles, Argo floats (3800084 and 380085) performed five full depth CTD profiles until the end of June 2005 (Fig.2.7). The Argo profiles are between 22 and 262 days apart. In layers above 600 dbar the variability is too high for any comparisons, but below this the variability drops to a more satisfactory value (Fig.2.7). All five Argo profiles were used to calculate the mean temperatures and the corresponding standard deviations below 500 dbar in 50 dbar intervals down to 1000 dbar. The differences between the mean temperatures and the CTD-SRDL measurements are shown in figure 2.7. Except one outlier, all CTD-SRDL measurements lie within variability measured by the Argo floats and most of them within  $\pm 0.1^{\circ}\text{C}$  to the mean temperature. This shows that these CTD-SRDL temperature profiles (8 out of 1934) are of an accuracy of about  $\pm 0.1^{\circ}\text{C}$ . Although I know that the temperature sensor should be much better, with this data for reference and its distribution in time and space, a more definite answer is not possible. This shows the limitation of remote data quality control, when only limited data for cross-comparisons are available.

When many reference measurements are available, a statistical approach might be possible, but great care must be taken in minimizing deviations due to temporal and spatial separation. Objectively mapping a set of reference data to the CTD-SRDL/animal position thus producing comparison temperature on isobars and salinities on surfaces of constant  $\Theta$  allows checking of CTD-SRDL measurements where there is no calibrated data in the vicinity of the profile. Similar methods are presently used by the Argo community (Wong et al., 2003; Boehme and Send, 2005). The main

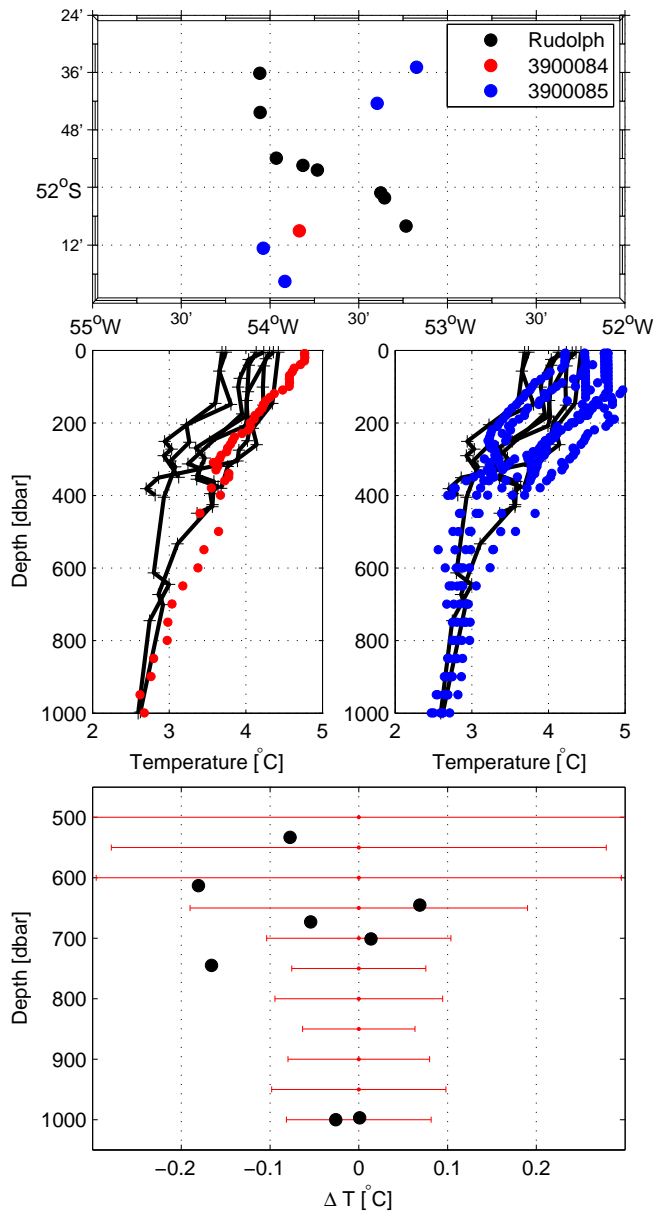


**Figure 2.7:** Positions (*top*) and temperature profiles (*middle*) of a CTD-SRDL (*Rudolph*) and Argo floats. CTD-SRDL profiles between 1 and 2 October 2004 (black), Argo float 3900084 profile at 24 October 2004 (red) and Argo profiles of float 3800085 from 22 May to 21 June 2005 (blue). Standard deviation of temperature on different depth levels as derived from these five Argo temperature profiles in red (*bottom*). Differences between the calculated mean temperatures and the CTD-SRDL measurements in black.

advantages are the global coverage of the hydrographic database, its automated system and the provision of confidence intervals, which makes this method suitable to handle the increasing set of CTD-SRDL data. I adapted the algorithm of Boehme and Send (2005) to check the salinity of one CTD-SRDL, which recorded data between February and November 2005 to the northwest of South Georgia (Fig. 2.8). The scale parameters used for this objective mapping are calculated from the correlation func-

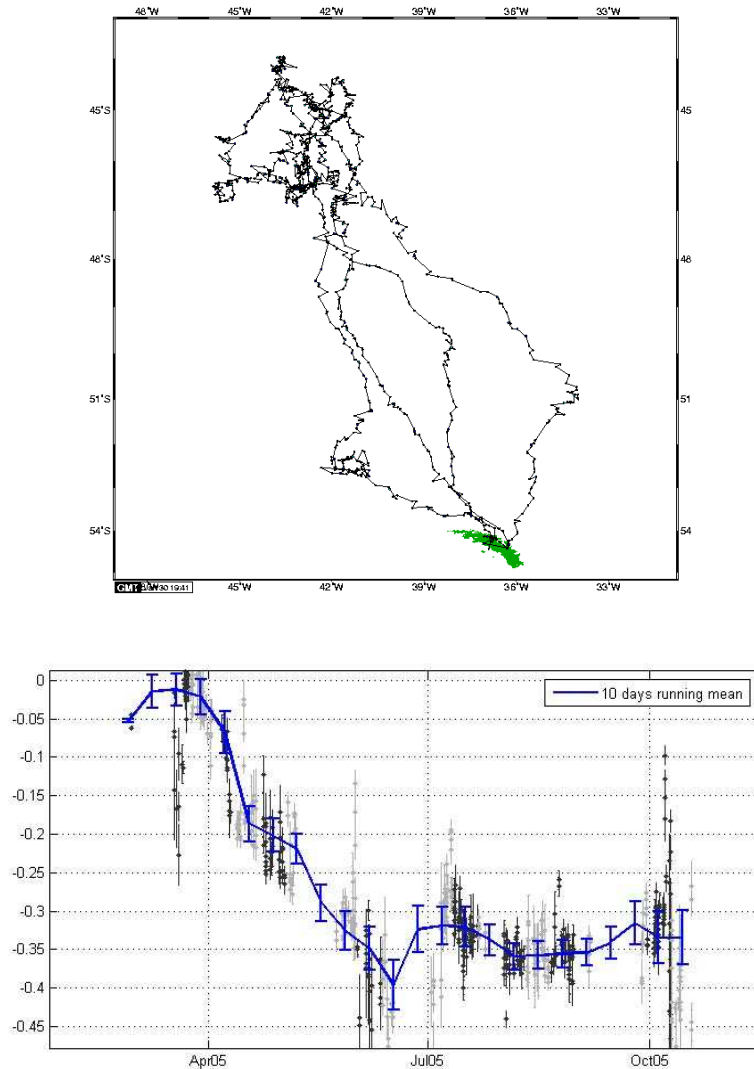


**Figure 2.8:** Positions (*top*) and estimated correction of the recorded salinity (*bottom*) of a CTD-SRDL (28494) between February and November 2005.

tion of in-situ measurements. Please refer to chapter 3 for more information. This animal visited a feeding site to the north of the Falkland Plateau between moulting and breeding. Four trips between South Georgia and the feeding site were recorded (Fig. 2.8). Argo float data and ship-based measurements were used to calculate a

reference salinity for each CTD-SRDL recording. The differences of the the actual measurements and the references provide a time series of corrections to the measurements including errors (Boehme and Send, 2005). The calculated corrections for this CTD-SRDL suggest a drift of the sensor in the first four months towards higher values, stabilizing afterwards with a constant offset of  $-0.34 \pm 0.05$  (Fig. 2.8). However, the region covered by the data is one of big changes in the hydrography, not only in longitudinal range but also on a seasonal or even monthly basis (Meredith and Hughes, 2005, Ch. 3). This results in a higher error of the correction factor and complicate the interpretation of the estimated correction. As usually only data from previous years are available as reference profiles, the drift in salinity observed by the CTD-SRDL compared to these historical profiles can also be partially attributed to a change in water mass properties within the Antarctic Circumpolar Current at that particular time. Again, this shows the limits of a delayed-mode quality control technique and the only way to improve the technique is to get as many accompanying reference CTD profiles as close by in time and space as possible. Another way to improve the quality of this technique is to use data of the CTD-SRDLs themselves, when enough different CTD-SRDLs are operating in the same area, as described in Boehme (2004).

So far, I checked more than 40 CTD-SRDLs deployed in 2004, 2005 and 2008 for offsets and drifts using both methods mentioned above. All CTD-SRDLs showed an offset in salinity, which is due to the effect of the seals' head on the external inductive field as mentioned above. The measured salinity was on average  $0.22 \pm 0.14$  too high. One example is shown in figure 2.9. A CTD-SRDL was deployed on a female Southern elephant seal on South Georgia in February 2008. The seal travelled south into the Weddell Sea and turned east. The salinity data collected during this migration were 0.1406 too high in salinity when compared to Argo float data, which was collected at the same time in the wider area. This shows that the real-time data should be

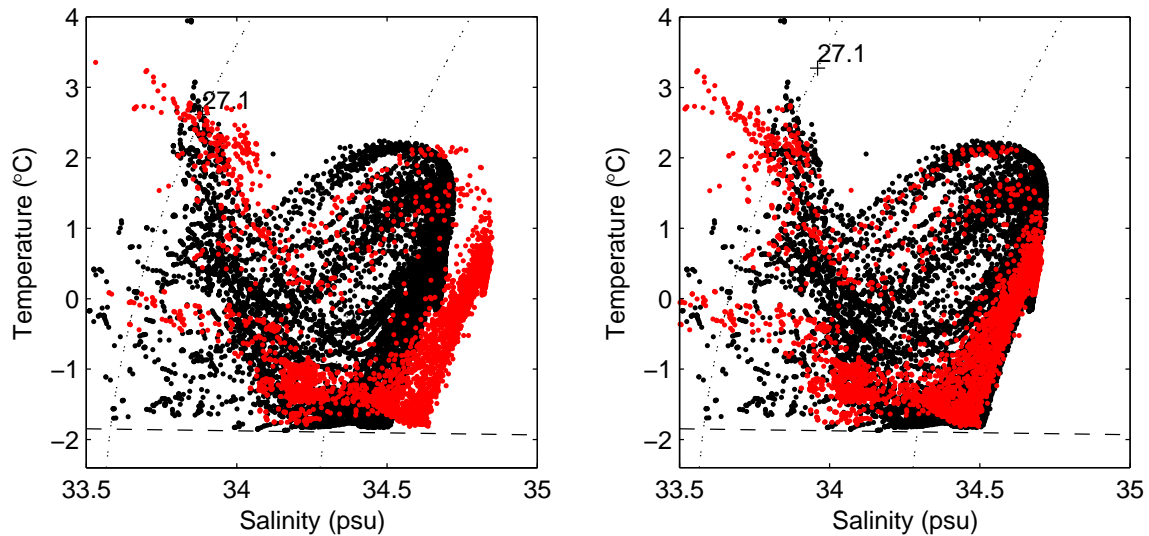


**Figure 2.9:** Temperature vs. salinity diagram. Data collected by Argo floats in black and data from a CTD-SRDL in red. Uncorrected CTD-SRDL data are shown in the left panel, while CTD-SRDL data in the right panel are corrected by an constant offset of  $-0.1406$  in salinity.

handled with care as with data from all oceanographic instruments. However, such offsets are easily detectable by direct comparison of real-time CTD-SRDL data with e.g. Argo float data and a real-time correction can be employed to enhance this real-time data. By using delayed-mode quality methods an accuracy of better than 0.02 in temperature and salinity for a dataset can be achieved.

### 2.3.5 Costs (as-of 1 June 2008)

The cost of one CTD-SRDL is £3950 (1 June 2008). However, you have to add the costs for relaying data using the Argos satellite system. To use the Argos system you have to pay €15 for each month data are received from one CTD-SRDL. Every day is divided in to four 6-hour periods and for each period in which data are received and additional €0.75 charge is added. In general, a CTD-SRDL transmits several messages within each 6-hour period, so that this charge can be simplified to a €3 charge per day. Assuming a deployment over 8 months (240 days), the total costs are

then £4609.47 (\$ 9139.61) (see table 2.3).

The expectation is to receive between 2 and 3 full CTD profiles a day, resulting in 600 CTD profiles per CTD-SRDL per 240 days deployment. Each CTD profile would then cost £7.68 and each C-T-P triplet £0.51. So, how does this compare to ship-based measurements? The daily costs of research vessels vary hugely from small ocean going vessels at £12500 (e.g Celtic Voyager) to icebreakers at £45000 (e.g. Polarstern). Assuming that a 2000m ship-based CTD cast takes about 90 minutes and a station spacing of about 30 miles, which would take about 3 hours to cover, would result in 5 CTD profiles a day from a research vessel. To get ship-based data similar to the animal-borne measurements, a ice capable ship is needed. Assuming daily costs of £30000, each CTD cast would cost £6000. Assuming that the final CTD profile is binned into 1 dbar intervalls, each C-T-P triplet would cost £3. An Argo float costs about £15000 delivering about 125 CTD-profiles within its lifetime. Therefore, each Argo float CTD-profiles costs £120 with 82 depth levels resulting in £1.46 per C-T-P triplet. However, these calculations are just academic as all methods don't compete but rather complement each other. Each of these methods to gather ocean data has its strength and weaknesses and these calculations are only shown for the sake of completeness.

Item	Number	Single Price	Total Price	Total in £
CTD-SRDL	1x	£3950		£3950.00
Monthly Argos charges	8x	€15	€120	£94.21
Daily Argos charges	240x	€3	€720	£565.26
Total Costs				£4609.47

**Table 2.3:** Costs of one CTD-SRDL and its data transmission for a typical 8 months deployment.

## 2.4 Field Experiences

The CTD-SRDLs were deployed on a number of marine mammals from hooded seals in the Arctic to Weddell seals in Antarctica. Here I will show, how different species can be utilised to gather data on different scales.

The main oceanographic aim of the Southern Elephant Seals as Oceanographic Samplers (SEaOS<sup>1</sup>) project was to cover the vast area of the Southern Ocean and demonstrate and implement this cost-effective means of gathering routine observations of hydrographic data from such remote environments. We deployed 21 CTD-SRDLs on South Georgia gathering more than 8200 hydrographic profiles to depths up to 2000 dbar from the Drake Passage to east of the Mid-Atlantic Ridge (Fig. 2.10). The CTD-SRDLs were deployed after the elephant seals moult their skin in January/February.

The seals were immobilized with a teletamine/zolazepam mixture administered either intramuscularly (1.0 mg/kg) using a dart and blowpipe or intravenously (0.5 mg/kg), when the seal is constrained in a headbag. Subsequent intravenous injections were administered when necessary to maintain immobilization. Standard length and axillary girth were measure with a flexible tape before the CTD-SRDL was attached to the head with epoxy (Araldite, AW2102, Intertronics, Oxfordshire, UK) (Fig. 2.11). For more details on the attachment technique see Fedak et al. (1983). The CTD-SRDLs remain attached for periods of several months and are lost when the animals moult again.

Some of the animals travelled several thousands of kilometers away from South Georgia during their migrations. During these migrations about 90% of two successive CTD-profiles were seperated by less than 34 km and the instruments delivered about 2 profiles a day, providing a station spacing similar to ship-based transects. Marine

---

<sup>1</sup><http://biology.st-andrews.ac.uk/seaos/index.html>

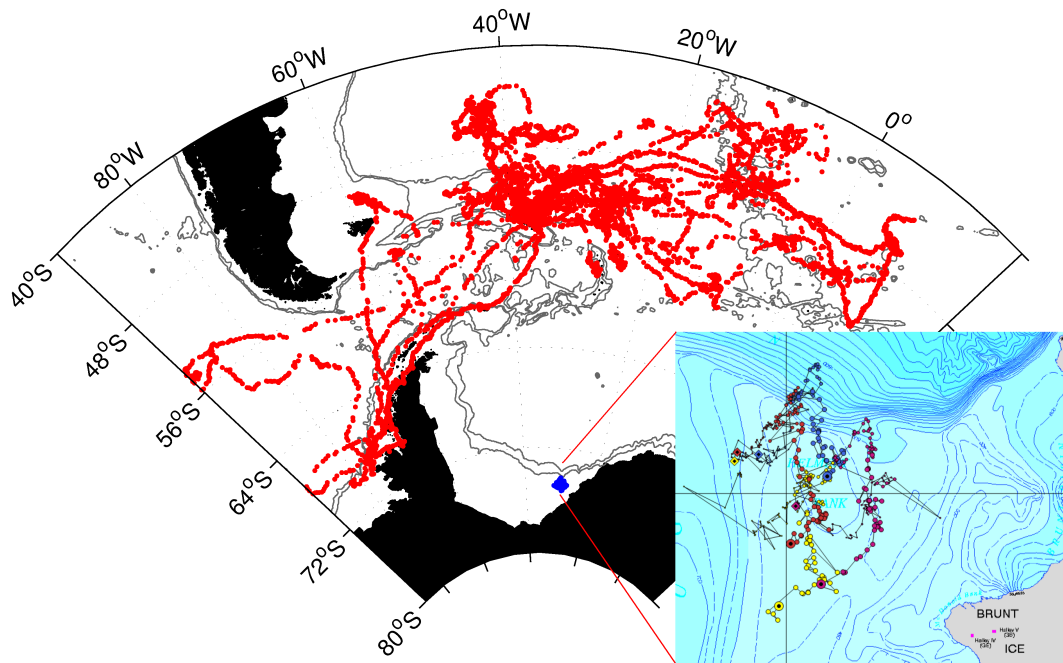


**Figure 2.10:** Spatial coverage of the two studies discussed in the text. The large map shows the locations of CTD profiles gathered during the SEaOS project (red) and the Weddell Sea project (blue). The inset is a magnification of this particular study area.



**Figure 2.11:** Picture of a CTD-Satellite Relay Data Logger (CTD-SRDL).

mammals are ‘adaptive’ samplers generating a higher number of profiles in regions with higher oceanographic gradients (Ch. 4). Such data is therefore particularly useful to investigate the general oceanography in this area (Ch. 3).

To study small scale oceanographic feature another setup is needed. This can be

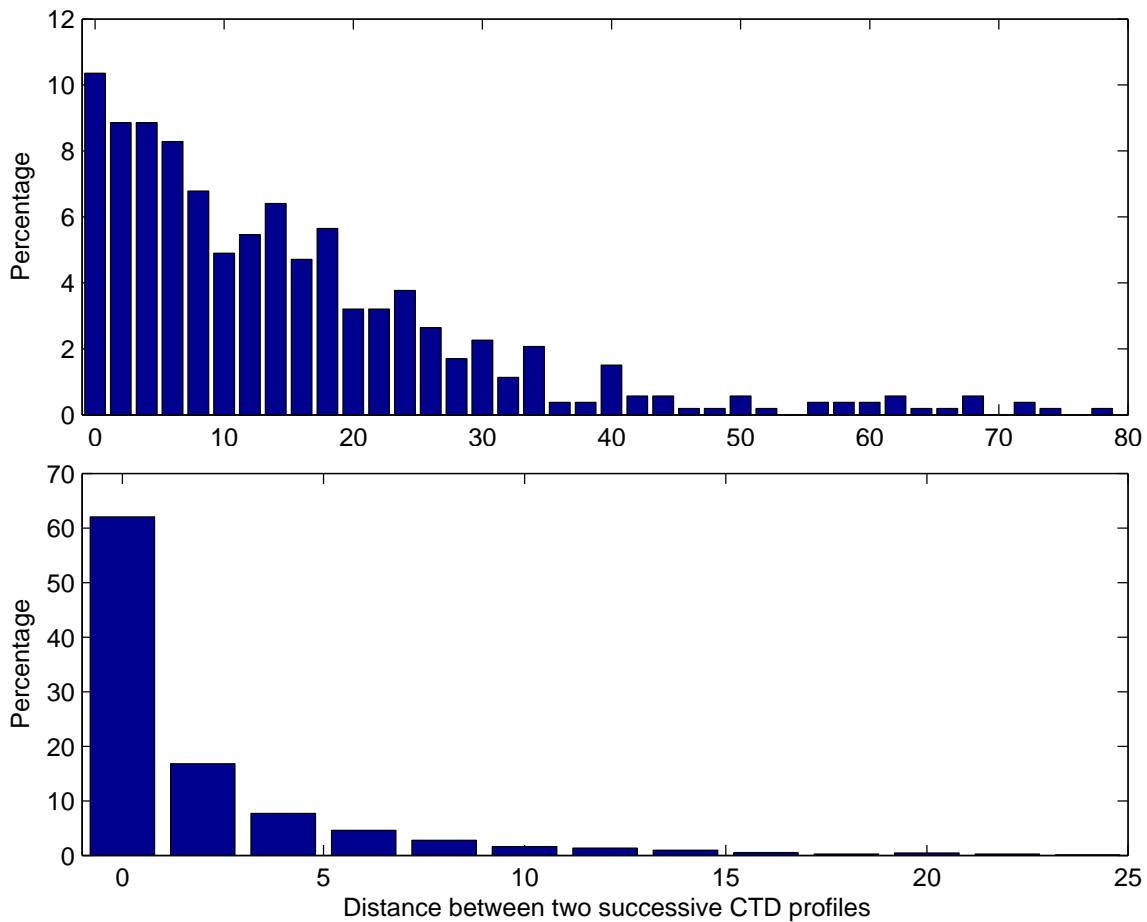


**Figure 2.12:** Distance between two successive CTD profiles. The top panel shows data from the SEaOS project, while the lower panel shows the data obtained by the Weddell Seals.

either achieved by choosing a different software for the CTD-SRDL or by choosing another species. In February 2007, 4 CTD-SRDLs were deployed on Weddell seals (*Leptonychotes weddellii*) just south of the shelf break in the southeastern Weddell Sea (Fig. 2.10). The CTD-SRDLs were deployed in a similar way as on Southern elephant seals (Fig. 2.13). However, the configuration of the instruments was slightly different and not based on 6-hours periods, so these instruments delivered 4-5 CTD profiles per day from beneath the pack ice, complete from the surface to the sea floor over the continental shelf. For more than 90% of the data, the station spacing was less than 6 km (Fig. 2.12) delivering a spatially focused view of the cross-shelf



**Figure 2.13:** CTD-SRDL attached to the fur of a Weddell Seal after their moult (January/February) in 2007. Photo by R. Stevens.

processes north of the Filchner Ice Shelf. When compared to sea ice cover obtained by remote sensing, these seals were shown to deliver data from below 95% pack ice coverage. This near-real time data is thus virtually unobtainable by other means.

## 2.5 Summary and Conclusions

The uniqueness of the series 9000 CTD-SRDL (Fig.2.1) lies in its data collection, processing and transmissions strategies and this study clearly demonstrates that animal-borne sensors have the potential to provide high quality oceanographic measurements in near real-time. Vertical profiles of temperature and salinity to depths of up to 2000 m were recorded with a sufficient accuracy to be useful for operational oceanography. The CTD-SRDLs record temperature with an accuracy of better than  $0.01^{\circ}C$ . But due to the limited availability of reference data for post-processing, data are often associated with an error of  $0.02^{\circ}C$  as a more definite answer is not possible. Salinity measurements are in general very good, but afflicted with an offset of the order of 0.2 during the deployment due to the effect of the seal's body onto the inductive field. The salinity data therefore need post-processing, which can be a real-time correction to enhance the real-time data, and must comprise of a delayed-mode

quality control. Nevertheless, such sensors are a powerful complement to existing hydrographic sampling methods and data quality will improve further in the future. Other enhancements include different parameters that can be measured, and at the moment a fluorometer is developed to be incorporated in to the existing CTD-SRDL to enhance the sensor suit.

The international SEaOS project collected more than 22000 profiles (Ch. 1) over 3 years in the Southern Ocean and were added to the World Ocean Database. However, data are collected in near real-time and a system is now in place to forward the data to the Global Telecommunication System (GTS). As defined by the World Meteorological Organization (WMO) the GTS is the co-ordinated global system of telecommunication facilities and arrangements for the rapid collection, exchange and distribution of observations and processed information within the framework of the World Weather Watch, i.e. providing data for numerical weather prediction centers. CTD-SRDL data of ongoing projects are therefore converted into an appropriate format and will be loaded to the GTS on a daily basis. This system started in July 2008. Thus, CTD-SRDL data will be freely available and will advance the output of model and assimilation systems producing forecasts of temperature, salinity and currents of the oceans, e.g. the Forecasting Ocean Assimilation Model<sup>2</sup> (FOAM).

Here I showed just two examples of species covering the Southern Ocean (Fig. 2.10)). Nevertheless, research projects using CTD-SRDLs exist on a variety of species, including white whales (Lydersen et al., 2002), ringed seals (Lydersen et al., 2004), hooded seals (Fisheries and Oceans, Canada), grey seals (Fisheries and Oceans, Canada), sea lions, Weddell seals (British Antarctic Survey, UK), northern elephant seals (Tagging of Pacific Pelagics), crabeater seals (University of California, Santa Cruz, USA) and southern elephant seals (UK, USA, France, Australia, Brazil, South Africa, Germany). With the current knowledge of animal behaviour the data collection is pre-

---

<sup>2</sup><http://www.metoffice.gov.uk/research/ncof/foam/index.html>

dictable by choosing the right species.

The CTD-SRDL described in this study shows an innovative approach in collecting oceanographic data from remote, previously inaccessible parts of the oceans and meets the goals of the Global Ocean Observing System of improving ocean data availability in delayed and real-time modes.



### **3 The ACC frontal system in the South Atlantic: monitoring using merged Argo and animal-borne sensor data.**

Manuscript accepted in

Boehme, L., M. P. Meredith, S. E. Thorpe, M. Biuw, and M. Fedak (2008), The ACC frontal system in the South Atlantic: monitoring using merged Argo and animal-borne sensor data., *J. Geophys. Res.*, doi:10.1029/2007JC004647, in press.

### 3.1 Abstract

I described large-scale features of the Antarctic Circumpolar Current (ACC) by merging Argo data and data obtained by novel animal-borne CTD sensors. Twenty one CTD-Satellite Relay Data Loggers (CTD-SRDLs) each recording conductivity, temperature and pressure were attached to Southern elephant seals (*Mirounga leonina*) on South Georgia. I merged the data from the CTD-SRDLs with concurrent data from Argo floats in the South Atlantic Ocean to yield a unified dataset of gridded fields of hydrographic data with high temporal and spatial resolution, enabling determination of features absent in each of the datasets separately. The structure and variability of the frontal field revealed by this dataset was compared with those in daily quarter-degree, optimally interpolated sea surface temperature fields and fields of weekly gridded sea level anomaly. In general, the frontal positions derived using my dataset are in agreement with previous work, especially where the pathways are constrained by topography, e.g at the North Scotia Ridge, South Scotia Ridge and the Mid-Atlantic Ridge. However, with the improved temporal and spacial resolution provided by the CTD-SRDLs, I were able to observe some novel features. All frontal positions are more variable than previously indicated across the Scotia Sea and west of the Mid-Atlantic Ridge on seasonal timescales. The merged dataset shows the temporal variability of the Southern ACC Front (SACCF) retroflection north of South Georgia and in its position east of the island, where the SACCF lies further north than has been suggested in previous work. In addition, the Subantarctic Front crosses the Mid-Atlantic Ridge also further north indicating a northward shift of the ACC frontal system east of 40°W.

## 3.2 Introduction

The most pronounced feature of the Southern Ocean circulation is the eastward flow of the Antarctic Circumpolar Current (ACC) (Fig. 3.1), which plays a crucial role in the global climate system by connecting the major oceans and redistributing oceanic properties, such as heat, salt and nutrients. This flow is also associated with a steep rise of isopycnals toward the south through the entire water column. This poleward rise of isotherms and isohalines is not uniform, but occurs in a series of clear step-like patterns. Between zones of relatively uniform water mass properties lie bands of large horizontal density gradients characterising the ACC fronts, which are associated with relatively narrow, deep-reaching current cores and large surface velocities in the order of 20 – 30 *cm/s* (Nowlin et al., 1977; Nowlin and Clifford, 1982; Nowlin and Klinck, 1986). Understanding the structure and location of the major fronts of the Southern Ocean is of considerable importance due to their influence on climate and ecosystem processes.

Using historical data, Orsi et al. (1995) and Belkin and Gordon (1996) were the first to map the circumpolar distribution of the Southern Ocean fronts. From north to south, the fronts and zones of the Southern Ocean are: the Subtropical Front (STF), Subantarctic Zone (SAZ), Subantarctic Front (SAF), Polar Frontal Zone (PFZ), Polar Front (PF), Antarctic Zone (AAZ), Southern ACC Front (SACCF), Southern Zone and the southern boundary of the ACC (SB) (Whitworth, 1980; Orsi et al., 1995). A variety of definitions based on water mass properties have been used to identify these fronts. (see Orsi et al., 1995; Belkin and Gordon, 1996, for useful summaries of these definitions). However, the frontal properties are not uniform in all sectors of the Southern Ocean. The variations in frontal structure from region to region and the multiplicity of definitions used by various authors have led to some confusion in identifying particular fronts. In addition, many areas have remained relatively poorly

sampled and in very few locations have sufficient repeat measurements been made to permit the variability of the fronts to be assessed. These earlier studies were based on ship-based measurements with their high accuracy and depth-resolving capability, but this data are scarce in the Southern Ocean and are focused on the summer season due to inherent logistic difficulties.

Others studies (e.g. Gille, 1994; Moore et al., 1999; Kostianoy et al., 2003) have examined the time-varying frontal locations on a circumpolar scale using satellite measurements. Indeed, the spatial and temporal resolution of the altimetric sea surface height (SSH) measurements used by e.g. Gille (1994) were comparatively coarse, i.e. larger than mesoscale ( $> 100$  km and  $> 100$  days). Moore et al. (1999) determined the surface PF location from weekly composites of the daily images of sea surface temperature (SST) measured from satellite-borne infrared sensors hampered by cloud cover. Dong et al. (2006) use the recently launched Advanced Microwave Scanning Radiometer for the Earth Observing System (AMSR-E), which provides global all-weather SST measurements, though with lower spatial resolution than more traditional infrared SST.

The studies based on remote sensing were limited to analyses of fronts with a surface expression in SST and only a few studies were able to collect in situ data with a sufficient temporal resolution to investigate the frontal variability using the subsurface expressions (Sokolov and Rintoul, 2002; Thorpe et al., 2002; Meredith et al., 2003b; Sokolov et al., 2006). None of these studies describe the three major fronts of the ACC (SAF, PF and SACCF) simultaneously with at least mesoscale coverage. Here I use a comprehensive in situ dataset collected during 2004 and 2005 to determine the location, structure and variability of the three major fronts in the South Atlantic sector of the Southern Ocean (Fig. 3.1). I focus on data obtained by free-drifting profiling floats seeded by the Argo project (Gould et al., 2004) and

complement this data with hydrographic profiles recorded by animal-borne sensors.

Argo is a global array of autonomous profiling floats that provides vertical profiles of salinity and temperature of the upper 2000 m of the open ocean at 10-day intervals. This array samples the seasons evenly, so the measurements are not biased toward the summer period favorable for ship-based work (Gould et al., 2004). Although the profiling float has enormous potential for broad-scale ocean observations, it does not provide a complete observational strategy. The coverage of floats in the Southern Ocean is more sparse than elsewhere, especially in seasonally ice-covered regions.

Marine mammals, however, can help to overcome these limitations and provide a complimentary high resolution data source. They can operate deep in ice-covered regions (Lydersen et al., 2004) and animal-borne sensors can accurately record hydrographic data at high frequency and in near real-time from remote, relatively inaccessible parts of the ocean (Lydersen et al., 2004; Charrassin et al., 2004; Bailleul et al., 2007). Autonomous CTD-Satellite Relay Data Loggers (CTD-SRDLs) can be attached to marine animals and report vertical profiles of salinity, temperature and pressure to a depth of up to 2000 m. Enlisting marine animals as sampling platforms is not a new idea. The earliest published reference to this approach is from 1970 (Evans, 1970). Nowadays these instruments have the potential to collect information about the oceans that is not only relevant to the study of physical structure of the oceans but also for studying the ecology of animals carrying the instruments (Lydersen et al., 2002; Hooker and Boyd, 2003; Lydersen et al., 2004; Charrassin et al., 2004, Ch. 5). While CTD-SRDL measurements are neither regular in terms of spatial and temporal coverage (compared, for example, with satellite measurements of oceanographic fields) nor completely random (such as those from drifting buoys), these studies provide valuable in situ information about the subsurface structure of the ocean. Accurate satellite positioning of diving marine animals, high-accuracy sensors, and

the potential to collect large numbers of profiles cost-effectively make these studies particularly important in regions where traditional oceanographic measurements are scarce. CTD-SRDLs can be programmed to sample and transmit hydrographic profiles on a daily basis and is therefore intrinsically an eddy-resolving device, rather than a broad-scale one. The natural niche for CTD-SRDLs in the observing system is in providing complementary measurements of boundary currents and fronts, as well as coverage of undersampled ocean basins (Chs. 1, 2 and 4). They thus provide a powerful complement to floats rather than a replacement for them. Only by combining these two datasets, I am able to investigate the variability of the frontal system from Drake Passage to the Mid-Atlantic Ridge on short temporal scales ( $< 100$  days).

In this chapter, I describe the characteristics of the dataset and methods I used to identify the SAF, PF and SACCF, including the optimal interpolation method used to calculate gridded fields of temperature on selected depth levels. Then I present the data as gridded horizontal fields to determine the mean position and variability of the fronts. Finally, I discuss the findings in the broader Southern Ocean context.

## **3.3 Data and Methods**

### **3.3.1 Hydrographic in situ Data**

Between 2004 and 2005, more than 120 profiling floats populated the southern South Atlantic Ocean as part of the Argo project. One disadvantage of sampling by autonomous floats is that most of the measurements are without accompanying ship-board data for absolute calibration. This deficiency is especially problematic for salinity, as conductivity cells are prone to changes that can cause sensor drifts in float salinity measurements. Several methods of calibration are available to adjust sensor drift by comparison with ship-board CTD data or statistical estimates of background

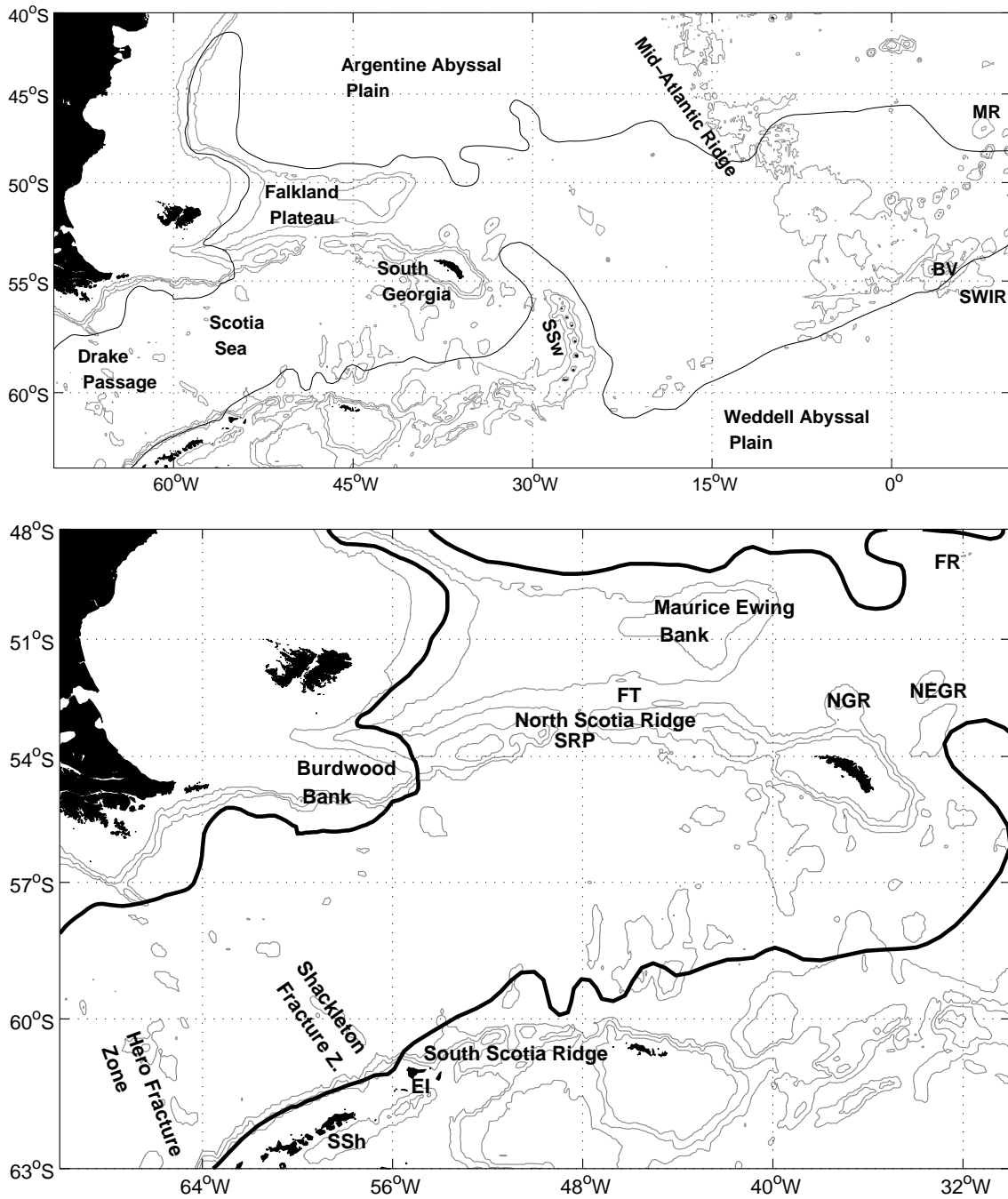


**Figure 3.1:** Schematic of the southern South Atlantic (top) and the Scotia Sea (b). Some important topographic features are marked: Meteor Rise (MR), Bouvetøya (BV), South West Indian Ridge (SWIR), South Sandwich Islands (SSw), Falkland Ridge (FR), Falkland Trough (FT), Northwest Georgia Rise (NGR), Northeast Georgia Rise (NEGR), Shag Rocks Passage (SRP), Elephant Island (EI) and South Shetland Islands (SSh). The 1000 m, 2000 m and 3000 m isobaths are marked. The two solid lines show the extent of the ACC. The northern line corresponds to the Subantarctic Front and the southern line to the Southern Boundary from Orsi et al. (1995).

temperature and salinity relations (Wong et al., 2003; Boehme and Send, 2005). For this work, I only used profiles that passed the Argo real-time quality control, containing information on their position, date, temperature ( $T$ ) and salinity ( $S$ ) profiles, with their first measurement point shallower than 20 m (Fig. 3.2). I used either the delayed-mode data or, if not available, I used the method of Boehme and Send (2005) to check the float salinity for any drift.

The CTD-SRDL data come from the SEaOS project<sup>1</sup> (Southern Elephant Seals as Oceanographic Samplers), an international interdisciplinary program aimed at increasing our understanding of how Southern elephant seals interact with their physical environment and also at demonstrating and implementing this cost-effective means of gathering routine observations of hydrographic data from remote environments. All CTD-SRDLs were checked in a calibration facility before deployment and these comparisons yield errors of less than 5 mK in temperature and less than 0.007 mS/cm in conductivity leading to salinity values with an error up to about 0.010 in the worst case scenario. Again a method similar to Boehme and Send (2005) has been created and implemented to compare the CTD-SRDL measurements with historical CTD data and calibrated Argo float data to correct any sensor drift in temperature and salinity (Ch. 2). This lack of absolute post-deployment calibration adds an uncertainty to the dataset. Nevertheless, I expect the CTD-SRDL data to be better than 0.02 in temperature and salinity (Ch. 2).

During the SEaOS program we used CTD-SRDLs, custom-built by the Sea Mammal Research Unit, St Andrews, UK and Valeport Ltd., Devon, UK. We deployed 8 CTD-SRDLs in 2004 and 13 instruments in 2005 at Husvik, South Georgia (54° 11' S, 36° 42.5' W). The CTD-SRDLs were fixed harmlessly to seals' fur after the elephant

---

<sup>1</sup><http://biology.st-andrews.ac.uk/seaos/index.html>

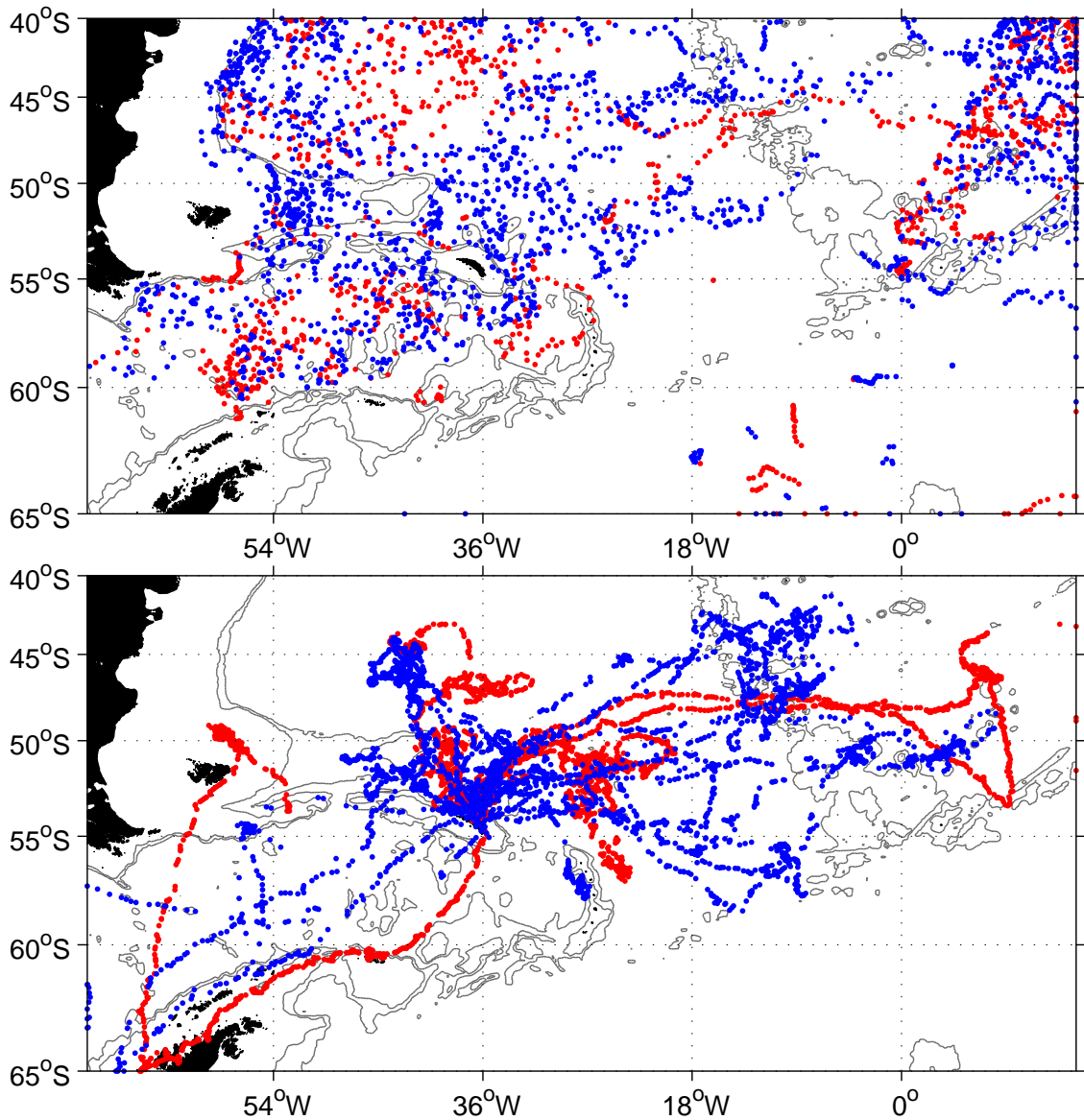


**Figure 3.2:** Spatial distribution of Argo float data (top) and CTD-SRDL data (bottom) in the years 2004 (red) and 2005 (blue).

seals completed their annual moult in January/February. A CTD-SRDL configuration was chosen to ensure batteries last throughout as much of the winter migration as possible, ideally until seals return to breed in September. During the animals' migration the CTD-SRDLs recorded and transmitted hydrographic profiles at a rate of approximately 2 profiles/day to an average depth of about 560 m, representing a combination of transect-type sections with a spatial resolution of 25-50 km along

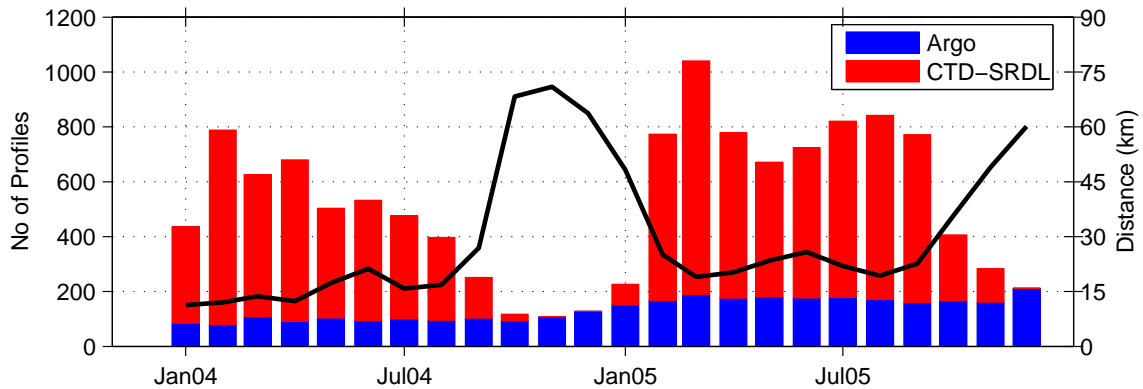


**Figure 3.3:** Monthly number of hydrographic profiles (bars) and mean distance to the neighbouring profile (line) from the combined Argo/SRDL dataset.

the migratory routes and mooring like data in the foraging areas of the seals. The CTD-SRDLs were finally lost when the animals moulted again. In 2004 and 2005, we obtained more than 8200 hydrographic profiles to depths up to 2000 m, from the Drake Passage to east of the Mid-Atlantic Ridge (Fig. 3.2).

Figure 3.2 shows the complementarity of the two datasets (Argo and CTD-SRDLs), especially in the area between South Georgia and the Mid-Atlantic Ridge. These two data sources produce a dataset with a temporal and spacial resolution, which were previously unavailable. This dataset includes up to 1000 hydrographic profiles per month (Fig. 3.3), of which CTD-SRDLs contribute up to 90%. Figure 3.3 shows a reduction when the CTD-SRDLs stopped working between September and December each year. The spatial resolution of each subset also changed from less than 20 km to more than 60 km when less profiles were present. With reference to Fig. 3.3, it can be seen that the Argo float data provide the background field, and the CTD-SRDL data are used to increase the temporal and spatial resolution of the dataset yet the only source of data between the South Sandwich Islands and the Mid-Atlantic Ridge (Fig. 3.1).

### Optimal Interpolation of Gridded Fields

This combined dataset was used to generate gridded horizontal potential temperature ( $\Theta$ ) fields. To calculate the best estimate of temperature at each grid point, an optimal interpolation scheme similar to the one introduced by Boehme and Send (2005) is used. At each grid point the objective estimate of temperature  $T^{obj}$  is then given by:

$$T^{obj} = \langle \mathbf{d} \rangle + \omega \cdot (\mathbf{d} - \langle \mathbf{d} \rangle), \quad (3.1)$$

where  $\mathbf{d} = [d_1, \dots, d_n]$  denotes the set of temperature values,  $\langle \mathbf{d} \rangle$  denotes the mean value of the set of  $\mathbf{d}$  and  $\omega$  is the weighting matrix. I assume the covariance of the data  $\mathbf{d}$  to be exponential. However, the flow of the ACC follows the topography and a Gaussian function is not satisfactory. To take the complex topography into account each in situ profile is weighted by three distances: the spatial distance  $\mathbf{D}$ , the fractional distance in potential planetary vorticity  $\mathbf{F}$  and the temporal distance  $\Delta t$  to the grid point (Davis, 1998);

$$\begin{aligned} D &= |\mathbf{0} - \mathbf{I}| \\ F &= \frac{|PV(\mathbf{0}) - PV(\mathbf{I})|}{\sqrt{PV^2(\mathbf{0}) + PV^2(\mathbf{I})}} \\ \Delta t &= |t_0 - t_I|. \end{aligned} \quad (3.2)$$

In eq. 3.2 the position  $(x_i, y_i)$  of the in situ data point is given in  $\mathbf{I}$  and the date in  $t_I$ , while the grid point position is  $\mathbf{0}$  and the date  $t_0$ .  $\mathbf{D}$  is the spatial distance between the two points.  $\mathbf{F}$  takes account of the differences in barotropic potential vorticity  $PV$ :

$$PV = \frac{f}{H}, \quad (3.3)$$

with the planetary vorticity  $f$  and the water depth  $H$  (taken from the 5-minute gridded global relief data TerrainBase<sup>2</sup>). The PV criterion might be misleading in some cases, as two points with similar potential vorticity but lying in different basins separated by a ridge could have very different properties. This problem also exists when using a simple Gaussian mapping scheme. The modification by introducing the potential planetary vorticity into the mapping scheme gives superior results as outlined in Boehme and Send (2005).

The covariance is a function of the temporal and spatial separation, and the exponential decay scale is determined by the spatial scale  $\lambda$  [km], the cross-isobathic scale  $\Phi$  [dimensionless], as well as the temporal scale  $\tau$  [days] (Wong et al., 2003; Boehme and Send, 2005). The covariance matrix for the temperature–grid data ( $\mathbf{C}dg$ ) and the temperature–temperature covariance matrix ( $\mathbf{C}dd$ ) then take the form:

$$\begin{aligned} \mathbf{C}dd_{ij}(x, y, t) &= \langle \mathbf{s}^2 \rangle \cdot \exp \left\{ - \left[ \frac{D_{ij}}{\lambda} + \frac{F_{ij}}{\Phi} + \frac{\Delta t^2}{\tau^2} \right] \right\}, \\ \mathbf{C}dg_i(x, y, t) &= \langle \mathbf{s}^2 \rangle \cdot \exp \left\{ - \left[ \frac{D_{i0}}{\lambda} + \frac{F_{i0}}{\Phi} + \frac{\Delta t^2}{\tau^2} \right] \right\}. \end{aligned} \quad (3.4)$$

$\langle \mathbf{s}^2 \rangle$  is the signal variance of the temperature data. The inverse solution then is (McIntosh, 1990)

$$\omega = \mathbf{C}dg \cdot [\mathbf{C}dd + \mathbf{I} \cdot \langle \eta^2 \rangle]^{-1}, \quad (3.5)$$

where  $\mathbf{I}$  denotes the identity matrix.

The scale parameters used for objective mapping are as important as the method itself, as they will represent the hydrographic structure of the ocean, hence it is necessary to calculate these scale parameters from the correlation function of in situ measurements.

---

<sup>2</sup><http://www.ngdc.noaa.gov>

According to the objective mapping method used a time-independent spatial scale, a cross-isobath scale and a temporal scale are required. Following Boehme and Send (2005), the normalized autocorrelation function  $R(D, F)$  is calculated and then fitted by an exponential distribution, which yields the scaling parameters  $\lambda$  and  $\Phi$ . All available hydrographic data were used to calculate these scales on a gridded horizontal field (Fig. 3.4). The longest spatial scales are found close to the shelf together with the smallest cross-isobath scales, indicating a flow along the isobaths. Away from the shelf in the Scotia Sea the spatial scales are much smaller ( $< 150$  km) and the cross-isobath scales bigger than 0.5. These small spatial scales are the result of the big horizontal gradients by the ACC fronts, which cannot be resolved by a cross-isobath scale. Instead of using a separate scale for each grid point based on figure 3.4, I used one spatial and one cross-isobath scale for the whole domain in the South Atlantic. I was limited by the horizontal resolution of the hydrographic data and needed to resolve the flow along the shelf, so that I set the scales to  $\lambda=200$  km and  $\Phi=0.3$ .

Due to a lack of reliable in situ information with which to calculate the temporal scale, I instead used daily SST data. Using these data, processes with time scales from one day to two years are resolved. At each location the square difference  $\epsilon_i^2(SST) = (SST_0 - SST_i)^2$  between two temperature measurements (at the locations 0 and  $i$ ) and the corresponding time difference  $T_i = |t_0 - t_i|$  are calculated (Boehme and Send, 2005). For each time difference a lot of temperature differences are observed and a mean is taken to compute the normalized autocorrelation function  $R(T)$  of the mean square difference  $\overline{\epsilon^2}(T)$ :

$$R(T) = \frac{1}{\overline{\epsilon^2}} \sum \overline{\epsilon^2}(t) \overline{\epsilon^2}(t - T).$$

$R(T)$  seems to follow a Gaussian distribution (Fig. 3.5). However, there is an increased correlation around 180 days, which is due to the similar temperatures around

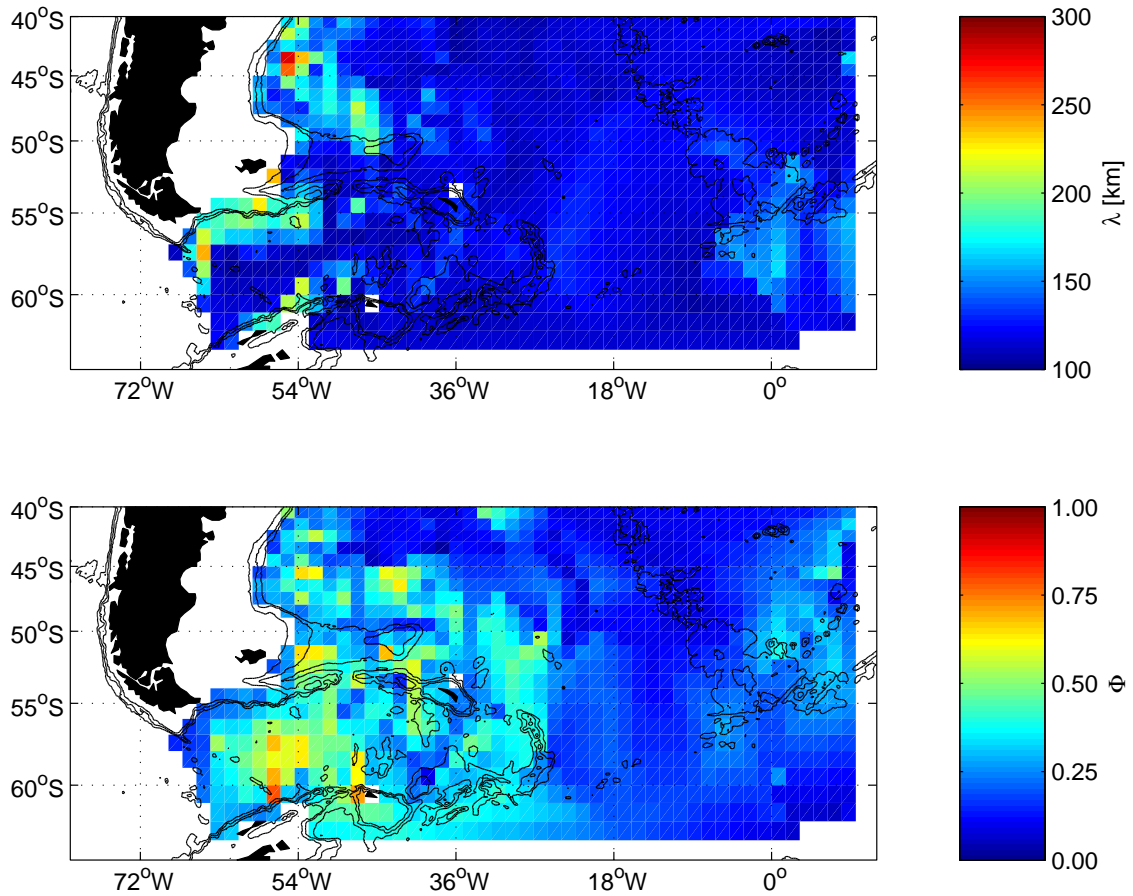


**Figure 3.4:** Spatial and cross-isobath scales of the Southern Ocean in the South Atlantic. The upper panel shows the spatial scale  $\lambda$  (km) and the lower panel shows the cross-isobath scale  $\Phi$  (no units).

spring and autumn about 180 days apart. Nevertheless, I assume a Gaussian distribution with

$$W(T) = e^{-\frac{T^2}{\tau^2}} \quad (3.6)$$

The unknown coefficient  $\tau$  can be computed by doing a least squares fit, which minimizes the sum of the squares of the deviations of the data R from the model W. This

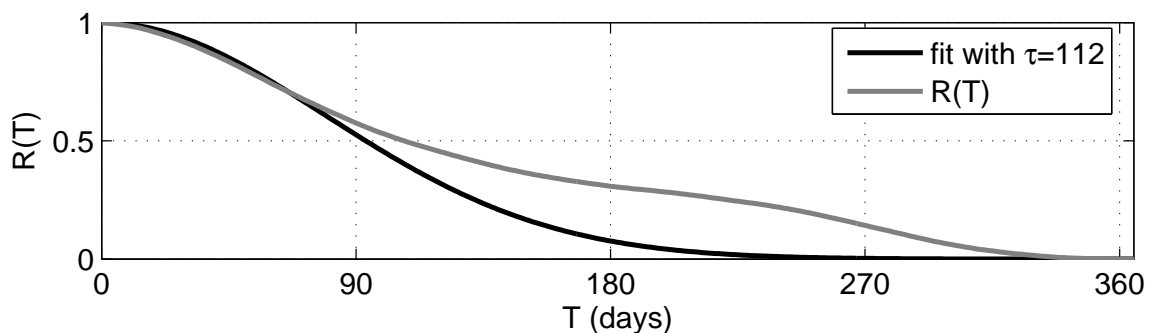


**Figure 3.5:** Time scale of the Southern Ocean in the South Atlantic. The difference of two SST measurements for different times but at the same location were used to compute the normalized autocorrelation function  $R(T)$  (grey). A least squares fit is used to get a Gaussian function (black) with a resulting time scale of  $\tau = 112$  days.

problem can be set up in a linear system:

$$\mathbf{G} = \mathbf{X}\mathbf{m}$$

with  $G = [\log(R_1), \dots, \log(R_n)]$ ,  $X = [T_1^2, \dots, T_n^2]$  and  $m = -\frac{1}{\tau^2}$ . If no offset is allowed, the solution of  $\mathbf{m} = \mathbf{X}^{-1}\mathbf{G}$  is  $\tau = 112$  days (Boehme and Send, 2005).

This interpolation scheme and the calculated scales are used to calculate the potential temperature field on different depth levels. All these calculations are done on a  $0.4^\circ \times 0.25^\circ$  grid ( $\sim 25$  km) from  $80^\circ$  W to  $15^\circ$  E and  $63^\circ$  S to  $40^\circ$  S. The first run used all available Argo and CTD-SRDL data from 2004 and 2005 with no time scale to calculate the average temperature field of this time period. I mapped temperature fields at 200, 300 and 500 dbar and the temperature of the temperature minimum layer. To avoid eddy-like features I only used the most unbroken isotherms from west to east.

To resolve the high temporal variability of the fronts, I used the same scheme to calculate the frontal positions on a monthly basis. Using the detected temporal scale  $\tau$ , I mapped the temperature fields to the middle of each month in 2004 and 2005

and extracted the dedicated isotherms. This gives us 24 monthly positions for each front from January 2004 to December 2005.

### 3.3.2 Sea surface temperature

I also used an optimally interpolated daily, quarter degree ( $\pm 25\text{km}$ ) SST product (available at <http://www.ssmi.com>). This product is computed by a combination of two satellites, the TRMM Microwave Imager (TMI) and NASDA's (National Space Development Agency of Japan) Advanced Microwave Scanning Radiometer for EOS (AMSR-E)<sup>3</sup>. TMI and AMSR-E observations are used to retrieve SST and this combination provides nearly complete global coverage each day. Two years (January 2004 to December 2005) of daily SST observations are used in this study. Following Moore et al. (1999) and Dong et al. (2006), I calculated the standard deviation of SST and derived the mean SST gradient  $\delta SST = \sqrt{(\delta T/\delta x)^2 + (\delta T/\delta y)^2}$  at the frontal positions from the daily SST data, including its standard deviation.

### 3.3.3 Sea level anomaly

Sea level anomaly is the difference between the total sea level and the average sea level. Anomalies are used because the total level made by the Satellite based altimeter varies from  $\pm 100$  metres. Although most of this is constant and is due to the Earth's gravity and the ocean circulation, sea level variations caused by e.g. El Nino account for only 1% of the signals and if the constant part were not removed, the signals would not be observable.

Satellite altimeter sea level anomaly (SLA) data used in this chapter were obtained from AVISO on a  $1/3^\circ$  Mercator grid at 7 day intervals (Ducet et al., 2000). These are multimission gridded sea surface heights computed with respect to a seven-year

---

<sup>3</sup>[http://aqua.nasa.gov/about/instrument\\_amsr.php](http://aqua.nasa.gov/about/instrument_amsr.php)

mean and consist of processed data from different altimeter missions (Jason-1, T/P, ENVISAT, GFO, ERS1/2 and GEOSAT). Combining data from different missions significantly improves the estimation of mesoscale signals (Le Traon and Dibarboure, 1999; Le Traon et al., 2001). I used data from August 2001 to June 2006 in this study to calculate the SLA variance.

## 3.4 Results

### 3.4.1 Definition and Determination of Fronts

Fronts are identified by apparent horizontal gradients at various depth levels. However, the particular frontal properties can change both in time and space due to air-sea interaction and cross-frontal mixing (Belkin and Gordon, 1996). To minimise these effects, one needs a database of sufficient spatial resolution. Belkin and Gordon (1996) suggest that a distance of less than 200 km between measurements should be used, which I easily achieve with my combined dataset (Fig. 3.3). In the present paper, I used the dataset of temperature and salinity profiles provided by CTD-SRDLs combined with the Argo data to describe the properties and positions of three major fronts of the ACC. Here, I show CTD-SRDL data to determine the frontal properties.

Figure 3.6 presents a section across the Drake Passage measured between 7 June 2004 and 24 June 2004 by a CTD-SRDL that recorded only temperature and pressure. This is the location most routinely sampled by ships in the Southern Ocean, and hence the one at which the frontal structures are best known. Note, however, that most historical sections have been performed during the months of the austral summer, when ship-based operations are easiest. As typically seen in meridional sections across the ACC, the temperature decreases to the south in a series of steps or fronts, separated by zones of weaker meridional gradient. Although this winter section shows

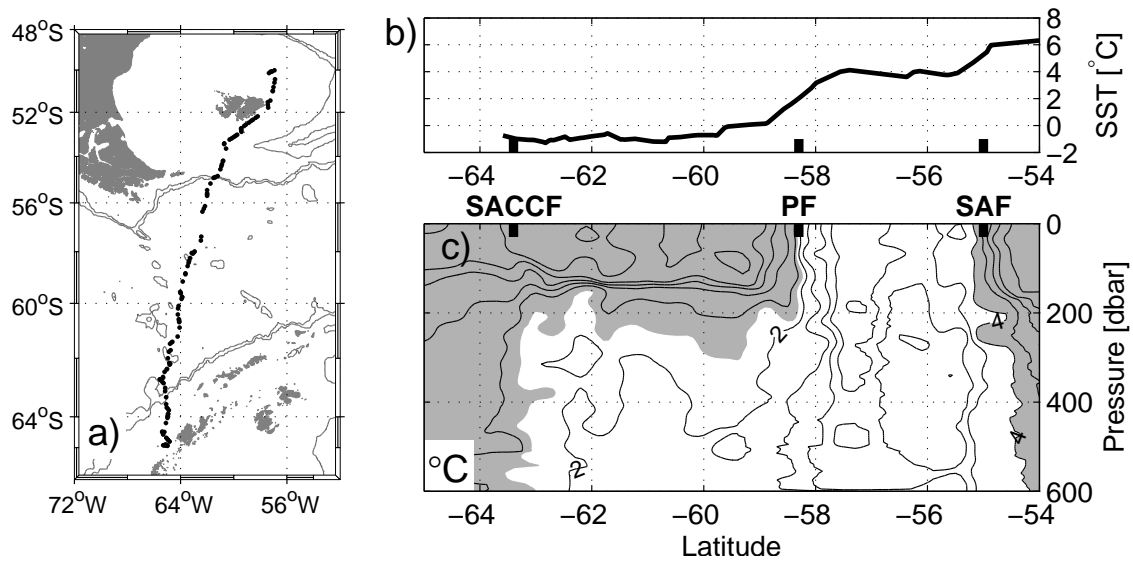


**Figure 3.6:** *a)* Station locations from a CTD-SRDL between 7 June 2004 and 24 June 2004. 2000 m and 3000 m isobaths are plotted and land is shaded. *b)* High resolution satellite SST interpolated onto profile location and time. *c)* In situ temperature along the animal's migration. Contour intervals are every 0.5° C and areas below 1.8° C and above 4° C are shaded. Front locations are marked on the upper axis. **SACCF**: Southern ACC Front; **PF**: Polar Front and **SAF**: Subantarctic Front.

clear vertical temperature gradients, which are associated with the SAF at about 55° S very close to the Burdwood Bank, the PF at about 58° S and the SACCF close to the continental shelf at about 63.6° S, it also reveals some differences to previous work. In figure 3.6, the SAF is associated with the vertical 4° C isotherm, while the PF is associated with the vertical 2° C isotherm above 200 dbar. The mixed layer south of the PF does not show any evidence of the SACCF, while below the thermocline the SACCF is shown by the vertical 1.8° C isotherm below 200 dbar (Fig. 3.6c). The satellite SST data in Fig. 3.6b also show no evidence of the SACCF, while the other two fronts are clearly seen in the meridional temperature gradients from 0° C to 4° C (PF) and 4° C to 6° C (SAF).

Between 14 January 2005 and 26 February 2005 a CTD-SRDL recorded a hydrographic section further to the east and north from South Georgia (54° S, 36° W) to the Mid-Atlantic Ridge at 43° S, 17° W (Fig. 3.7a). This section did not cross the

ACC perpendicularly, but Fig. 3.7e shows the strong horizontal density gradients associated with the SAF and PF at 47° S and 49.5° S respectively. There was also an eddy just north of the PF and a loop of the SACCF at the southern end of the section (Fig. 3.7). The tongue of the SACCF is marked by  $\Theta$  minimum at around 150 m and the doming of the isopycnals between 54° S and 52° S in Fig. 3.7e. The PF is again associated with the vertical 2° C isotherm in the  $\Theta_{min}$  layer (Fig. 3.7c). The surface expression of the PF is very weak with only a slight satellite SST gradient of about 1° C (Fig. 3.7b). The SAF however has a clear increase of satellite SST from 7° C to 10° C. In Fig. 3.7c, the subsurface expression of the SAF correlates with the descent of the 4° C isotherm from 100 dbar to 350 dbar to the north.

At the beginning of winter 2004, a CTD-SRDL sampled a meridional section northeast of Bouvetøya from 54° S, 9° E to 45° S, 5° E (Fig. 3.8a). While there was no obvious satellite SST gradient marking the frontal positions (Fig. 3.8b), the subsurface hydrography in Fig. 3.8 reveals two of the three major ACC fronts. In this figure, the SACCF is marked by vertical 1.6° C to 2° C isotherms from the surface to below 600 dbar. The PF coincides with the northward limit of the 2° C isotherm in the  $\Theta_{min}$  layer (Fig. 3.8c). Both fronts show also a large horizontal density gradient (Fig. 3.8e).

The  $\Theta$ - $S$  properties within fronts can change alongstream. This can be seen in the different salinities between the section from South Georgia to the Mid-Atlantic Ridge (Fig. 3.7d) and the section further to the east (Fig. 3.8d) with its higher salinity. However, the temperature ranges belonging to certain fronts were very stable in my area of interest, so I choose to define the frontal positions based on temperature criteria at given depth levels (Tab. 3.1). I found the SAF's axial indices to be very stable in my area of interest with a vertical 4° C isotherm from 150 m to 350 m. This is slightly different from previous work (Peterson and Whitworth III, 1989; Orsi et al.,

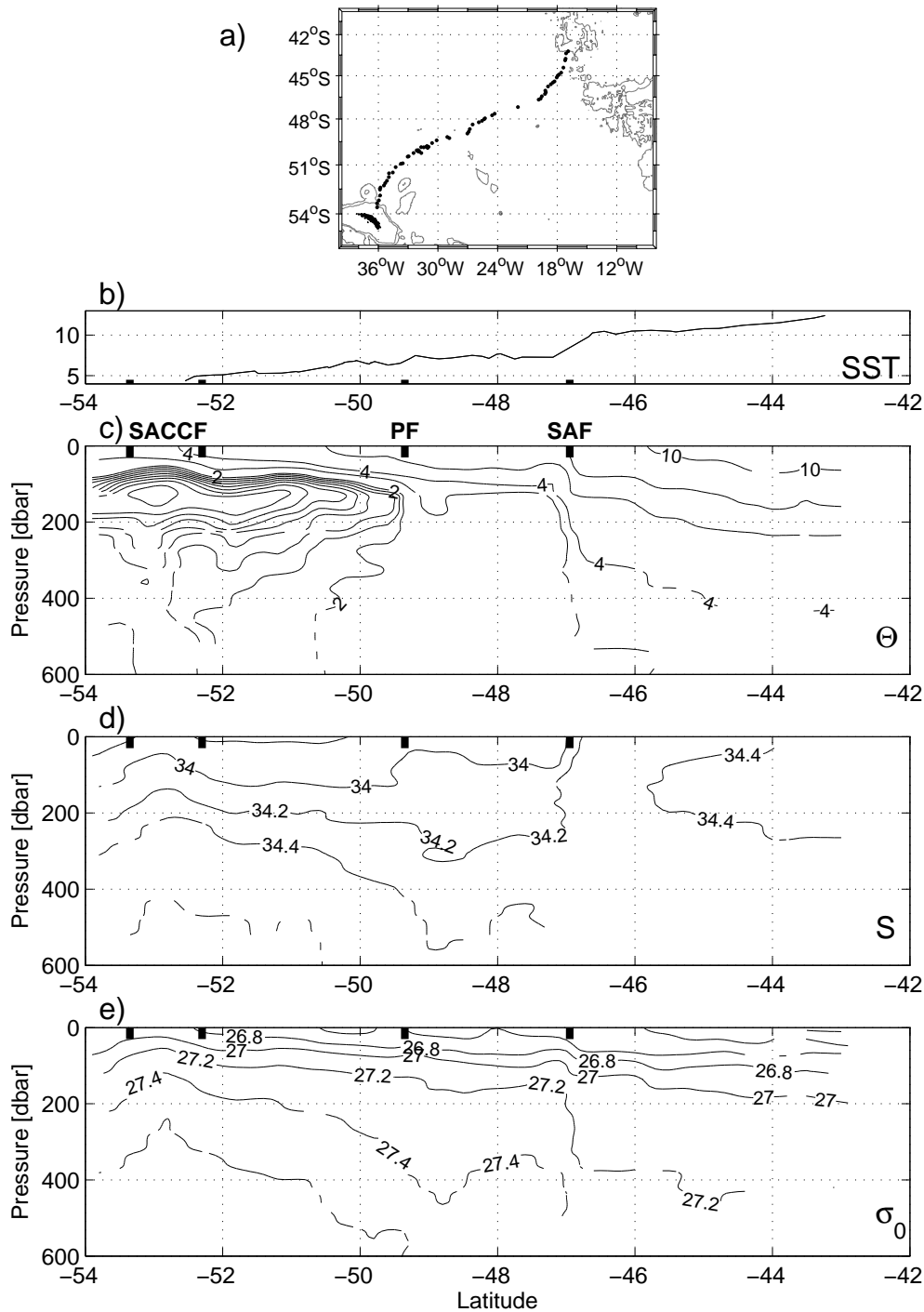


**Figure 3.7:** *a)* Station locations from a CTD-SRDL between 14 January 2005 and 26 February 2005. Isobaths are 2000 m and 3000 m and land is shaded black. *b)* High resolution satellite SST interpolated onto profile location and time. *c)* Potential temperature along the animal's migration. Contour intervals are every 0.2° C to 2° C then 3° C, 4° C and then every 2° C. Front locations are marked on the upper axis. **PF**: Polar Front and **SAF**: Subantarctic Front. *d)* Salinity along the animal's migration. Contour intervals are every 0.2. *e)* Potential density relative to surface pressure. Contour intervals are every 0.2 kg/m<sup>3</sup>.

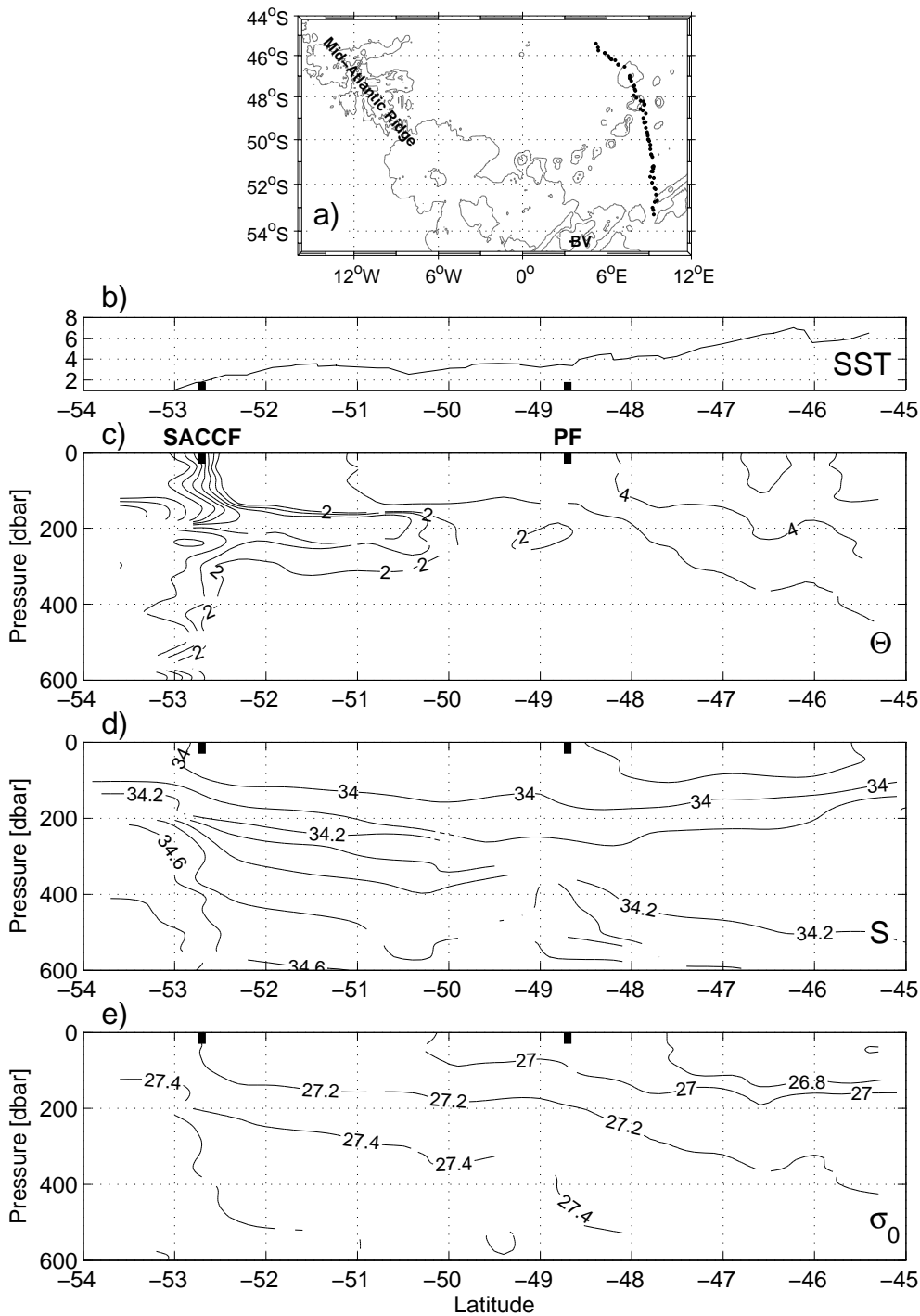


**Figure 3.8:** *a)* Station locations from a CTD-SRDL between 13 April 2004 and 4 May 2004. Isobaths are 2000 m and 3000 m. Bouvetøya is highlighted (BV). *b)* High resolution satellite SST interpolated onto profile location and time. *c)* Potential temperature along the animal's migration. Contour intervals are every 0.2°C to 2°C, then 3°C, 4°C and every 2°C. Front locations are marked on the upper axis. **SACCF**: Southern ACC Front and **PF**: Polar Front *d)* Salinity along the animal's migration. Contour intervals are every 0.1. *e)* Potential density relative to surface pressure. Contour intervals are every 0.2 kg/m<sup>3</sup>.

1993, 1995), but proved to be the best indicator in my area and time period. The criterion for identification of the PF is similar to that used in previous work (Botnikov, 1963; Belkin and Gordon, 1996). The vertical  $2^{\circ}\text{C}$  isotherm in the  $\Theta_{min}$  layer is an indicator of the PF almost everywhere in the Southern Ocean and is in agreement with the definition of the PF as the location of rapid descent of the  $\Theta_{min}$  by Gordon (1971). Detailed descriptions of the hydrographic sub-surface properties are scarcer for the SACCF than for the SAF or PF. The SACCF, as with the other ACC fronts, is identified by large horizontal density gradients through the water column (Fig. 3.8e). The northern limit of the front can be identified from horizontal changes in the properties of Upper Circumpolar Deep Water (UCDW), a type of the Circumpolar Deep Water that occupies most of the deep layers of the ACC. From analysis of historical hydrographic sections, Orsi et al. (1995) locate stations north of the SACCF by a potential temperature greater than  $1.8^{\circ}\text{C}$  along the temperature maximum of the UCDW at depths greater than 500 m. It is apparent that this large-scale criterion presented does not provide a reliable indicator for the position of the SACCF in local areas (as shown previously by Thorpe et al. (2002) and Meredith et al. (2003b)) and it has been shown at other locations that the fronts change along-stream as they split and merge and are subject to seasonal cycles in heat and freshwater flux (e.g. Belkin and Gordon, 1996). Notwithstanding this, the  $\Theta = 1.8^{\circ}\text{C}$  isotherm at 500 m depth proved to be the best one to track the SACCF in my area of interest and time period.

To map the frontal positions, I used the gridded potential temperature fields and extracted the dedicated isotherm for each front as described above. For the position of the SAF I used the position of the  $\Theta = 4.0^{\circ}\text{C}$  isotherm at a pressure ( $p$ ) of 300 dbar. For the PF I extracted the  $\Theta = 2.0^{\circ}\text{C}$  isotherm in the  $\Theta_{min}$  layer and, if not present, the  $\Theta = 2.0^{\circ}\text{C}$  isotherm at  $p = 200$  dbar pressure. The SACCF was located by selecting the  $\Theta = 1.8^{\circ}\text{C}$  isotherm at  $p = 500$  dbar pressure (Tab. 3.1).

### 3.4.2 Frontal positions

#### Subantarctic Front

The mean position of the SAF derived from my merged dataset corresponds very well with the position of Orsi et al. (1995) in the western part of the study region, while the position in the eastern part lies further north than in previous work. The path of the SAF is constrained by the bathymetry (Fig. 3.9). In this figure, the SAF flows close to the shelf slope in the western part of Drake Passage until it reaches  $60^\circ$  W. Here, south of Burdwood Bank, the SAF moves away from the shelf slope before turning northward. The SAF crosses the North Scotia Ridge and the Falkland Trough before the SAF follows the 1500 m depth contour on the west side of the Argentine Abyssal Plain as the Malvinas Current. At  $40^\circ$  S the SAF retroflects upon encountering the Brazil Current. The SAF then flows southward at about  $55^\circ$  W until it is shifted eastward and flows north of the Falkland Plateau and the Falkland Ridge along  $48^\circ$  S. During this southward movement the SAF starts to meander. Further to the east the mean SAF position of Orsi et al. (1995) shows two big loops to the south and north, which are not represented by my mean position of the SAF. The SAF crosses the Mid-Atlantic Ridge at  $45^\circ$  S,  $15^\circ$  W.

The monthly SAF positions (Fig. 3.9b and c) reveal areas with high variability and

Front	Sub-surface criteria	satellite SST criteria
SAF	$\Theta = 4.0^\circ$ C at $p = 300$ dbar	SST gradient
PF	$\Theta = 2.0^\circ$ C in $\Theta_{min}$ layer (100-300 m) or $\Theta = 2.0^\circ$ C at $p = 200$ dbar	SST gradient can be weak
SACCF	$\Theta = 1.8^\circ$ C at $p = 500$ dbar	most times no SST gradient

**Table 3.1:** Summary of front indicators of the ACC in the South Atlantic used in this chapter. The last column indicates whether a SST gradient can be utilised to locate a front.

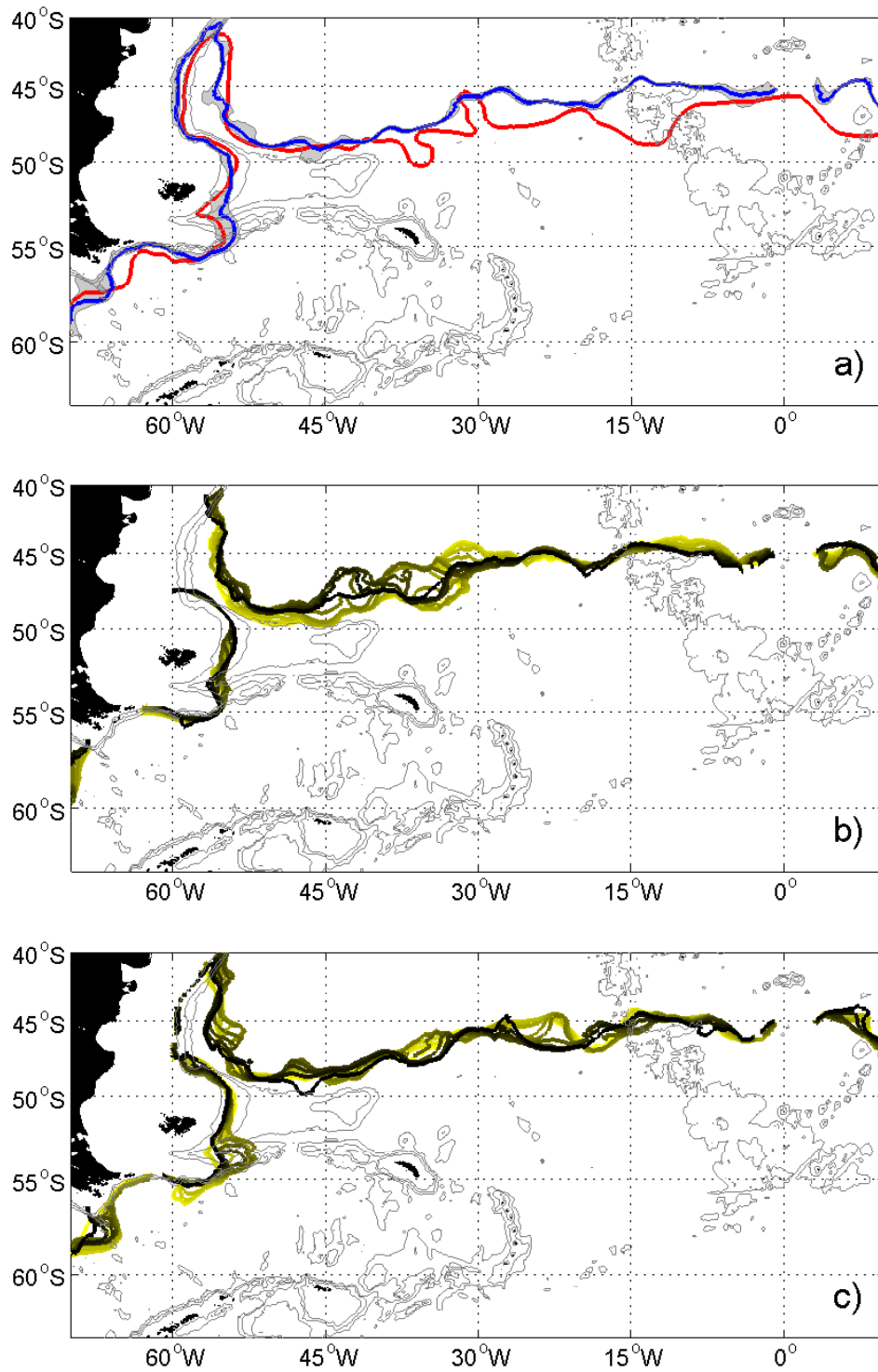


**Figure 3.9:** Position of the Subantarctic Front during 2004 and 2005. Isobaths are 1000 m, 2000 m, 3000 m and land is shaded black. *a)* Mean Position of the Subantarctic Front (blue) and mapping error (grey) of the interpolation scheme. Position of the front by Orsi et al. (1995) in red. *b)* Monthly position of the Subantarctic Front in 2004 (yellow to black). *c)* Monthly position of the Subantarctic Front in 2005 (yellow to black).

their differences between 2004 and 2005. The path from south of the Burdwood Bank crossing the Falkland Plateau and the position along the Brazil/Malvinas Confluence seems always to be an area of higher variability of the frontal position. The areas of higher variability between  $45^{\circ}$  W and  $15^{\circ}$  W shifted from the western part in 2004 to the eastern part in 2005. The path of the SAF across the Mid-Atlantic Ridge seems to be strongly constrained by the underlying topography as indicated by a very small variability in the frontal positions (Fig. 3.9b and c).

### **Polar Front**

The derived position of the PF lies north of the position of the PF of Moore et al. (1999) and corresponds well with the PF of Orsi et al. (1995) (Fig. 3.10a). As with the SAF, the path of the PF is also controlled by the topography. In Figure 3.10a the mean path of the PF starts west of Drake Passage south of  $60^{\circ}$  S, but north of the Hero Fracture Zone at  $66^{\circ}$  W. It then continues to the northeast until it reaches the North Scotia Ridge. Here it seems to be pushed eastward into a meander on the east end of the ridge until it finds a way through the Shag Rocks Passage to the north towards the Maurice Ewing Bank. Here, the position of the PF lies further to the east than indicated in Orsi et al. (1995). The PF then flows around the northwest side of the bank looping to the east and following the  $50^{\circ}$  S parallel. At  $50^{\circ}$  S,  $10^{\circ}$  W the PF is shifted to the north crossing the Mid-Atlantic Ridge. It then loops back to the southeast and follows again the  $50^{\circ}$  S parallel (Fig. 3.10a).

All the monthly positions of the PF follow this mean path (Fig. 3.10b and c), but show a much greater variability than the monthly SAF positions (Fig. 3.9b and c). In 2004, the PF showed a big northward loop at  $65^{\circ}$  W before continuing to the northeast with less variability. During 2004 the PF increased the loop to the southeastern end of the North Scotia Ridge before crossing the North Scotia Ridge through the Shag

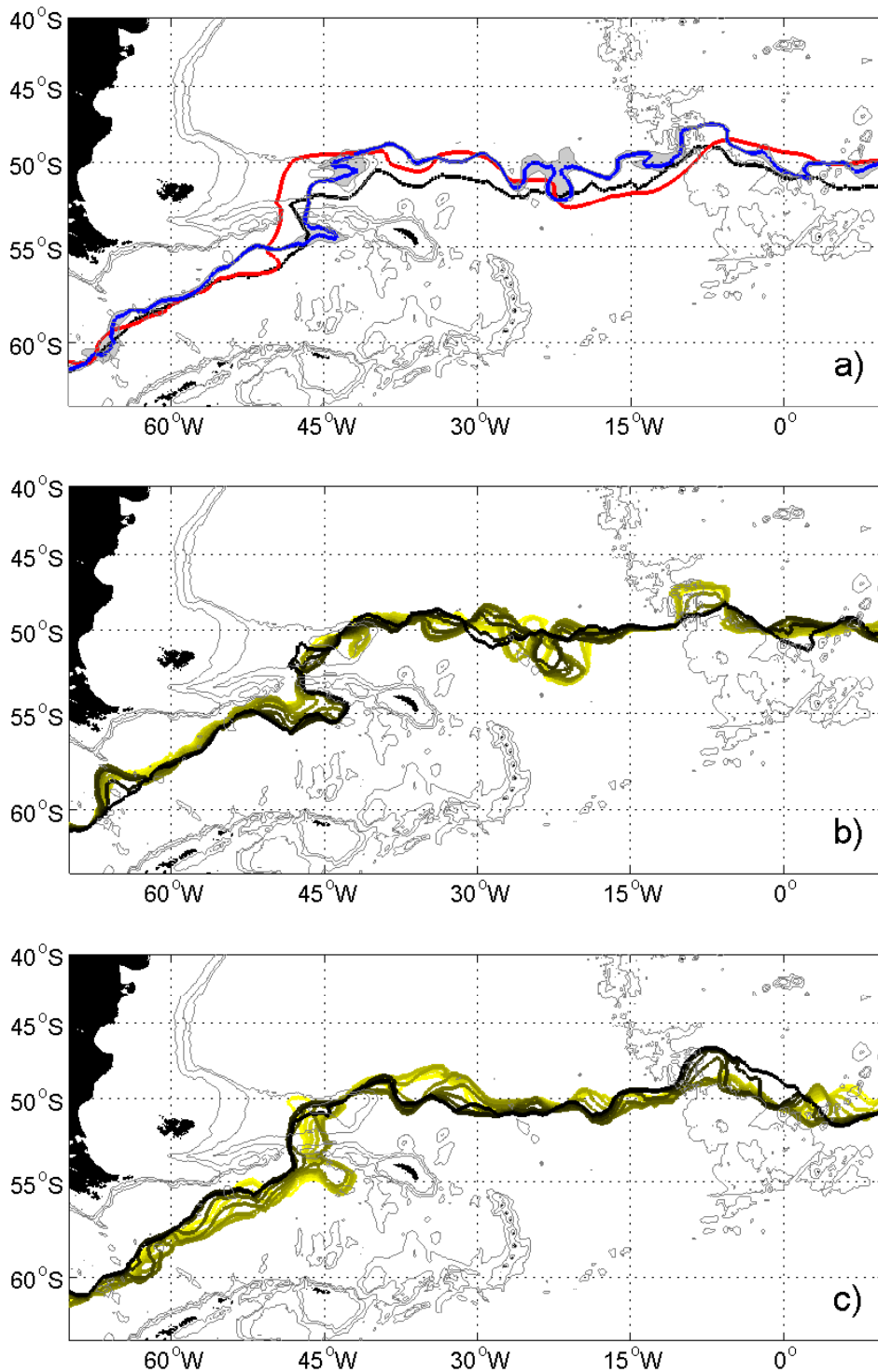


**Figure 3.10:** Position of the Polar Front during 2004 and 2005. Isobaths are 1000 m, 2000 m, 3000 m and land is shaded black. *a)* Mean Position of the Polar Front (blue) and mapping error (grey) of the interpolation scheme. Position of the front by Orsi et al. (1995) in red and Moore et al. (1999) in black. *b)* Monthly position of the Polar Front in 2004 (yellow to black). *c)* Monthly position of the Polar Front in 2005 (yellow to black).

Rocks Passage (Fig. 3.10b). After looping cyclonically around the Maurice Ewing Bank it then meandered to the east with strong variability of up to  $3^\circ$  in latitude between  $35^\circ$  W and  $18^\circ$  W. Constrained by the topography, it crossed the Mid-Atlantic Ridge at  $50^\circ$  S,  $10^\circ$  W before looping northward above the Mid-Atlantic Ridge.

In 2005, the PF did not show the northward movement at  $65^\circ$  W but stronger variability within Drake Passage (Fig. 3.10c). The loop to the west before crossing the North Scotia Ridge diminished in 2005. On its way north to the western side of the Maurice Ewing Bank the PF showed strong variability in 2005. It then turned east following the topography. Immediately east of the Maurice Ewing Bank the PF started to meander up to  $3^\circ$  in latitude between  $42^\circ$  W and  $30^\circ$  W. This was further to the west than in 2004 (Fig. 3.10b and c). It then crossed  $50^\circ$  S,  $10^\circ$  W with strong variability on the east side of the Mid-Atlantic Ridge before following the bathymetry to the southeast (Fig. 3.10c).

### **Southern ACC Front**

The average position of the SACCF is shown in Fig. 3.11a. It is in good agreement with the frontal position of Orsi et al. (1995) modified by Thorpe et al. (2002). The SACCF lies close to the shelf break of the Antarctic Peninsula (Fig. 3.11a). It loops to the northwest north of Elephant Island, very similar to the positions of Orsi et al. (1995). The SACCF then meanders to the northeast to the southwestern side of South Georgia. It wraps anticyclonically around South Georgia from the south and then retroflects north of the island across the Northeast Georgia Rise looping cyclonically to the southeast. At about  $57^\circ$  S,  $15^\circ$  W it lies further north than in previous work (Orsi et al., 1995). The crossing of the Mid-Atlantic Ridge is not resolved due to a lack of data (Fig. 3.11a).

The monthly positions reveal the high variability of the SACCF (Fig. 3.11b and

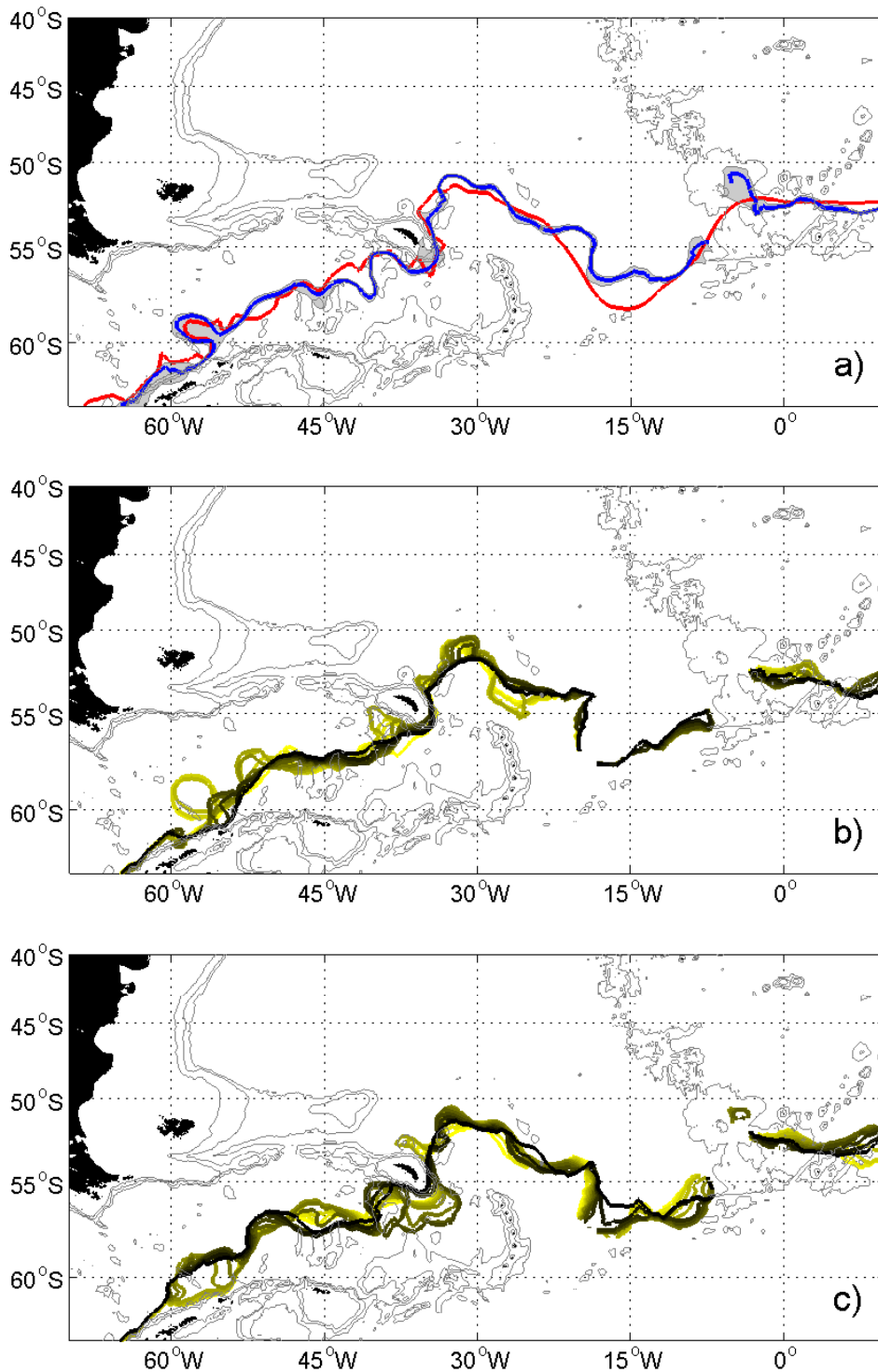


**Figure 3.11:** Position of the Southern ACC Front during 2004 and 2005. Isobaths are 1000 m, 2000 m, 3000 m and land is shaded black. *a)* Mean Position of the SACCF (blue) and mapping error (grey) of the interpolation scheme. Position of the front by Orsi et al. (1995) modified by Thorpe et al. (2002) in red. *b)* Monthly position of the SACCF in 2004 (yellow to black). *c)* Monthly position of the SACCF in 2005 (yellow to black).

c). At the beginning of 2004 the SACCF showed a big cyclonic loop just east of the Shackleton Fracture Zone, which disappeared during 2004 (Fig. 3.11b). It then meandered in a  $1^\circ$  wide band to the northeast. The area on the southwest side of South Georgia showed high variability in the frontal position, with a cyclonic loop building up and disappearing again during 2004. The front followed the continental shelf of South Georgia until the approximate region of the Northwest Georgia Rise, as per Meredith et al. (2003a). Although an area of high variability, the SACCF seemed to be constrained by the Northeast Georgia Rise until it reaches its northernmost point at  $31^\circ$  W. It then turned southeastward until it reached  $54^\circ$  S,  $20^\circ$  W where it turned sharply southward (Fig. 3.11b). At  $58^\circ$  S it turned eastward again, but the lack of data in 2004 hampered resolution of the frontal position properly in this area. I was able to map the SACCF again from  $52^\circ$  S,  $5^\circ$  W from where it followed the north side of the SW Indian Ridge (Fig. 3.11b).

In 2005 the SACCF showed even more monthly variability than in the previous year, with movements covering a range of  $3^\circ$  in latitude in the Scotia Sea (Fig. 3.11c). Especially south of South Georgia the SACCF meandered and looped over a great range until it followed the shelf break on the east side of South Georgia. It then extended its position to the north of the island across the Northwest Georgia Rise during 2005 (Fig. 3.11c). (This tongue was already seen in Fig. 3.7.) Again constrained by the Northeast Georgia Rise the SACCF reached the northernmost point further to the west than in the previous year at about  $34^\circ$  W. It then turned southeastward but lay further north than in 2004. Again at  $54^\circ$  S,  $20^\circ$  W it turned sharply southward showing high variability in crossing the ocean basin between the South Sandwich Islands and the Mid-Atlantic Ridge. The crossing of the Mid-Atlantic Ridge is not resolved in Fig. 3.11c due to a lack of data. In the figure the SACCF reappears again at  $52^\circ$  S,  $5^\circ$  W, possibly suggesting that the crossing is constrained by the bathymetry and follows the front of Orsi et al. (1995). North of Bouvetøya the SACCF lay on the

north side of the South West Indian Ridge (Fig. 3.11c).

### 3.4.3 SST and SLA

The satellite SST at the frontal positions is closely related to their meridional positions (Fig. 3.12). The southernmost position of the SAF is in Drake Passage, where the SST is at its minimum of about 5° C. The same is true for the PF with a SST of below 2° C at the western edge of Drake Passage (Fig. 3.12). Both fronts turn then sharply northward; this is reflected in the increasing SST. The standard deviation of the SST increases due to the more meridional orientation of the front. During the northward loop of the SAF the SST expression rises from 6° C to 9° C between 60° – 50° W. The SST of the PF increases between 50° – 40° W from about 4° C to 6° C. The SSTs of the SAF and PF decrease by about 2° C to the east, although the fronts stay at the same latitude (PF) or even lie further north (SAF). The same is true for the SACCF but less pronounced and the SACCF lies further south in the east. The maximum SST of the SACCF is 2.5° C at 30° W with a drop to 0.5° C at 10° W (Fig. 3.12). Figure 3.12 also shows the longitudinal distribution of the SST gradient. The SST gradient at the SACCF is around 1° C per 100 km, which is close to the 'normal' meridional increase in SST to the north. Over short time periods and small areas this gradient can be above this background noise, suggesting that the SACCF could occasionally be detected using remotely-sensed SST information as shown by Meredith et al. (2003b).

When comparing the average frontal positions to the standard deviation of daily SST data for the period 2004 - 2005, it is obvious that the SAF and PF are in general associated with bands of high variability of SST (Fig. 3.13). Although the seasonal cycle is included here, areas of high variability ( 1.5° C) are related to meandering of the fronts and eddy activity. On the contrary, areas with low standard deviation of

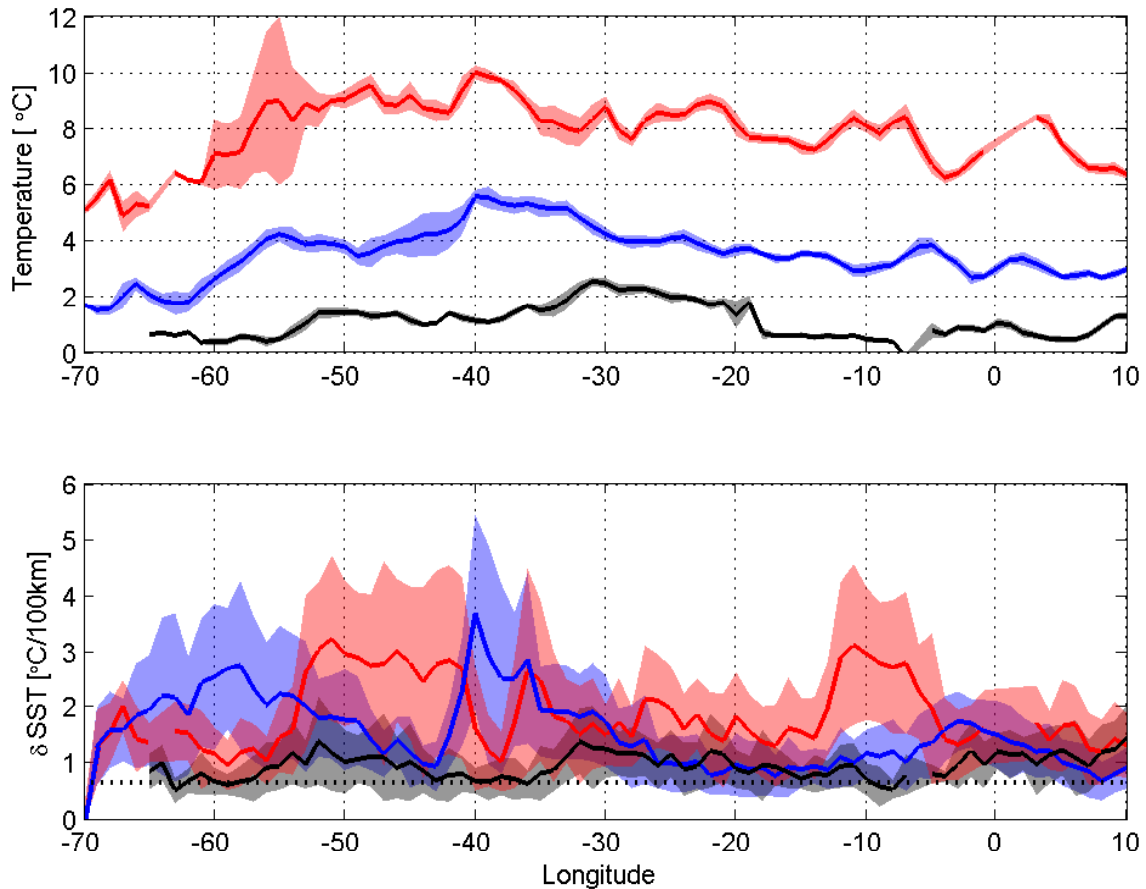


**Figure 3.12:** SST (*top*) and SST gradient (*bottom*) at frontal positions with mean as solid line and standard deviation as patch from monthly data for the period 2004 - 2005, inclusive. The SAF is in red, the PF in blue and the SACCF in black. The horizontal dotted black line in the bottom panel shows the mean meridional increase in SST to the north.

SST indicate low variability of the frontal position and less eddy activity. The area southwest of Burdwood Bank along the continental shelf shows low variability in SST and coincides with low variability in the position of the SAF (Fig. 3.9). This feature continues further north, where the SAF is again constrained by bathymetry along the shelf north of the Falklands (Fig. 3.13). When the SAF turns southward, it is associated with stronger variability in SST indicating higher variability of the frontal position, which I also found in the monthly positions (Fig. 3.9). The band of high SST variability along the PF confirms the variability of the PF position from Drake Passage to the Mid-Atlantic Ridge (Fig. 3.10). From Drake Passage to south of South

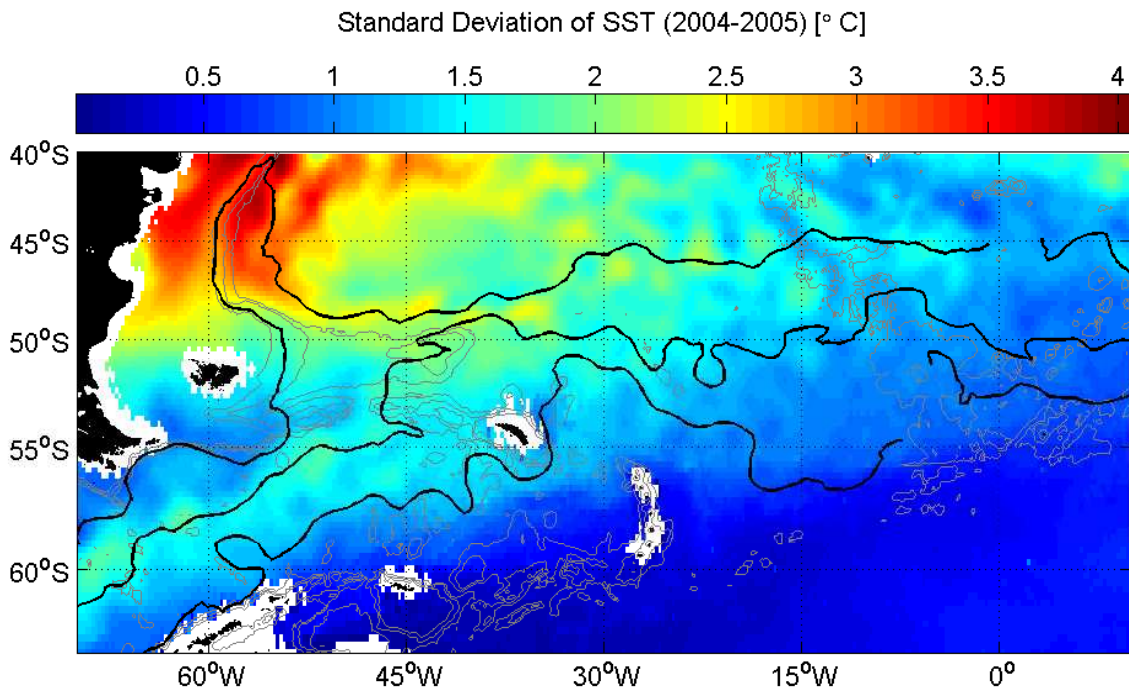


**Figure 3.13:** Standard deviation of daily SST data for the period 2004 - 2005, inclusive and the mean frontal positions of SAF, PF and SACCF as derived by this study (solid black lines). Isobaths are 1000 m, 2000 m and 3000 m and land is shaded black.

Georgia the standard deviation of SST of  $1.3^{\circ}\text{C}$  coincides with the southernmost extent of the SACCF (Fig. 3.11). On the eastern side of the island a patch of low SST variability indicates that the SACCF is constrained close to the shelf slope on this side of the island (Fig. 3.13). However, north of the island the SST deviation increases related to a higher variability of the frontal position (Fig. 3.11).

The variance of sea level has been used for many years to identify regions of intense mesoscale variability (Kostianoy et al., 2003). Figure 3.14 shows the SLA variance calculated from weekly gridded altimeter data. In my area of interest are two regions of high SLA variance. The first one lies within the ACC in the Drake Passage south of the SAF and along the PF. This intense mesoscale variability shows that the PF in the Drake Passage is generally dominated by current meanders and mesoscale eddies. Following the path of the PF two branches of higher SLA variance can be seen close to the west and south flanks of the Maurice Ewing Bank, while the mean PF path

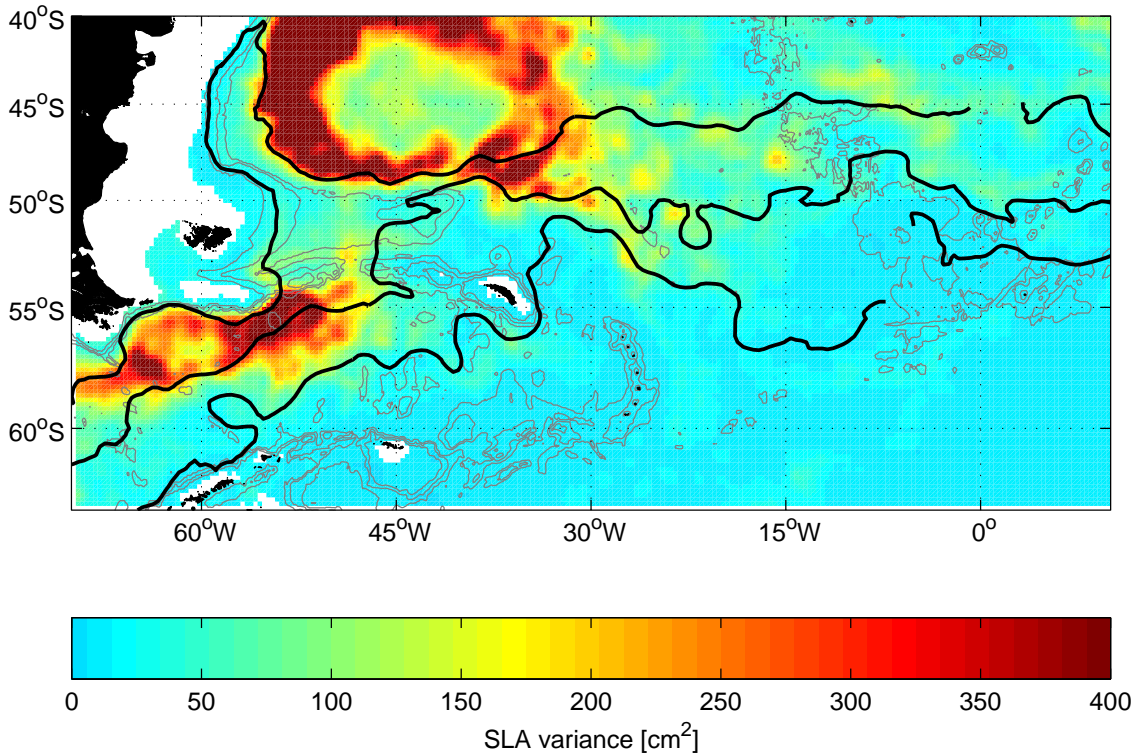


**Figure 3.14:** Variance of sea level anomaly based on weekly gridded altimeter data for the period 08/2001-06/2006, inclusive. Mean frontal positions of SAF, PF and SACCF as derived by this study. Isobaths are 1000 m, 2000 m and 3000 m and land is shaded black.

is across this topographic feature. The other area of high SLA variance lies north of the mean SAF in the Brazil/Malvinas Confluence. This confluence of currents creates mesoscale meanders and eddies with energy levels ranked at the top of the world's oceans (Fu et al., 2001; Goni and Wainer, 2001; Vivier et al., 2001). The mean SAF path is nestling to the west and south side of this area, indicating that all variability takes place north of the front. At around 40° W a transition zone starts where this energy is shifted from the north side of the SAF to the south, in particular in the vicinity of the SACCF at about 30 – 25° W.

## 3.5 Discussion

In general, the average frontal positions derived from my dataset are in agreement with previous work (Orsi et al., 1995; Thorpe et al., 2002), especially where the pathways are constrained by topography, e.g at the North Scotia Ridge, South Scotia Ridge and the Mid-Atlantic Ridge. However, some novel features are observed, which I outline here. First, I discuss the derived positions of the frontal system in comparison to previous work. Then, I examine the possible causes for the observed zonal shift of the ACC. Finally, I discuss the relationship between the surface and sub-surface expressions of the three major fronts.

### 3.5.1 The frontal positions

The mean position of the SAF in 2004 to 2005 correlates well with data from previous work (Orsi et al., 1995) on the western side of the study region, i.e. west of South Georgia. East of the island the SAF lay further north. I compared the position with the 4° C isotherm at 200 dbar, which is used for identification of the SAF in previous work (Peterson and Whitworth III, 1989; Orsi et al., 1993) to conclude that both criteria give very similar results. Also the SST gradient shows a value above noise levels (Fig. 3.12) indicating that the position of the SAF is at least very close to the surface expression of the front (Fig. 3.12). The mean SAF position also lacks the southward loop between the Maurice Ewing Bank and the Falkland Ridge seen in the mean position by Orsi et al. (1995). Arhan et al. (2002) state that this area at 37° W is a key injection site of North Atlantic Deep Water into the ACC. However, the location of the SAF used in this study is based on the 300 dbar temperature field and a penetration of northern water into the SAF occurs at much greater depth (Arhan et al., 2002). An effect on the SAF as determined in this study by injected northern water is therefore unlikely. Nevertheless, I see strong meandering of the monthly SAF

positions north of the Maurice Ewing Bank and the Falkland Ridge along  $48^{\circ}$  S (Fig. 3.9). Arhan et al. (2002) also describe an anticyclonic flow over the Falkland Plateau and such a flow could have been the cause for this meandering. An interesting feature is that the monthly SAF positions east of the Maurice Ewing Bank are on average north of the mean position by Orsi et al. (1995), suggesting a northward shift of the northern boundary of the ACC in 2004 and 2005 (Fig. 3.9).

Despite the differences in defining the PF, the mean PF path from previous studies agrees well with my observations, particularly in the vicinity of strong topographic features, such as the Drake Passage and the Mid-Atlantic Ridge. However, a relatively large difference is seen in the north Scotia Sea before the PF crosses the North Scotia Ridge. In 2004 and 2005 the PF extended far more to the east than in previous work and showed high spatial variability. A longer time series is needed to verify if this is particular to the studied time period or is a regular occurrence. The mean PF path is across the Maurice Ewing Bank, while two branches of higher SLA variance can be seen close to the west and south flanks of the Maurice Ewing Bank. This may result from a topographically-induced lateral splitting of the PF south of the bank as suggested by Naveira Garabato et al. (2002). However, the monthly PF positions show that the PF loops cyclonically around the bank with a recirculation on the eastern side. If this discrepancy is due to a lack of representativeness of the data used in Naveira Garabato et al. (2002) or in my dataset needs further investigations on a smaller temporal and spatial scale. The monthly positions show also strong variability of the front due to meandering and meridional movements. Dong et al. (2006) suggested a correspondence between the tendency of the PF location and the meridional shift of the wind field resulting in a move equatorward during winter, but my findings do not support this. This might be due to the fact that the short temporal variability is larger compared with the seasonal variability and that a seasonal signal is much smaller in the sub-surface expression than at the surface. The PF positions

show a large short term variability due to meandering and eddy activity. These eddies seem to be much more important for the frontal position than the wind field.

The SACCF shows great variability north of Elephant Island. Data from the WOCE section SR1b between 1993 and 2000 show that there are very often small, vertically-coherent eddies to the southern end of this section just north of Elephant Island (Cunningham et al., 2003). These eddies have the characteristics of water from south of the SB, but can be found almost as far north as the PF. This rich eddy field with associated low temperatures could be a factor in the high variability of the SACCF to the northwest of Elephant Island.

Another interesting feature is the strong variability of the SACCF in the vicinity of South Georgia. The SACCF looped to the north before wrapping anticyclonically around South Georgia in early 2004. Meredith et al. (2005) used six years (1996 - 2001) of high-resolution hydrographic data collected during the austral summer to show the interannual variability of the water mass properties around South Georgia and concluded that significant variability occurs at sub-annual timescales. Indeed, the monthly SACCF positions show the large sub-annual variability (Fig. 3.11). During summer 2004/2005 the path of the SACCF moved further south, while the PF extended a loop along the North Scotia Ridge to the east before turning back to the west and crossing the North Scotia Ridge. At the end of 2005 the PF again lay further west, while the SACCF again looped northward before wrapping around South Georgia. This interplay and the strong variability north of the island as shown in Figures 3.10 and 3.11 must have implications on the South Georgia ecosystem.

### **3.5.2 A shift of the ACC**

Interestingly, the mean SAF, as positioned by my dataset, crossed the Mid-Atlantic Ridge about 400 km further north than the SAF of Orsi et al. (1995). The mean

SACCF path follows the path by Orsi et al. (1995) and Thorpe et al. (2002) very closely, but at  $15^{\circ}$  W the SACCF lies further north. When the spatial resolution of the dataset is best in this area (at the end of 2005), the SACCF was situated up to 150 km further north when compared to the location of Orsi et al. (1995). The SAF and SACCF are deep reaching fronts and are constrained by the bathymetry in many places. This change from one constrained passing place to another one further north suggests a major shift in the location of the ACC between Orsi et al. (1995) and my findings.

It has been argued that such shifts can happen in response to changes in wind stress. Such changes have been happening in recent decades. For example, Thompson and Solomon (2002) show an increased strength of the zonal winds over the Southern Ocean in the past three decades. A recent study argued that this will be followed by a significant increase in transport and a poleward change in position of the ACC (Fyfe and Saenko, 2006). Contrary to these expectations, I see a northward shift of the ACC in 2004 and 2005 compared to previous work. However, Meredith and Hogg (2006) cast doubt on whether this process described by Fyfe and Saenko (2006) is real or an artefact of coarse-resolution climate models. Dong et al. (2006) suggest that there is observational evidence for this process. A northward shift of the maximum zonal wind stress may also force the PF to move to the north as suggested by Dong et al. (2006), with variations in the wind field leading variations in the PF path. However, my findings suggest that eddies are much more important and the observed shift in the ACC position does not lend weight to the argument that the ACC location depends on zonal wind stress.

According to Meredith and Hogg (2006), eddies act to constrain changes in ACC transport that occur when changes in wind forcing occur. These eddies will also tend to constrain any changes in the position of fronts. In 2004, the SAF shows strong

meandering and eddy activity west of  $30^\circ$  W, while the PF shows the same further downstream east of  $30^\circ$  W. This transition takes place, where the two fronts are in close proximity, suggesting a transfer of eddies from the SAF to the PF. This is confirmed by the large variance in SLA in this region to as far south as the SACCF (Fig. 3.14). Strong meandering and eddy activities are associated with the SAF from  $45^\circ - 40^\circ$  W, with the PF from  $40^\circ - 30^\circ$  W and with the SACCF around  $30^\circ - 25^\circ$  W. This indicates that the fronts are not really individual discrete features that are circumpolarly continuous, but rather split and merge and re-split (Pollard et al., 2002). Using only satellite SST data, frontal loops across the same longitude more than once cannot be resolved and will lack these features (e.g. Dong et al., 2006). This demonstrates the advantage of being able to track such movements of ACC fronts even more clearly using in situ data.

This transition zone from  $45^\circ$  W to  $25^\circ$  W also supports the argument of Sun and Watts (2002), who suggested that the mean flow of the ACC transports heat from warm subtropical regions to cold subpolar regions. Sun and Watts (2002) also showed that the ACC warms in the western South Atlantic, cools until south of Africa, gaining heat again in the Indian Ocean and cools in the South Pacific. This heat loss is shown in Fig. 3.12 by a decrease of SST of about  $2^\circ$  C to the east, although the fronts stay at the same latitude (PF) or even lie further north (SAF).

### **3.5.3 Correlations between the surface and sub-surface expressions**

Previous studies used satellite SST to define the positions of the ACC fronts. While this can be appropriate for the PF, and to a lesser extent the SAF, it could be quite difficult for determining the SACCF position (Fig. 3.12). Nevertheless, Meredith et al. (2003b) showed a SST signal that was associated with the SACCF close to South

Georgia, indicating the potential of SST for remote detection of this front for certain times and places.

Consistent with previous studies, Dong et al. (2006) and others suggested that the surface PF location tends to be south of the subsurface PF location. Fig. 3.10a supports this argument, showing my derived locations of the PF generally north of the PF locations of Moore et al. (1999). Admittedly, the topography seems to play an important role. My comparisons between the PF positions and satellite SST data showed that when the PF path is constrained by topography, the SST gradient is high, suggesting a concurrence of surface and subsurface locations. However, over deep ocean basin regions with weak topographic variations, the PF meanders substantially, and the SST gradient is weak (Moore et al., 1999; Dong et al., 2006).

The SST gradient at the PF in Fig. 3.12 varies between  $1^{\circ}\text{C}$  and  $3.5^{\circ}\text{C}$  with a peak of more than  $5^{\circ}\text{C}$ , which is similar to Dong et al. (2006). Interestingly Moore et al. (1999) show a peak in the SST gradient for the PF from the Drake Passage to  $20^{\circ}\text{W}$ , while I found two peaks, one at  $60^{\circ}\text{W}$  and another one at  $40^{\circ}\text{W}$ . The minimum is in between where the PF crosses the North Scotia Ridge. Either the SST gradient is very small or the surface and sub-surface expression of the PF are different here. I suggest the latter, because this is also the place with the biggest differences between the mean path and the path based on the surface expression by Moore et al. (1999) (Fig. 3.10a). Also to the east of  $30^{\circ}\text{W}$  the SST gradient of the PF is very weak, suggesting a higher separation between the surface and sub-surface expression. Here the small SST gradient of the SAF suggests a separation between the surface and sub-surface expression too. The SST gradient of the SAF is relatively weak except at two locations, where the SAF is constrained by the topography at  $50 - 40^{\circ}\text{W}$  north of the Falkland Plateau and at  $10^{\circ}\text{W}$  after crossing the Mid-Atlantic Ridge. This feature is also present in the PF and SACCF east of the Mid-Atlantic Ridge. However, all

fronts show high SST gradients when they reach their northermost point (Fig. 3.12).

### 3.6 Summary and Conclusions

Analysis of in situ hydrographic data of the years 2004 and 2005 in the southwest Atlantic sector of the Southern Ocean has produced maps of the SAF, PF and SACCF within the ACC at high spatial and temporal resolution. The availability of Argo float data and the complementary CTD-SRDL data has allowed us to examine the fronts simultaneously in much more detail than previously possible. In defining the fronts, I have placed most weight on the distribution of horizontal temperature gradients. Defining the fronts in this way corresponds to various scalar criteria used by earlier investigators. The data collected by animal-borne CTD-SRDLs proved to be very useful in obtaining several cross-sections of the ACC at different locations and seasons. The existence of suitable proxies expressed in terms of subsurface temperature or satellite SST has allowed us to examine the spatial and temporal variability of the front locations. The results can be summarised as follows:

- New technology has enabled production of an in situ dataset with high temporal and spatial resolution in the Southern Ocean. The Global Ocean Observing System required the establishment of Argo, which is designed for broad-scale ocean sampling. Smaller scale eddy-resolving sampling is complementary to the broad-scale mode and can be achieved using autonomous CTD-Satellite Relay Data Loggers attached to marine animals. These high-accuracy sensors proved to have the ability to collect large numbers of profiles cost-effectively particularly in regions where traditional oceanographic measurements are scarce. They are a powerful complement to the array of Argo floats. Both technologies send data via satellites and have a great potential for observing the ocean in real-time,

when used in tandem.

- The comprehensive dataset enabled me to map the monthly positions of the SAF, PF and SACCF in 2004 and 2005. This time series indicates areas of high variability in these frontal locations. The SAF is constrained by the South American continental shelf, but shows high variability west of the Burdwood Bank and when crossing the ocean basin between South America and the Mid-Atlantic Ridge. The PF is the most active front with meandering along its entire path through the study region. It is constrained by the North Scotia Ridge and the Mid-Atlantic Ridge. Its pathway around/across the Maurice Ewing Bank is not sufficiently resolved in this study. The SACCF shows high variability in the Scotia Sea and to the northeast of South Georgia, but it is also constrained by specific topographic features, e.g. the South Georgia shelf, Northeast Georgia Rise and the Mid-Atlantic Ridge. All frontal variability seems to be much more influenced by meandering and eddies than possible seasonality in the wind field. The spatial pattern of higher variability changes between the two years.
- The position of the PF is highly variable south of the North Scotia Ridge. The front also extends much further to the east before crossing the North Scotia Ridge than in previous work. The extension of this eastward loop varies over time with the greatest extent in summer 2004/2005. The SACCF shows a northward loop on the west side of South Georgia before wrapping around the island. Again the size of this loop is highly variable with its peaks in winter 2004 and at the end of 2005. Whether these two frontal features are coupled needs further investigations.
- After looping anticyclonically around South Georgia, the SACCF shows a strong variability in the position of its retroflexion north of the island. This tongue of the SACCF has its greatest extent to the west during winter. In 2004 this

feature is less pronounced than in 2005, where it reached the Northwest Georgia Rise. Despite the meandering, the SACCF is constrained by the South Georgia shelf, the Northeast Georgia Rise and the Mid-Atlantic Ridge.

- Previous studies were limited by the sparse hydrographic data in the Southern Ocean or were constrained by the continuity of the SST at the fronts when using satellite SST maps. The frontal positions based on the sub-surface expressions within this study are compared to satellite SST. The SST gradient is in general the highest when the fronts are constrained by the bathymetry, induced by the concurrence of the surface and sub-surface expression.
- SST and SLA variance support the argument that there is a transition zone starting around  $40^\circ$  W where eddy energy is shifted from the north side of the SAF to the south, in particular in the vicinity of the SACCF at about  $30^\circ - 25^\circ$  W.
- East of  $40^\circ$  W all three fronts were shifted further to the north than historical positions suggested, varying between 400 km for the SAF and 150 km for the SACCF.



# **4 Monitoring Drake Passage with elephant seals: Frontal structures and snapshots of transport**

Manuscript accepted by  
*Limnology and Oceanography*

## 4.1 Abstract

CTD-Satellite Relay Data Loggers (CTD-SRDLs), each recording conductivity, temperature and pressure, were attached to Southern elephant seals (*Mirounga leonina*) on the island of South Georgia. During the animals' migration the CTD-SRDLs recorded and transmitted hydrographic profiles at a rate of approximately 2 profiles day<sup>-1</sup> to an average depth of about 547 m, representing transect-type sections with a spatial resolution of 16-47 km along the migratory routes of the seals. These sections can be used to clearly identify the locations of the Antarctic Circumpolar Current fronts across Drake Passage, providing in situ data complementary to satellite and other techniques. An empirical relationship between upper ocean temperature and baroclinic mass transport is used to determine the transport through Drake Passage at the times of the sections, and these transports are compared with estimates derived by other techniques. An absolute geostrophic velocity section across Drake Passage is calculated using CTD-SRDL data and data of absolute geostrophic surface velocities from altimetry. The mean total baroclinic transports in June 2004 and April 2005 are estimated to be  $124 \times 10^6 \pm 14 \times 10^6 \text{ m}^3 \text{ s}^{-1}$  and  $112 \times 10^6 \pm 14 \times 10^6 \text{ m}^3 \text{ s}^{-1}$  respectively.

## 4.2 Introduction

The Antarctic Circumpolar Current (ACC) dominates the horizontal circulation of the circumpolar Southern Ocean, and is a key component of the global ocean overturning circulation (Rintoul et al., 2001). The clockwise circulation around the Antarctic continent provides a vital link for transporting heat and freshwater between the Atlantic, Indian, and Pacific Oceans. The transport of the ACC and its variability are therefore of considerable importance, due to their influence on climate and ecosystem processes over large areas. With increasing expectations for weather and ocean predictions at increasingly fine resolutions, models must become more sophisticated, and the need for detailed in-situ observations has never been more acute and is accelerating. Data are needed from regions and seasons where traditional hydrographic data (e.g. ship-based measurements, Argo floats etc.) are scarce and/or difficult and expensive to implement. New approaches are being developed to fill this gap.

The flow of the ACC is not spatially uniform, with zones of relatively uniform water mass properties separated by narrow, deep-reaching current cores associated with the ACC fronts (Nowlin et al., 1977; Nowlin and Clifford, 1982; Nowlin and Klinck, 1986). Before these narrow fronts were fully resolved, estimated net transports of the ACC in Drake Passage ranged unrealistically widely, from  $236 \times 10^6 \text{ m}^3 \text{ s}^{-1}$  to  $-15 \times 10^6 \text{ m}^3 \text{ s}^{-1}$ , due to coarse spatial and temporal sampling and inappropriate assumptions in transport calculations (Reid and Nowlin, 1971; Foster, 1972). Subsequently, repeat hydrographic measurements were made as early as the mid 1970s as part of the International Southern Ocean Studies (ISOS) experiment. ISOS fully revealed the banded structure of the ACC, and derived a mean transport of  $134 \times 10^6 \pm 13 \times 10^6 \text{ m}^3 \text{ s}^{-1}$  using the repeat hydrography and moorings data (Whitworth, 1983; Whitworth and Peterson, 1985).

Whitworth and Peterson (1985) suggested that the ACC is in geostrophic bal-

ance and concluded that although about three-quarters of the net transport is in the baroclinic component, transport variability is mainly barotropic on timescales up to around annual. Reanalysis of the ISOS moorings data led Cunningham et al. (2003) to argue that the barotropic and baroclinic variability in Drake Passage transport are comparable even on subseasonal timescales. More recent analyses have demonstrated that barotropic variability dominates the transport through Drake Passage on timescales up to around seasonal, with baroclinic variability becoming important at annual and interannual timescales (Hughes et al., 2003; Meredith et al., 2004).

Annual occupations of a repeat hydrographic section (WOCE SR1) began in 1993 during the World Ocean Circulation Experiment (WOCE). Cunningham et al. (2003) estimated the baroclinic transport to be  $136.7 \times 10^6 \pm 7.8 \times 10^6 \text{ m}^3 \text{ s}^{-1}$  from six SR1 hydrographic sections and reanalysed the ISOS data and found the uncertainty of the mean net transport to be around  $35 \times 10^6 \text{ m}^3 \text{ s}^{-1}$ , significantly larger than suggested by Whitworth and Peterson (1985). Cunningham et al. (2003) and Sprintall (2003) observed the two northernmost fronts of the ACC to be highly variable, meandering on interannual timescales. This interannual frontal variability was confirmed in chapter 3, showing the high variability of the Polar Front (PF) in Drake Passage on subannual timescales.

Today it is known that the circumpolar transport variability of the ACC on time scales from days to years is forced by fluctuations in the Southern Annual Mode (SAM), the dominant extra-tropical mode of climate variability in the Southern Hemisphere (Thompson and Wallace, 2000). Despite a trend toward a higher-index state in recent decades, the SAM is strongly modulated by season (Thompson and Solomon, 2002). The range in transports shown by the ACC on interannual timescales is seen to be rather small, however, and this is believed to be due to energy being cascaded to smaller (mesoscale) length scales via baroclinic instability (Meredith and Hogg, 2006).

Equally importantly, Meredith et al. (2004) showed that the interannual changes in the seasonal signal in the SAM are reflected in changes in the seasonal signal in the ACC transport.

Repeat hydrographic and XBT sections are continuing (e.g., Sprintall, 2003; Sokolov et al., 2004), but these measurements alone are not adequate for monitoring the interannual variability in the ACC transport, or changes to the seasonal signal in ACC transport due to changes in the SAM (Meredith and Hughes, 2005). Such estimates are hugely aliased by short-term variability, e.g., eddies and higher-frequency transport changes. High frequency variability in Drake Passage can produce aliased signals even with a 10-day altimeter sampling (Gille and Hughes, 2001). Meredith and Hughes (2005) showed that sampling intervals very much shorter than 10 days are needed.

Whilst estimates of ACC transport variability on interannual timescales that derive from ship-based repeat hydrographic and XBT sections data are badly aliased (Meredith and Hughes, 2005), it remains open to question whether such data are capable on longer timescales (decadal) of monitoring changes in transport. The key would be to have a sufficient number of occupations so that the estimated mean for a given period would be a robust indicator of the actual mean, against the background of inherent variability at higher frequencies. If this approach were to work, it is likely that a very large number of sections across Drake Passage would be needed, i.e., more than are currently obtainable with research ships. Another problem is the seasonal variability in the ACC transport (Meredith et al., 2004). Conductivity-Temperature-Depth (CTD) and XBT sections are conducted almost entirely in the austral summer, thus any estimates of mean transport based on these sections will be potentially biased.

Alternative approaches are proxy techniques based on less expensive measurements which can be obtained more frequently, also from the austral winter, and do not

require research vessels (Lydersen et al., 2002). Here I present a new set of under-way observations from Drake Passage, and show their usefulness in identifying and pinpointing ACC frontal features. Although not pre-planned, I show that the new technique of ‘adaptive-sampling’ results in higher resolution at the ACC fronts. I demonstrate further that these measurements have comparable utility to XBT and expendable conductivity-temperature-depth (XCTD) sections for studies seeking to monitor ACC transport variability. By including wintertime data into such efforts, we will help alleviate some of the problems with aliasing at interannual periods. At longer periods these new data may help define more robust transport means, if sustained over several decades.

## 4.3 Data

### 4.3.1 Hydrographic data

Within the framework of the international SEaOS project (Southern Elephant Seals as Oceanographic Samplers), 21 Southern elephant seals (*Mirounga leonina*) on South Georgia were equipped with CTD-Satellite Relay Data Loggers (CTD-SRDLs). This interdisciplinary program is aimed at increasing our understanding of how Southern elephant seals interact with their physical environment (Ch. 5) and also at demonstrating and implementing this cost-effective means of gathering routine observations of hydrographic data from remote environments (Chs. refGI and 3). CTD-SRDLs, custom-built by the Sea Mammal Research Unit, St Andrews, UK and Valeport Ltd., Devon, UK, were fixed harmlessly to seals’ fur after the elephant seals completed their annual moult in January and February and were finally lost when the animals moulted again the following season. During the animals’ migration, the CTD-SRDLs report vertical profiles of salinity, temperature, and pressure to a depth of up to 2000 m with

an accuracy of better than 0.02 in temperature and salinity (Ch. 2); hence of at least same quality as XBT data (Boyd and Linzell, 1993).

Several animals traveled west from South Georgia towards the Antarctic Peninsula and two crossed Drake Passage nearly perpendicular to the flow (Fig. 4.1). Here I show two hydrographic sections obtained by the Southern elephant seals *Rudolph* and *Jason* in 2004 and 2005 (Fig. 4.1). *Rudolph* crossed the western Drake Passage between 07 June 2004 and 20 June 2004 from the Antarctic Peninsula towards the western side of Burdwood Bank. He sampled 96 temperature profiles with an average station spacing of 16 km, an average profile depth of 469 m and a range of profile depths between 118 m and 1000 m (Fig. 4.2). Between 01 April 2005 and 15 April 2005, *Jason* travelled from Elephant Island to the southeastern side of Burdwood Bank very close to the WOCE repeat section SR1b. Eighteen CTD profiles were recorded with an average station spacing of 47 km and profile depth of 624 m with a profile depth range from 260 m to 1074 m (Fig. 4.3). The CTD-SRDL configuration was set to ensure batteries lasted until seals return to breed in September and only one CTD profile was sampled every six hours. However, the horizontal spacing of consecutive dives deeper than 200 m is less than 6 km on average for both animals. Hence, the configuration could be optimised in the future to increase the spatial and temporal resolution of such hydrographic sections made by Southern elephant seals.

### 4.3.2 Absolute dynamic topography

To calculate the absolute velocity from the hydrographic data, I use the Maps of Absolute Dynamic Topography product (MADT) of the Data Unification and Altimeter Combination System (DUACS), which is part of the multi-mission ground segment of the Centre National d'Études spatiales. This system processes Jason-1, Envisat, GFO, ERS-1, ERS-2, and Topex-Poseidon altimeter data and synchronises it with auxiliary

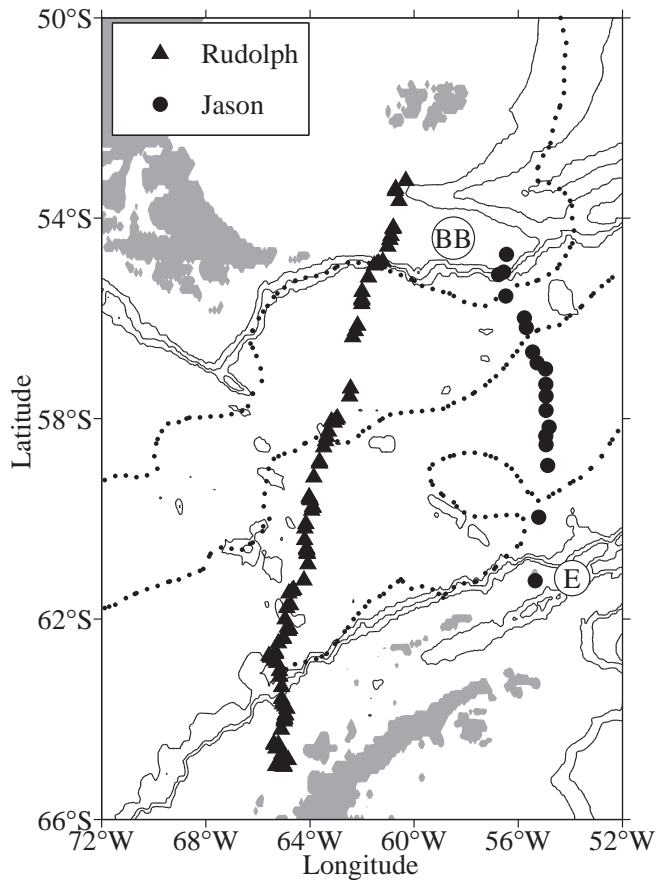


**Figure 4.1:** The positions of the CTD-SRDL hydrographic profiles from *Rudolph* (triangles) and *Jason* (circles) sampled between 7-20 June 2004 and 1-15 April 2005 respectively. The mean position for 2004 and 2005 of the Subantarctic Front, Polar Front and Southern ACC Front (from north to south) from chapter 3 are shown as solid lines. Burdwood Bank (BB) and Elephant Island (E) are marked. Isobaths are 1000 m, 2000 m and 3000 m and land is shaded black.

data. Each mission is homogenised using the same models and corrections. A multi-mission cross-calibration process removes any residual orbit error, or long wavelength error, as well as large scale biases and discrepancies between various data flows (CLS, 2007). All altimeter fields are interpolated at crossover locations and dates. After a repeat-track analysis, a mean profile is subtracted to compute sea level anomaly. Data are then cross validated, filtered from residual noise and small scale signals, and finally sub-sampled to give the Sea Level Anomaly product (SLA). Absolute Dynamic Topography (ADT) products are obtained by computing  $ADT = SLA + MDT$ , where MDT is a global Mean Dynamic Topography (Rio and Hernandez, 2004). The final mapping procedure generates a combined map merging measurements from all available altimeter missions (MADT). Geostrophic velocity maps are computed us-

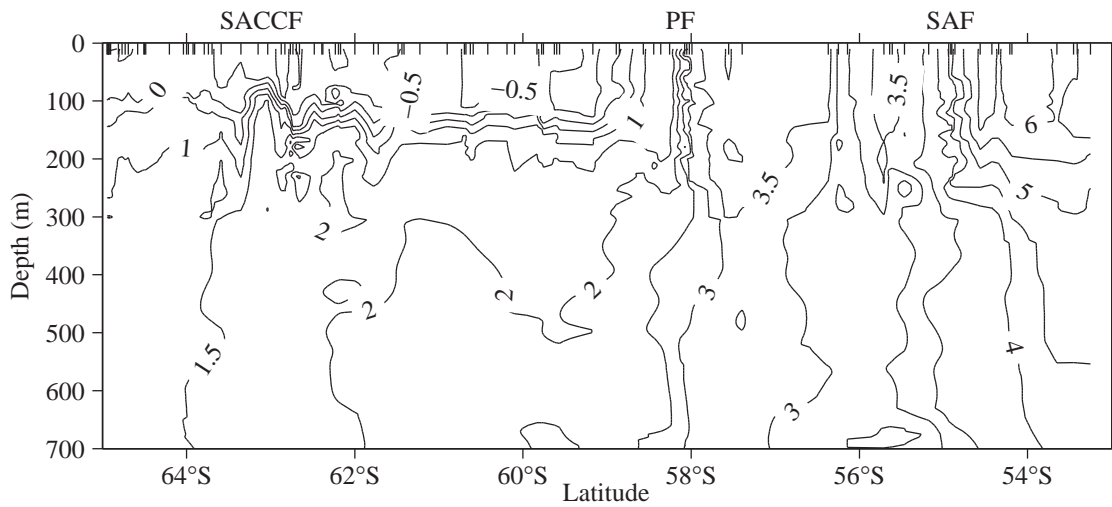


**Figure 4.2:** In situ temperature section sampled by *Rudolph*. The positions of the profiles are given on the top axis to show the horizontal resolution of the temperature data. This figure is adapted from chapter 3. Front locations are marked on the upper axis. **SACCF**: Southern ACC Front, **PF**: Polar Front and **SAF**: Subantarctic Front.

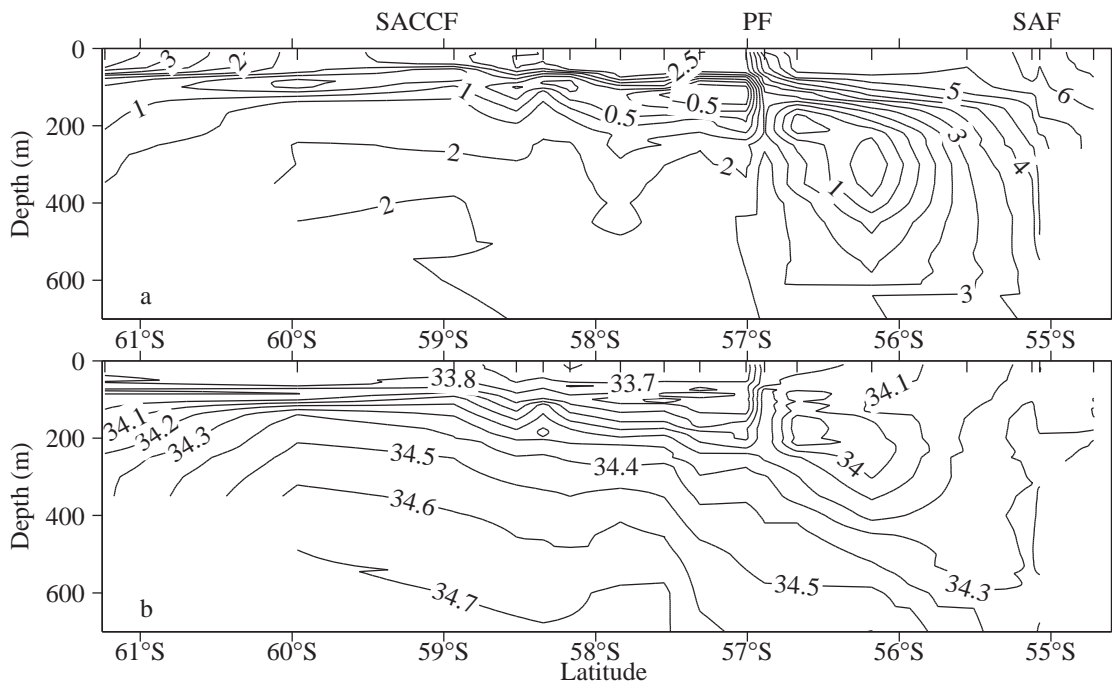


**Figure 4.3:** In situ temperature (*top*) and salinity (*bottom*) sections made by *Jason*. The positions of the CTD profiles are given on the top axis to show the horizontal resolution of the temperature data. Front locations are marked on the upper axis. **SACCF**: Southern ACC Front, **PF**: Polar Front and **SAF**: Subantarctic Front.

ing finite differences. The MADT have global coverage and include absolute dynamic topography and the corresponding geostrophic velocities on a third degree Mercator grid (CLS, 2007).

## 4.4 Results

### 4.4.1 Frontal structures in Drake Passage

*Rudolph* was equipped with a temperature-only SRDL and the data are shown in Fig. 4.2. There is no clear near-surface temperature minimum layer visible, indicating winter conditions along the entire section. As typically seen in meridional sections across the ACC, the temperature decreases to the south in a series of steps or fronts, separated by zones of weaker meridional gradients. Although this winter section shows clear horizontal temperature gradients, which are associated with the Subantarctic Front (SAF) at about 55°S very close to the Burdwood Bank and the PF at about 58°S, the Southern ACC Front (SACCF) close to the continental shelf at about 63°S is less pronounced. Between the PF and the SAF lies a zone of nearly homogeneous water without a pronounced thermocline. Of great interest, and potentially great usefulness, is the fact that *Rudolph* spent more time close to the fronts, which can be seen in the closer station spacing (Fig. 4.2).

About a year later, *Jason* recorded a full CTD transect across the Drake Passage further to the east at the end of the austral summer (Fig. 4.3). The temperature minimum layer between 100 m and 200 m depth is still visible. The first profile of the section at 61°S is on the Antarctic shelf to the southwest of Elephant Island. These shelf waters are indicated by a warmer surface layer of more than 2°C south of 60°S. Further north the higher salinities of the Circumpolar Deep Water (CDW) become apparent below 300 m depth, while further north still the relatively horizontal

isotherms and isohalines get distorted by the strong current cores and eddies within the ACC (Fig. 4.3). Orsi et al. (1995) defined the SACCF as the southern-most eastward core of the ACC that carries waters with circumpolar characteristics, which is distinct from the Antarctic regime farther south. Using this definition and the vertical isotherms locates the SACCF at about 59°S. The surface expression of the PF is by contrast marked clearly by the increase of the sea surface temperature from 2.5°C to 5°C at about 57°S.

Between 57°S and 56°S there is a cold extension of water descending from south to north (Fig. 4.3). Figure 4.4 shows the potential temperature versus salinity relationships for this section by *Jason*. The low temperature and salinity immediately identifies it as being derived from the temperature minimum layer, i.e., winter water, with a potential density of  $\sigma_{\Theta} = 27.3 \text{ kg m}^{-3}$ . It is of Antarctic origin with a depth of about 150 m south of the PF, and subducts to the north of the PF to intermediate depths of more than 500 m (Fig. 4.3). The SAF has again no strong surface expression, but is indicated by the vertical isotherms at 55°S close to Burdwood Bank.

#### 4.4.2 Estimating transports from in situ temperature

Monitoring ocean transports requires measurements of the density field as well as changes in the pressure field associated with the barotropic flow. To calculate the geostrophic transport from only temperature sections it is necessary to first obtain a relationship between the steric height, relative to a specified reference level, and temperature (Sprintall, 2003). In regions characterized by a single well-defined temperature-salinity ( $T$ - $S$ ) relationship, a mean  $T$ - $S$  curve can be formulated using historical salinity data to identify the salinity corresponding to each temperature observation. Steric height is then estimated from this salinity and the temperature observation relative to their deepest common depth (e.g., McCarthy et al., 2000).

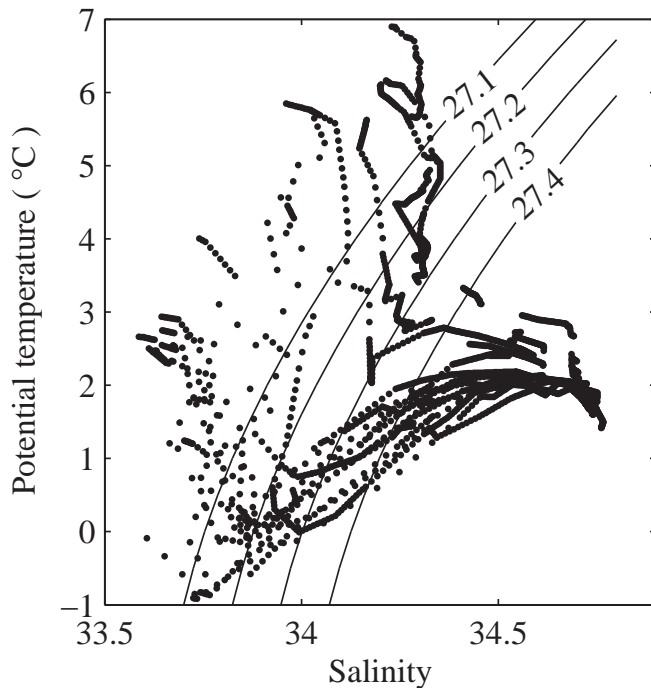


**Figure 4.4:** Potential temperature versus salinity for the stations made by *Jason*. The  $\sigma_{\Theta} = 27.3 \text{ kg m}^{-3}$  isopycnal marks the approximate density of the Antarctic Intermediate Water of the Drake Passage.

However, this is complicated in the Southern Ocean. Inversions and frontal variability mean that at some locations the  $T$ - $S$  relationship is not unique; hence one temperature can correspond to several salinity values. Nevertheless, the envelope of the  $T$ - $S$  relations does not change much with time and each streamline can be associated with a particular  $T$ - $S$  curve. This relationship between upper ocean temperatures to some known (determined) structure function of steric height, potential energy anomaly or transport stream function has been used extensively in regions where there are only limited numbers of deep hydrographic stations but a copious quantity of temperature data (Rintoul et al., 1997; Sprintall, 2003; Sokolov et al., 2004).

Most studies applying this technique to estimate the transport in Drake Passage use a reference level of 2500 m, because it is the deepest depth that lies above the height of the mid passage topography and also appears to be an appropriate reference depth as determined by the historical analysis of baroclinic transport in Drake Passage (Whitworth and Peterson, 1985; Rintoul et al., 2002). Some studies used a simple

relationship between the mass transport function and a single temperature variable. This could be the mass transport function regressed against a single temperature measurement (Ridgway and Godfrey, 1994), dynamic height against the average temperature from the surface to 600 m (Rintoul et al., 1997) or the baroclinic transport stream function,  $\chi_{2500}$ , against the averaged temperature ( $T_h$ ) between 600 m and 700 m depth (Sokolov et al., 2004):

$$\begin{aligned} \chi_{2500} = & (2.1024\overline{T_h^7} - 26.815\overline{T_h^6} + 138.81\overline{T_h^5} \\ & - 385.31\overline{T_h^4} + 641.27\overline{T_h^3} - 643.39\overline{T_h^2} \\ & + 360.61\overline{T_h} + 1.4552) \cdot 10^5 \end{aligned} \quad (4.1)$$

The zonal transport per unit width,  $U_\chi$ , is then (Sokolov et al., 2004):

$$U_\chi = -\frac{1}{\rho_{2500}f} \frac{\partial}{\partial y} \chi_{2500} \quad (4.2)$$

where  $\rho_{2500}$  is the reference density and  $f$  is the Coriolis parameter. Sprintall (2003) finds a relationship between the mass transport function,  $Q_{2500}$ , and the temperatures at 100 m ( $T_{100}$ ), 400 m ( $T_{400}$ ) and 700 m ( $T_{700}$ ):

$$Q_{2500} = 47.25 + 4.76T_{100} - 2.54T_{400} + 28.47T_{700} \quad (4.3)$$

The transport per unit width,  $U_Q$ , is then estimated from the gradient of the mass transport function  $Q_{2500}$  multiplied by  $g/f$ , where  $g$  is the acceleration due to gravity (Sprintall, 2003).

Both relationships are used here to calculate the transport from each temperature section shown in Figs. 4.2 and 4.3. The transports derived from the transect of *Rudolph* are shown in Fig. 4.5a. The transports derived from  $Q_{2500}$  include much more detail

and suggest that small current cores and branches only affect the upper layer above 600 m depth. These are then only resolved by the method based on Sprintall (2003) including temperatures at shallower depths,  $T_{100}$  in particular. Hence, the transports based on  $\chi_{2500}$  lack these details and deliver unrealistic high values close to the shelf at 54°S. However, both methods show similar results, by placing the current core of the SAF at 55°S. The main PF current core lies at 58.1°S. The PF seems to have several shallow cores to the south with transports up to  $10 \times 10^6 \text{ m}^3 \text{ s}^{-1}$  based on  $Q_{2500}$ , while the transport based on  $\chi_{2500}$  shows only one main core of more than  $10 \times 10^6 \text{ m}^3 \text{ s}^{-1}$ . The SACCF shows again many current branches between 64°S and 62°S when derived from  $Q_{2500}$ . The transports based on  $\chi_{2500}$  show only a small core at 63.5°S. This richness in detail close to the fronts in both derived transports is only realistically feasible by using ‘adaptive samplers’. Figure 4.2 shows the decreased station spacing close to the fronts, increasing the detail of the three ACC fronts in this transect.

Figure 4.5b shows the transports derived from the transect of *Jason*. Both methods show similar results, but lack the detail of Fig. 4.5a (this transect consists of only 15 deep profiles compared to 81 in Fig. 4.5a). Again, transports derived from  $Q_{2500}$  include much more detail and show two current cores of the PF, the northern one less pronounced in the transports derived from  $\chi_{2500}$ . The SAF lies very close to the continental shelf (Fig. 4.3), and the calculated transports should be treated with caution in areas with less than 2500 m water depth. However, both methods seem to resolve the SAF at the northern end of the transect. The PF is associated with a stronger current than the SAF in contrast to Fig. 4.5a.

The cumulative transports integrated from Fig. 4.5 are shown in Fig. 4.6. Including different depths to represent different water masses and a shallow depth  $T_{100}$  to capture the seasonal changes in  $Q_{2500}$  seems to deliver much more detail than the

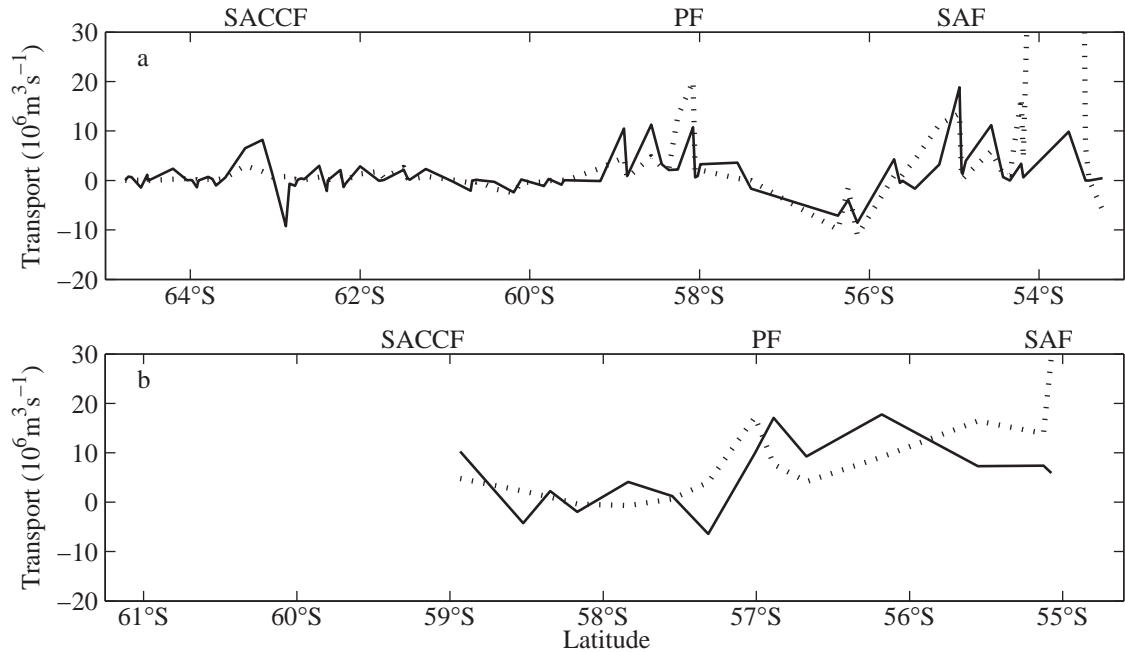


**Figure 4.5:** The transport per unit width ( $10^6 \text{ m}^3 \text{ s}^{-1}$ ) above 2500 m depth derived from mass transport function  $Q_{2500}, U_Q$  (solid line) and the baroclinic transport stream function  $\chi_{2500}, U_\chi$  (dotted line) for the Drake Passage transects of (a) *Rudolph* in June 2004, and (b) *Jason* in April 2005. Front locations are marked on the upper axis. **SACCF**: Southern ACC Front, **PF**: Polar Front, and **SAF**: Subantarctic Front.

transport derived from  $\chi_{2500}$ . The cumulative transports of both methods derived from *Rudolph*'s dataset correlate very well. Here, the method based on  $Q_{2500}$  captures the SACCF including a counter-current just north of the SACCF (Fig. 4.5), while the method based on  $\chi_{2500}$  lacks this transport. South of 60°S, the temperature corresponds to several salinity values and  $\chi_{2500}$  fails to resolve the different relationships between temperature and the stream function. However,  $Q_{2500}$  shows more detail in this region and seems to resolve the streamlines even close to the shelf at 64°S. The strongest current cores correlate well with the positions of the PF and SAF derived above (Fig. 4.2). Interestingly, both relationships show a decrease in transport between 57.5°S and 55.5°S between the two fronts and is due to the colder water below 200 m. Here, the two methods show a decline of about  $20 \times 10^6 \text{ m}^3 \text{ s}^{-1}$  (Fig. 4.6a) and a counter-current just south of the SAF. Both relationships deliver estimates for the

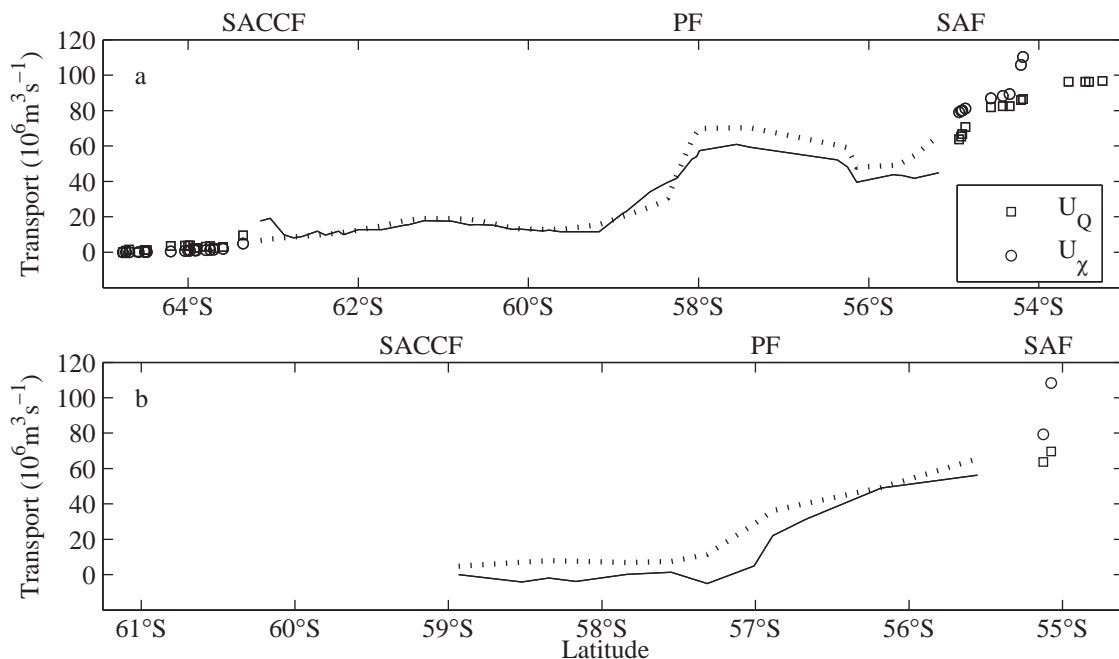


**Figure 4.6:** Cumulative transport ( $10^6 \text{ m}^3 \text{ s}^{-1}$ ) above 2500 m depth derived from mass transport function  $Q_{2500}$ ,  $U_Q$  (solid line) and the baroclinic transport stream function  $\chi_{2500}$ ,  $U_\chi$  (dotted line) for the Drake Passage transects of (a) *Rudolph* in June 2004, and (b) *Jason* in April 2005. The data are integrated from south to north, starting at the first profile with a water depth of more than 2500 m. Data from positions with water depths of more than 2500 m are lines, while others are marked with a circle and square. Front locations are marked on the upper axis. **SACCF**: Southern ACC Front, **PF**: Polar Front, and **SAF**: Subantarctic Front.

cumulative transports of  $80 \times 10^6 \text{ m}^3 \text{ s}^{-1}$  ( $Q_{2500}$ ) and  $90 \times 10^6 \text{ m}^3 \text{ s}^{-1}$  ( $\chi_{2500}$ ) above and relative to 2500 m depth, with errors of  $\pm 11 \times 10^6 \text{ m}^3 \text{ s}^{-1}$  ( $Q_{2500}$ ) and  $\pm 13 \times 10^6 \text{ m}^3 \text{ s}^{-1}$  ( $\chi_{2500}$ ) respectively. These errors are due to the temperature accuracy and to the uncertainties in the empirical relationships  $Q_{2500}$  and  $\chi_{2500}$  (Sprintall, 2003; Sokolov et al., 2004). Sokolov et al. (2004) showed that the transport of the upper 2500 m accounts for about  $67.6 \pm 1.3\%$  of the total baroclinic transport. Utilising this number yields a total baroclinic transport of  $118 \times 10^6 \text{ m}^3 \text{ s}^{-1} \pm 19 \times 10^6 \text{ m}^3 \text{ s}^{-1}$  for the method based on  $Q_{2500}$  and  $133 \times 10^6 \text{ m}^3 \text{ s}^{-1} \pm 22 \times 10^6 \text{ m}^3 \text{ s}^{-1}$  for the method based on  $\chi_{2500}$  respectively. I then calculate the average of both estimates weighted by their variance, yielding a total baroclinic transport in June 2004 of  $124 \times 10^6 \text{ m}^3 \text{ s}^{-1} \pm 14 \times 10^6 \text{ m}^3 \text{ s}^{-1}$ .

The cumulative transports derived from the temperature transect of *Jason* are shown in Fig. 4.6b. This transport function further to the east in Drake Passage seems to lack small scale features. Unfortunately, I have no deep stations between 59°S and the Antarctic continental shelf and therefore might underestimate the transport through Drake Passage by lacking the SACCF transport. The main current is associated with the PF (Fig. 4.5b), hence the biggest increase of the cumulative transport is around 57°S. The method based on  $Q_{2500}$  shows a weak counter-current just south of the PF. As the SAF lies close to the continental shelf, the integrated data should be treated with care. The transports above and relative to 2500 m are  $70 \times 10^6 \text{ m}^3 \text{ s}^{-1} \pm 11 \times 10^6 \text{ m}^3 \text{ s}^{-1}$  ( $Q_{2500}$ ) and  $80 \times 10^6 \text{ m}^3 \text{ s}^{-1} \pm 13 \times 10^6 \text{ m}^3 \text{ s}^{-1}$  ( $\chi_{2500}$ ). Again, utilising the relationship between the transport in the upper 2500 m and the total baroclinic transport of Sokolov et al. (2004) yields a total baroclinic transport of  $104 \times 10^6 \text{ m}^3 \text{ s}^{-1} \pm 18 \times 10^6 \text{ m}^3 \text{ s}^{-1}$  and  $118 \times 10^6 \text{ m}^3 \text{ s}^{-1} \pm 22 \times 10^6 \text{ m}^3 \text{ s}^{-1}$  respectively for the transect of *Jason*. The weighted average of both transports in April 2005 is  $110 \times 10^6 \text{ m}^3 \text{ s}^{-1} \pm 14 \times 10^6 \text{ m}^3 \text{ s}^{-1}$ .

### 4.4.3 Estimating transports from density

Although relatively inexpensive, CTD-SRDLs deliver not only temperature data, but also provide conductivity measurements to calculate salinity (Fig. 4.3). Hence, I can calculate density and the internal pressure field, from which the relative geostrophic currents relative to the surface are calculated. I took the corresponding surface geostrophic velocities closest in space and time from the MADT dataset to derive a section of absolute geostrophic currents of the upper 1000 m of Drake Passage (Fig. 4.7). The standard deviation of this velocity field is expected to be less than  $0.1 \text{ m s}^{-1}$  (Rio and Hernandez, 2004). Using the upper ocean temperature relationships limits the dataset to profiles that are at least 700 m deep. Here I am not limited to these

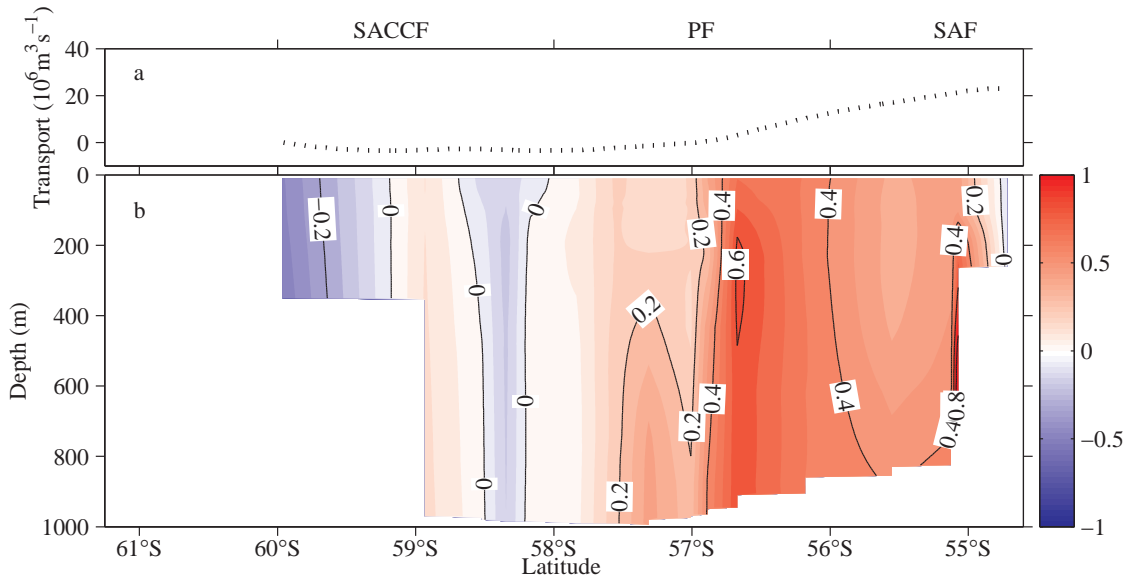


**Figure 4.7:** (a) Cumulative transport ( $10^6 \text{ m}^3 \text{ s}^{-1}$ ) (top) above 250 m depth (dotted line) derived from (b) absolute geostrophic velocities across the Drake Passage ( $\text{m s}^{-1}$ ) at the beginning of April 2005. Hydrographic data of *Jason* are used to derive relative geostrophic velocities and then corrected by corresponding surface geostrophic velocities obtained from Maps of Absolute Dynamic Topography. Positive velocities are to the east. Front locations are marked on the upper axis. **SACCF**: Southern ACC Front, **PF**: Polar Front, and **SAF**: Subantarctic Front.

deep profiles and can include shallower hydrographic profiles to extend the section further to the south and north, although I exclude profiles taken on the continental shelf. The flow can be seen to be ordered in vertically coherent, strong down-passage currents separated by much weaker mean currents. All three fronts are correlated with such strong current cores (Fig. 4.7). The SAF has a maximum velocity of more than  $0.4 \text{ m s}^{-1}$  just south of the position of the hydrographic front at  $55^\circ \text{S}$ . There is an indication of a stronger current core of more than  $0.8 \text{ m s}^{-1}$  below 400 m depth. Between the SAF and the PF lies a zone of eastward flow between  $0.4 \text{ m s}^{-1}$  and  $0.6 \text{ m s}^{-1}$ . The PF has two current cores at depth. The stronger one extends close to the surface north of the hydrographic-based position at  $57^\circ \text{S}$  with velocities higher than  $0.6 \text{ m s}^{-1}$ . Just south of the PF is a current core below 700 m depth with a maximum velocity of just over  $0.3 \text{ m s}^{-1}$ . Around  $58.4^\circ \text{S}$  lies a region with no flow to

the east and a slowly westward-flowing current core below 100 m depth. At 59°S the SACCF is visible with an eastward current of up to  $0.2 \text{ m s}^{-1}$ , although due to the lack of deep profiles further south, I miss the maximum current core. Nevertheless, this frontal jet supports the position of the SACCF based on the hydrographic data in Fig. 4.3. South of 59.5°S a westward flowing current marks the southern limit of the ACC and the position of the Antarctic Slope Front. In calculating the cumulative transport (Fig. 4.6b), the southern limit to the section means that the transport of the SACCF is not taken into account (Fig. 4.7). This is evidence that I underestimate the total transport across Drake Passage derived from the mass transport function  $Q_{2500}$  and the baroclinic transport stream function  $\chi_{2500}$ . The cumulative transport above 250 m depth is derived from the absolute geostrophic velocity section and shown in Fig. 4.7. The surface layer down to 250 m depth transports about  $38 \times 10^6 \text{ m}^3 \text{ s}^{-1} \pm 15 \times 10^6 \text{ m}^3 \text{ s}^{-1}$  to the east.

## 4.5 Discussion and Summary

### 4.5.1 Frontal structures

Various definitions exist for defining the positions of the ACC fronts (Orsi et al., 1995; Belkin and Gordon, 1996). Orsi et al. (1995) and Sprintall (2003) locate the SAF at the maximum subsurface temperature gradient between the 4°C and 5°C isotherms at 400 m depth, while I position the SAF at the 4°C isotherm at 300 m depth (Ch. 3). Both definitions give very close results when applied to the transect of *Jason* (Fig. 4.3). Very interesting is the wintertime occupation of Drake Passage by *Rudolph* (Fig. 4.2). Here, the definition of Orsi et al. (1995) would place the SAF incorrectly, while the definition in chapter 3 is still valid. This discrepancy is due to the fact that wintertime data of Drake Passage, which contributed to the definition of the criterion

in chapter 3, are rare and therefore not well-represented in the study of Orsi et al. (1995). The position of the SAF correlates closely with the mean frontal positions of chapter 3.

The PF is defined by the northernmost extent of the 2°C isotherm at 200 m depth (Orsi et al., 1995). This definition is also valid for the wintertime data in Fig. 4.2. The zone of nearly homogeneous water between the PF and the SAF can however blur this position. The position of the PF lies further north than the mean frontal position of chapter 3. However, I show that the position of the PF in Drake Passage is accompanied by a strong variability.

The subducting winter water in Fig. 4.3 can also distort the position of the PF when using this simple criterion. Orsi et al. (1995) constrain their definition by including the crossing of the temperature minimum layer from above to below 200 m depth, which would position the PF at the correct place. Nevertheless, this crossing of Antarctic waters across the PF and its influence on intermediate waters north of the SAF supports the arguments of freshening of intermediate waters in the Subantarctic Zone by Antarctic waters (*see* Meredith et al., 1999, and references therein). This modified water will ultimately contribute to the fresh Antarctic Intermediate Water (AAIW) layer north of the ACC and imprint characteristics of Antarctic origin on those derived by deep convection north of the SAF (Piola and Gordon, 1989; Talley, 1996).

Orsi et al. (1995) place the SACCF at the location where the temperature maximum layer is below 500 m depth and above 1.8°C, I apply a simple rule by selecting the 1.8°C isotherm at 500 m depth (Ch. 3). Both these definitions give the same results when applied to the transect of *Rudolph* (Fig. 4.2). The transect of *Jason* does not show such a clear vertical 1.8°C isotherm. However, the 1.8°C isotherm of the temperature maximum layer crossing the 500 dbar isobar and the current cores of Fig. 4.7 support the position of the SACCF at 59°S, which again agrees well with chapter

3.

Remotely-sensed sea surface temperature (SST) data are often used to determine the positions of the SAF and PF within the ACC (Moore et al., 1999; Dong et al., 2006). The meridional maxima of the SST gradient are allocated to the different ACC fronts. In this context, the very weak surface temperature signal of the SAF in Fig. 4.3 is interesting, supporting the argument of chapter 3 that the SST gradient across the SAF can be very weak in Drake Passage, and suggesting that remotely-sensed SST data are not always appropriate for determining the location of the SAF.

Figures 4.5 and 4.6 show that the main transport occurs very close to the three main ACC fronts. The transports derived from the high spatial resolution transect of *Rudolph* show many small current cores, resulting in a much more complex current system than the traditional conceptual model of the ACC frontal system. The high detail of the transports based on the method including shallower depths suggests that these weaker currents only occur in the upper layer. This branching structure of the ACC flow has also been observed in previous work (Moore et al., 1999; Sokolov and Rintoul, 2002; Lenn et al., 2007). Previous work using fine-scale sampling techniques in the upper waters of the Southern Ocean has also highlighted the complex nature of the ACC fronts. Pollard et al. (1995) used a towed undulator to obtain an upper-ocean hydrographic transect upstream of Drake Passage, and observed fine scale (5-10 km) undulations when crossing the ACC fronts here. Meredith et al. (2003b) made similar observations of ‘streakiness’ in the SACCF using 2 km-resolution data close to South Georgia. This was attributed to differential advection by the ACC fronts, with the large velocities advecting water mass properties along the axis of the front more rapidly than on either side, thus sharpening the cross-frontal gradients. I have demonstrated here that in situ fine-scale information on ACC frontal structures is obtainable with the CTD-tagged animals, and without recourse to cruise-based sampling.

In general, the fronts are better resolved in the transect of *Rudolph* (Fig. 4.2) than in the data of *Jason* (Fig. 4.3), due to the closer station spacing close to the fronts of *Rudolph*. *Rudolph* sampled 81 vertical hydrographic profiles with higher station density around the frontal positions. As a result, the horizontal detail of the frontal structures and the detail in transports across Drake Passage are better than analysis based on CTD sections (which typically consists of about 30 profiles), and hence are better able to resolve the fine-scale structures described above. XBT sections commonly have a greater detail, but lack in general salinity measurements. Typically these sections are also pre-planned, and so the spatial resolution is the same in the ACC zones as in the fronts, while seals target the fronts preferentially, which gives them great utility when wanting high spatial resolution in regions of rapid change over short distances.

This case shows that Southern elephant seals are ‘adaptive samplers’, directing sampling effort to particularly interesting and productive regions as they adaptively sample their environment based on previous experience. These foraging areas are also likely to coincide with the regions of most interest to oceanographers. This also has the added benefit that individuals are likely to retrace previous tracks, and can therefore provide repeat sections. Some seal species penetrate deep into polar regions where cloud and partial or near-total sea ice coverage can limit the applicability of oceanographic remote sensing, and where most profiling floats and ships cannot operate (Ch. 5).

### 4.5.2 Transports

The maximum transport per unit width above 2500 m at the position of the three major fronts of the ACC are between  $10 \times 10^6 \text{ m}^3 \text{ s}^{-1}$  and  $20 \times 10^6 \text{ m}^3 \text{ s}^{-1}$  (Fig. 4.5). Between the fronts lie regions of weak flow or counter-currents. The transect of *Rudolph*

shows a relatively strong counter-current of up to  $10 \times 10^6 \text{ m}^3 \text{ s}^{-1}$  to the west (Fig. 4.5) associated with the homogeneous water between the PF and SAF (Fig. 4.2). The eastward flows associated with the fronts can be distinct as derived from *Rudolph* or merge as the flow of the PF and SACCF do in the transect of *Jason*. The total transports of the fronts derived from Fig. 4.6 are between  $10\text{-}20 \times 10^6 \text{ m}^3 \text{ s}^{-1}$  for the SACCF,  $45 \times 10^6 \text{ m}^3 \text{ s}^{-1}$  for the PF and between  $10\text{-}35 \times 10^6 \text{ m}^3 \text{ s}^{-1}$  for the SAF. This correlates well with the results of previous work (Orsi et al., 1995; Sokolov and Rintoul, 2002; Sprintall, 2003).

The absolute geostrophic velocity section across Drake Passage at the beginning of April 2005 shows three current cores associated with the three fronts (Fig. 4.7). A low velocity of about  $0.2 \text{ m s}^{-1}$  is associated with the SACCF, while the PF and SAF show velocities of more than  $0.6 \text{ m s}^{-1}$ . These surface layer velocities and their vertically coherent structure correlate well with previous findings (e.g., Lenn et al., 2007).

I utilised relationships between upper ocean temperatures and stream functions to determine the cumulative baroclinic transports across Drake Passage based on two methods (Sprintall (2003) and Sokolov et al. (2004)). In general, transports  $Q_{2500}$  based on Sprintall (2003) are slightly lower than  $\chi_{2500}$  based on Sokolov et al. (2004) and show more detail. Sprintall (2003) showed that most of the mesoscale variability is only evident in the upper layer above 200 m depth.  $Q_{2500}$  incorporates this variability by including  $T_{100}$  and, therefore, shows a higher level of detail. I am able to resolve the high frequency variability in Drake Passage, only by including this upper layer into the estimates.

For the transect of *Rudolph* in June 2004, I estimate the total baroclinic transport to be  $124 \times 10^6 \text{ m}^3 \text{ s}^{-1} \pm 14 \times 10^6 \text{ m}^3 \text{ s}^{-1}$ . This agrees well with summertime estimates of previous work. I note however, that this is an estimate for the total baroclinic

wintertime transport through Drake Passage in June 2004 and I lack comparative data. The transect of *Jason* in April 2005 yields an estimate of  $110 \times 10^6 \text{ m}^3 \text{ s}^{-1} \pm 14 \times 10^6 \text{ m}^3 \text{ s}^{-1}$ . I assume that this is a low estimate, because of the limited data around the SACCF.

The total transport across Drake Passage in April 2005 in the upper 250 m is estimated at  $38 \times 10^6 \text{ m}^3 \text{ s}^{-1} \pm 15 \times 10^6 \text{ m}^3 \text{ s}^{-1}$  (Fig. 4.7). This estimate is higher than the mean transport of  $27.8 \times 10^6 \text{ m}^3 \text{ s}^{-1} \pm 1 \times 10^6 \text{ m}^3 \text{ s}^{-1}$  between September 1999 and December 2004 of Lenn et al. (2007). Lenn et al. (2007) also report that the upper 250 m account for 20% of the total transport. This yields a very high total transport of  $190 \times 10^6 \text{ m}^3 \text{ s}^{-1} \pm 75 \times 10^6 \text{ m}^3 \text{ s}^{-1}$  derived from the absolute geostrophic field, when compared to the total estimate based on the upper ocean temperatures. However, calculating the mean weighted by the variances based on all three transport estimates yields  $112 \times 10^6 \text{ m}^3 \text{ s}^{-1} \pm 14 \times 10^6 \text{ m}^3 \text{ s}^{-1}$  for April 2005.

In summary, a unique hydrographic dataset obtained by instruments attached to two Southern elephant seals reveals the frontal structure of the ACC and is analysed to estimate the total eastward transport in Drake Passage. New technology has enabled us to obtain an in situ dataset with high spatial resolution even in the wintertime across Drake Passage. The majority of the uncertainty is due to the accuracy of the sensors. New generations of animal-borne sensors have better sensors and higher accuracy. These high-accuracy sensors have the ability to collect large numbers of profiles cost-effectively, particularly at times where traditional oceanographic measurements are scarce. Southern elephant seals are ‘adaptive samplers’ with increased spatial resolution close to hydrographic fronts capable of resolving fine-scale structures in the frontal features, and are thus a powerful complement to the existing means of data collection. Future deployments will yield better estimates and provide further detailed information on the locations of the transport changes. These data will be of

great benefit in adding to the ship-derived Drake Passage transport estimates, and will help mitigate the seasonal bias in the in situ sampling of the ACC at this location. It is thus of great importance that the CTD-SRDL deployments are maintained, and enhanced in number, into the future.



## **5 Variations in behaviour and condition of a Southern Ocean top predator in relation to in-situ oceanographic conditions.**

Paper published in

Biuw, M., L. Boehme, C. Guinet, M. Hindell, D. Costa, J-B. Charrassin, F. Roquet, F. Bailleul, M. Meredith, S. Thorpe, Y. Tremblay, B. McDonald, Y-H. Park, S. Rintoul, N. Bindoff, M. Goebel, D. Crocker, P. Lovell, J. Nicholson, F. Monks and M.A. Fedak, 2007, Variations in behaviour and condition of a Southern Ocean top predator in relation to in-situ oceanographic conditions. Proceedings of the National Academy of Science, August 21, 2007, Vol 104, No. 34, pp 13705-13710, doi: 10.1073/pnas.0701121104

## **5.1 Preface**

This chapter presents the results of biological, physical and interdisciplinary work conducted predominantly by the lead author (Dr. Martin Biuw) and myself. Dr. Biuw led the ecological and behavioural aspects of the study. The physical oceanography aspects of the research, and the physical side of the interdisciplinary aspects, were led by myself.

## **5.2 Abstract**

Responses by marine top predators to environmental variability have previously been almost impossible to observe directly. By using animal-mounted instruments simultaneously recording movements, diving behavior, and in situ oceanographic properties, we studied the behavioral and physiological responses of Southern elephant seals to spatial environmental variability throughout their circumpolar range. Improved body condition of seals in the Atlantic sector was associated with Circumpolar Deep Water upwelling regions within the Antarctic Circumpolar Current, whereas High-Salinity Shelf Waters or temperature/salinity gradients under winter pack ice were important in the Indian and Pacific sectors. Energetic consequences of these variations could help explain recently observed population trends, showing the usefulness of this approach in examining the sensitivity of top predators to global and regional-scale climate variability.

## 5.3 Introduction

The Southern Ocean (SO) is one of the most productive of the world's oceans, mainly a result of short, intensive spring phytoplankton blooms (Smetacek and Nicol, 2005). Because of restrictions on land-ocean-atmosphere interactions by the Antarctic ice cap, nutrient supply via rivers and dust is generally small or absent. Input of sedimentary nutrients is limited to coastal shelves, whereas pelagic waters over deep basins can be enriched via nutrient release from melting sea ice (Brierley and Thomas, 2002), advection of nutrientrich water masses from upstream shelf regions (Sullivan et al., 1993), or upwelling from distant sediment sources (Prezelin et al., 2000). The spatial and temporal distribution of nutrients is therefore highly influenced by interactions between bottom topography, water mass properties, ocean currents, and sea-ice dynamics. Significant phytoplankton blooms occur mostly on continental or island shelves, in the wake of the retreating sea ice or along frontal systems within the Antarctic Circumpolar Current (ACC) (Moore and Abbott, 2000). Understanding the responses of higher trophic levels to such spatial and temporal variability is fundamental to the effective management of living resources in the SO, and for predicting how animals may respond to climate change and the consequent changes in ocean circulation, ice dynamics, and biogeochemistry.

It is often difficult or impossible to observe directly how marine predators interact with their environment and the prey within it. It is especially challenging to obtain information on diet and the distribution of potential prey for long-ranging migrating species. Stomach contents and fecal remains are rarely available, and sufficiently detailed surveys of prey distribution are often lacking. Most studies of foraging ecology of marine predators have instead attempted to correlate habitat use or movement patterns to environmental characteristics (McConnell et al., 1992; Pinaud and Weimerskirch, 2005; Lea and Dubroca, 2003). Such studies do not adequately examine prey

choice or food web interactions, but can characterize critical habitats for conservation and management purposes. Relating movement and behavioral data from animal tracking to specific local environmental features is also challenging. For instance, data on ocean surface properties may not be good indicators of environmental conditions relevant to deep-diving species, and subsurface data are often not available at relevant spatial and temporal scales. It is not surprising that some studies have found strong correlations between behavioral patterns and environmental characteristics (Lea and Dubroca, 2003; Guinet et al., 2001), whereas other results have been more ambiguous (Bradshaw et al., 2004).

To understand the effects of environmental variability on foraging success and, ultimately, reproductive performance requires not only direct measurements of reproductive output coupled with studies of movement patterns while at sea, but also some method of identifying where and when animals actually improve their body condition. Appropriate feeding indices are often difficult to obtain, and most studies instead use proxies such as changes in movement patterns and time spent within discrete areas. Although these patterns may indicate high search effort, they do not necessarily relate to foraging success or, even more importantly, changes in animal condition.

Southern elephant seals (*Mirounga leonina*) represent a unique opportunity for studying links between environmental variability, individual physiology, behavior, and population dynamics across a range of scales in space and time. They are long-ranging (McConnell et al., 1992; Hindell et al., 2003) and deep-diving (Hindell et al., 1992) predators that can potentially access a wide range of geographic and oceanographic regimes in the SO, from benthic shelf areas to midwater pelagic water masses. They require ample stored reserves obtained at sea to fuel their reproductive efforts on land. Declines occurred at key colonies in the Indian and Pacific sectors during the 1950s-1970s (Hindell and Burton, 1987; Guinet et al., 1999; Laws, 1994), whereas

populations in the Atlantic sector remained stable (McCann, 1985; Laws, 1994; Boyd et al., 1996). A recent reexamination concluded that changes in the marine environment were the most plausible cause of the observed declines (McMahon et al., 2005).

The diet of elephant seals is not well known. Because of their long migrations, stomach contents are almost entirely digested by the time seals return to land where prey remains can be studied. Cephalopods (squid and octopus) probably constitute their main diet (Clarke and MaxLeod, 1982; Rodhouse et al., 1992; van den Hoff et al., 2003), but new methods for diet study suggest that fish may, at least seasonally, make up a significant proportion (Bradshaw et al., 2003). The spatial and vertical distribution of potential prey species is also poorly understood, especially during the winter season. It is, nevertheless, critically important to describe seal movements and habitat use, and to describe the environmental features that characterize their feeding habitats. Movements, habitat use, and diving behavior have been intensively studied at some colonies (McConnell et al., 1992; Bradshaw et al., 2004; Hindell et al., 2003, 1991,?; Campagna et al., 1999), but there has been no comprehensive description of these across the entire range of the species. Attempts to physically characterize their feeding habitats have been limited to remotely sensed surface water properties.

Recent developments in animal-borne sensors and data loggers have resulted in an oceanographic instrument: the conductivity-temperature-depth satellite relay data logger (CTD-SRDL) (Lydersen et al., 2002), capable of providing high-accuracy vertical temperature/salinity (T-S) profiles relayed via satellite. See chapters 1 and 2 for details on instrument specifications, sensor accuracy, data compression, and transmission strategies, etc. When deployed on deep-diving and long-ranging marine vertebrates, these instruments provide extensive spatial coverage and high temporal resolution of key physical oceanographic variables while simultaneously resolving the spatial and temporal scales of importance to the behavior and physiology of individ-

uals. Species returning regularly to breathe at the surface (such as seals, whales, and turtles) allow data to be relayed via satellite in near-real time. This approach complements traditional oceanographic data collection methods, especially in logistically difficult regions such as the SO. Many seals inhabit seasonally ice-covered seas, and regularly dive beneath the ice where most ocean-observing techniques cannot operate effectively. Here, we present results from Southern Elephant Seals as Oceanographic Samplers (SEaOS), a circumpolar study demonstrating how this unique approach can be used to study interactions between large marine predators and their environment.

## 5.4 Results and Discussion

We deployed CTD-SRDLs on 85 Southern elephant seals from key colonies throughout the SO (Fig. 5.1) in the Austral summers of 2003-2006 at four locations: Macquarie Island (n=16), Kerguelen Islands (n=29), South Georgia (n=21), and South Shetland Islands of the Antarctic Peninsula (n=19), representing the main breeding populations around the SO (Fig. 5.1). Instruments were deployed in January and February at the end of the annual molt, and lasted throughout most of the Antarctic winter season (mean  $\pm 1$  standard deviation,  $160.9 \pm 83.3$  days). The longest track (326 days) covered the entire winter migration of a South Georgia female (February 14 to October 9, 2005). The tag remained attached during the 30-day breeding period at South Georgia, and covered almost the entire subsequent summer trip (November 8 to January 1). Overall, seals delivered  $2.3 \pm 0.4$  complete temperature (T)-S profiles per day, at an average spacing of 21.3 km (95% less than 62 km apart) (Fig. 5.2).

We assessed spatial and temporal changes in diurnal diving behavior by using weighted mean daytime and nighttime dive depths. These were calculated by using weights defined by Gaussian density curves centered at local noon and midnight, respectively, with the 5-95% interval extending to 3 h in either direction. Values

therefore represent the weighted mean dive depths over 6-h day and night periods. We estimated changes in body condition of seals from their buoyancy, measured by the vertical rate of passive descent or ascent during so-called ‘drift dives’. This method has previously been described by Biuw et al. (2003), and provides a qualitative, indirect measure of changes in relative fat content. Briefly, buoyancy of seals at depth is almost entirely determined by relative amounts of lipid and lean tissue, and important feeding habitats can be inferred by mapping the change in relative lipid content (i.e., buoyancy as measured by drift rate) across the animals’ range. Behavioral and physiological data were linked with the contemporaneous in situ measured physical properties collected by the seals, allowing us to study their responses to oceanographic features. See chapter 2 for details of sensor accuracy and compression algorithm. To define the most important seawater properties encountered by seals, Gaussian mixture models were fitted to the  $\Theta$  and S properties measured at the deepest point of each dive, where the entire range of a given property can be described by a mixture of several normal distributions. The individual mixture components (clusters) can then be conveniently defined by their means and standard deviations.

#### **5.4.1 Movements and Distribution**

The movements of the 85 seals extended the documented range of the species, and demonstrated the circumpolar coverage of their migrations, from subtropical waters in the north to continental polar waters in the south (Fig. 5.1). One conspicuous exception is the apparent avoidance of the Weddell Sea. Seals in the Atlantic sector did not cross the Weddell/Scotia Confluence into Antarctic waters. Instead, the majority remained within the ACC, and a few individuals migrated into waters to the north of the Subantarctic Front (SAF). Similarly, seals tagged at the South Shetland Islands that migrated east into the Atlantic Sector stayed north of the South Scotia Ridge

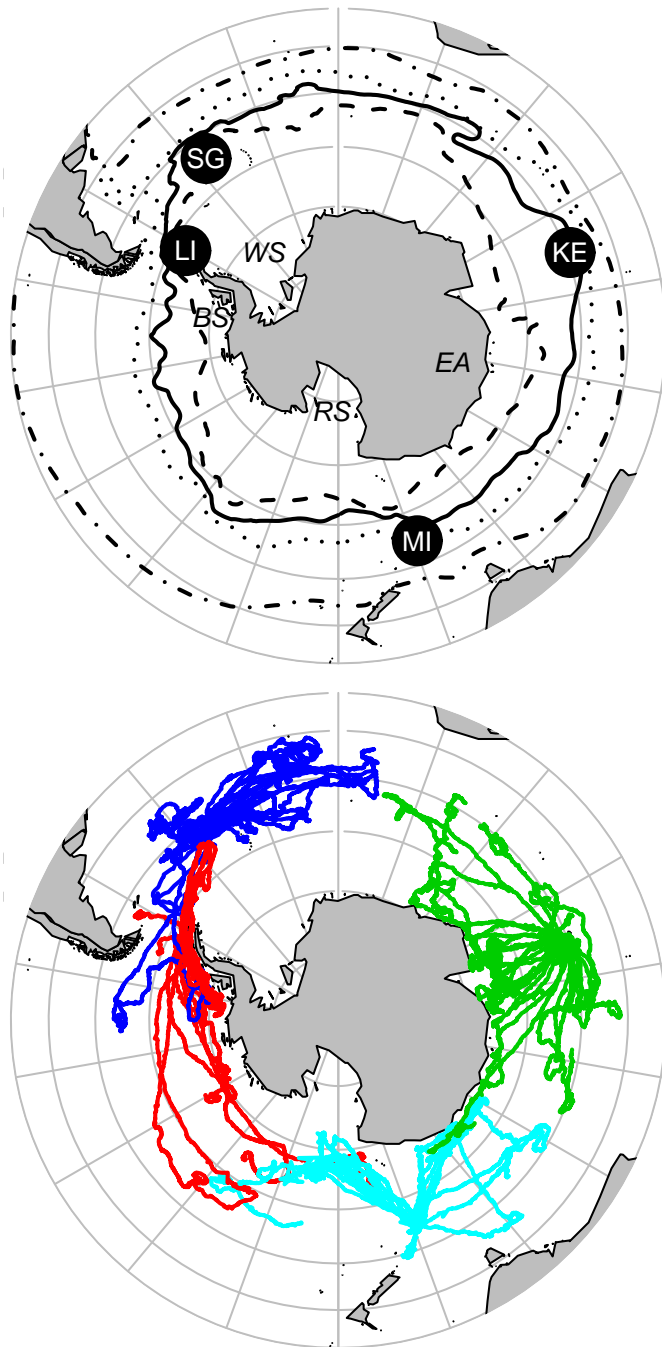


**Figure 5.1:** Orthographic view of the SO. (Upper) The four sites of instrument deployments are indicated by the filled black circles (SG, South Georgia; KE, Kerguelen Islands; MI, Macquarie Island; LI, Livingston Island), whereas the black lines represent mean locations of the major ACC fronts. From north to south, these include the Subtropical Front (dotted-dashed line) and SAF (dotted line) taken from Orsi et al. (1995), followed by the PF (solid line) and SACCF (dashed line), taken from Moore et al. (1999), the latter modified in the Scotia Sea region by data from Argo floats and CTD-SRDLs deployed on seals in this study (Ch. 3). The Weddell Sea (WS), East Antarctica (EA), Ross Sea (RS), and Bellingshausen Sea (BS) are also indicated. (Lower) The circumpolar movements of 85 Southern elephant seals between January 2004 and April 2006. Colors represent tracks from South Georgia (dark blue), Kerguelen (green), Macquarie (light blue), and the South Shetlands, Antarctica (red). Note the contrast between seals in the Atlantic sector showing a preference for ACC waters compared with the rapid southerly migrations by most Kerguelen and Macquarie seals across ACC waters toward the continental margin of East Antarctica or into the Ross Sea.

marking the border between the Scotia and Weddell Seas.

The only South Georgia seals to reach Antarctic waters did so along the shelf and shelf break west of the Antarctic Peninsula or in the Bellingshausen Sea during late

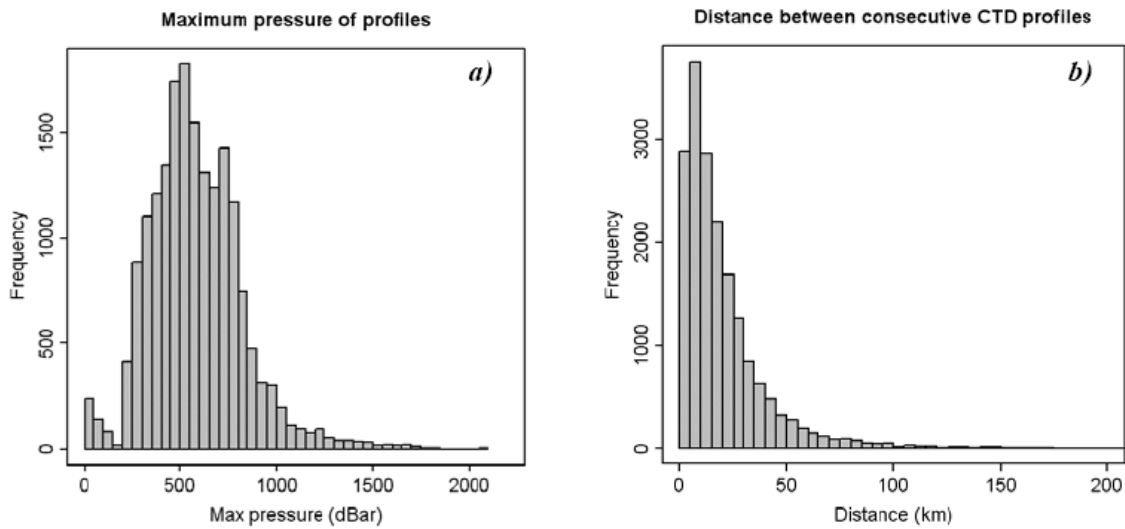


**Figure 5.2:** Histograms of (a) the maximum pressures of all T-S profiles and (b) the distance between consecutive T-S profiles obtained from the Southern elephant seals during the Southern Elephant Seals as Oceanographic Samplers (SEaOS) program.

summer before moving north into the ACC as the ice expanded in the autumn (Fig. 5.1). These patterns are consistent with previous studies (McConnell et al., 1992) suggesting limited use of Antarctic waters. Most seals from the South Shetlands remained on or close to the western Antarctic Peninsula shelf. However, some of the South Shetland seals undertook very long migrations to the west, either along the Antarctic Polar Front (PF) or the ice edge, overlapping with seals from the Macquarie Island population (Fig. 5.1). Migration patterns of seals from Kerguelen and Macquarie Island were less variable. Generally, a rapid southerly transit across the ACC frontal systems into Antarctic waters was followed by meandering movements, either in relatively confined, seasonally icecovered shelf waters along the East Antarctic coastline, or within the pack ice in the northern part of the Ross Sea (Fig 5.1). Few seals from Kerguelen and Macquarie remained within the ACC during the entire tracking period or moved northward into the ACC when the ice expanded in winter. In contrast to South Georgia, seals from these two populations spent very little time north of the SAF.

### 5.4.2 Diurnal Variations in Diving

Elephant seals from all colonies displayed strong diurnal patterns, presumably reflecting diurnal vertical migrations of prey. But day and night dive depths were not uniform across the SO. Overall, dives were deeper in the northern parts of the SO and became shallower toward the south. This was especially evident for nighttime dives, which were substantially deeper ( $>500$  m) north of the PF than further south ( $\approx 200$ - $400$  m; Fig. 5.3). The greatest diurnal differences were found between the SAF and the Southern ACC Front (SACCF), where seals typically dived to  $\approx 200$ - $300$  m at night and  $400$ - $600$  m or more during daylight hours. South of the SACCF, diurnal variations gradually diminished, in some regions because of the continental shelf where seals typically dived to or near the seafloor during both day and night. Interestingly, a similar pattern was observed over deep water in the northern Ross Sea, where dive depths were relatively consistent between  $200$  and  $400$  m, regardless of the time of day. Small-scale variations in dive depth were observed in some areas, such as within the main ACC system in the Atlantic sector (Fig. 5.3), possibly indicating association with high eddy activity and increased vertical mixing processes at these frontal regions.

### 5.4.3 Drift Rate and Relative Body Condition

Changes in animal buoyancy (i.e., relative fat content; see Biuw et al. (2003)) varied substantially across the SO (Fig. 5.4). For most South Georgia seals, the largest positive changes occurred within the ACC, especially between the SAF and the SACCF, but seals migrating to the west of the Antarctic Peninsula also displayed substantial positive changes while on the shelf break and in the Bellingshausen Sea. Most seals from Kerguelen and Macquarie showed strong negative changes while migrating across the ACC, especially between the PF and SACCF. In the Indian Ocean

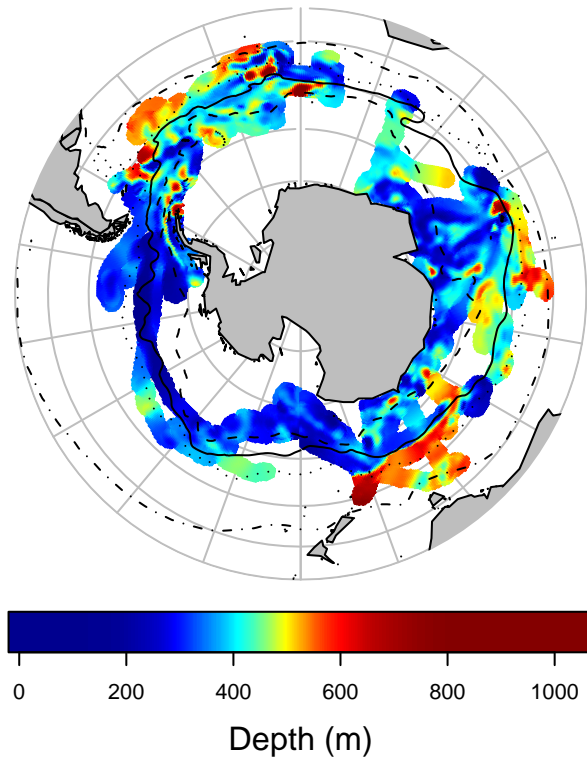


**Figure 5.3:** Circumpolar interpolated surface map of weighted mean nighttime dive depths of Southern elephant seals.

sector, this zone broadens meridionally around the Kerguelen Plateau (Orsi et al., 1995), representing a large region of apparently unfavorable foraging conditions. For these two populations, positive changes in drift rate were observed mainly south of the SACCF, either along the continental margin and shelf break along East Antarctica or within the marginal ice zone in the Ross Sea. Kerguelen and Macquarie seals remaining within the ACC showed positive changes mainly associated with the PF. There were many smaller-scale variations in the change in buoyancy, particularly in the Atlantic sector. These small-scale variations likely reflect the patchy distribution of prey resulting from the high eddy activity and small-scale dynamics of these frontal ACC regions.

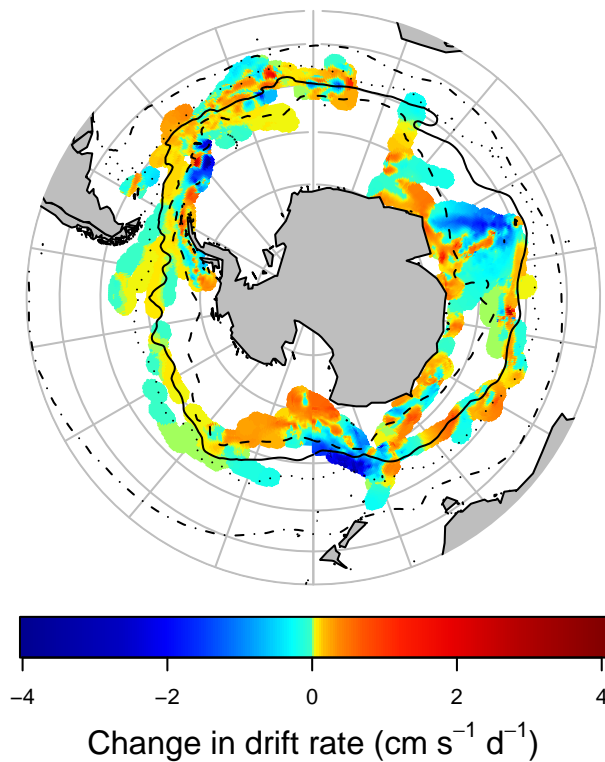


**Figure 5.4:** Circumpolar map of physiological changes during winter migrations of elephant seals. Daily change in drift rate was calculated for 36 individuals during their winter migrations in 2004 and 2005. Blue shading represents a decrease in vertical change in depth during passive drifts, indicating reduced relative lipid content, whereas green-red shading indicates increased vertical depth change and increasing relative lipid content. Interpolated surfaces were created by using the same mapping as that used for Fig. 5.3. Differences in coverage between here and Fig. 5.3 are a result of the fact that drift dives (for which vertical change of depth during passive drifts can be calculated) represent only  $\approx 8\text{-}10\%$  of all dives. Thus, this surface is calculated based on a smaller dataset than those in Fig. 5.3.

#### 5.4.4 Physical Ocean Properties

The following analyses focus on the seawater properties at the deepest point of each dive (Ch. 2). The South Shetland dataset was excluded from these analyses because

of the limited number of seals for which the entire set of physical and behavioral data were available. Seals from South Georgia encountered a wide range of physical water properties but tended to target waters typical of the ACC. Potential temperatures were relatively uniform at  $2.02 \pm 0.27^\circ \text{C}$ , whereas salinities showed two clusters at  $34.38 \pm 0.05$  and  $34.58 \pm 0.09$ . These values correspond either to Upper Circumpolar Deep Water or, in the case of the lower salinities, the boundary between Upper Circumpolar Deep Water and Antarctic Intermediate Water (AAIW) (Heywood and King, 2002). A smaller cluster was also observed at significantly higher temperatures and lower salinities ( $5.34 \pm 0.12^\circ \text{C}$  and  $34.16 \pm 0.08$ , respectively). These characteristics were observed mainly from one seal spending  $\approx 2$  months in a well defined area at  $\approx 20^\circ$  west of Drake Passage north of the SAF, and are consistent with deep-reaching highly mixed surface waters in late winter indicative of the formation of Subantarctic Mode Water and AAIW in this region (Tsuchiya and Talley, 1998).

Physical water properties encountered by Kerguelen and Macquarie seals were strikingly different from those for South Georgia seals, but were consistent with their geographic distributions. Although some seals remained in ACC waters similar to those of South Georgia seals [two potential temperature/salinity ( $\Theta$ -S) clusters at  $1.98 \pm 0.56^\circ \text{C}$  and  $34.38 \pm 0.13$  or  $34.60 \pm 0.06$ , indicating waters between the PF and the SAF], most used colder and/or more saline waters. The main cluster showed  $\Theta$ -S characteristics typical of waters of the Antarctic Slope Front and shelf waters, with temperatures approaching the seawater surface freezing point ( $-1.70 \pm 0.16^\circ \text{C}$ ) and salinities ranging from  $\approx 34.0$  to  $34.6$ . Some of these profiles measured along the continental margin of East Antarctica had  $\Theta$ -S characteristics consistent with High-Salinity Shelf Water, a precursor of Antarctic Bottom Water. These preferences were even more obvious when  $\Theta$ -S values corresponding to positive changes in drift rate were highlighted. Most of the positive changes for Kerguelen seals occurred in these extremely cold water masses associated with the Antarctic shelf regions (Fig. 5.5),

although  $\Theta$ -S characteristics associated with positive changes in drift rate for the few individuals remaining within the ACC were similar to those of the majority of the South Georgia seals. Although temperatures close to the freezing point were also observed in profiles from Macquarie seals over deep water in the Ross Sea pack ice, seals in this region appeared to favor warmer waters ( $1.47 \pm 0.13^\circ \text{C}$ ) with salinities of  $34.70 \pm 0.52$ . This corresponds to the subsurface  $\Theta$  and S maxima at depths of  $\approx 200$ - $300$  m, immediately below the permanent thermocline at the interface between cold winter surface waters and the Circumpolar Deep Water. This is consistent with the lack of diurnal pattern in this region and the restricted vertical depth coverage, suggesting that elephant seals feeding within the pack ice over deep basins dive through the cold surface mixed layer to target sharp discontinuities that may represent important overwintering areas for mesopelagic fauna (Lawson et al., 2003). Most of the observed positive changes in drift rate for Macquarie seals occurred within these well defined  $\Theta$ -S and depth ranges, although some also displayed positive changes in waters encountered within the ACC with characteristics typical for the SAF ( $2.52 \pm 0.20^\circ \text{C}$  and  $34.17 \pm 0.13$ ).

#### **5.4.5 Global Snapshot of Elephant Seal Habitats**

This study of Southern elephant seal migrations from some key breeding and moulting sites during their long-ranging winter feeding migrations provides a unique simultaneous circumpolar view of the habitat use of any SO predator. The in situ hydrographic measurements of water masses across both their horizontal and vertical ranges also provide a direct description of the detailed environmental conditions experienced by them. Because our information about the distribution and abundance of potential prey is sparse at best, this study does not attempt to correlate seal movements, behavior, and changes in condition to prey fields and diet per se. Our approach instead

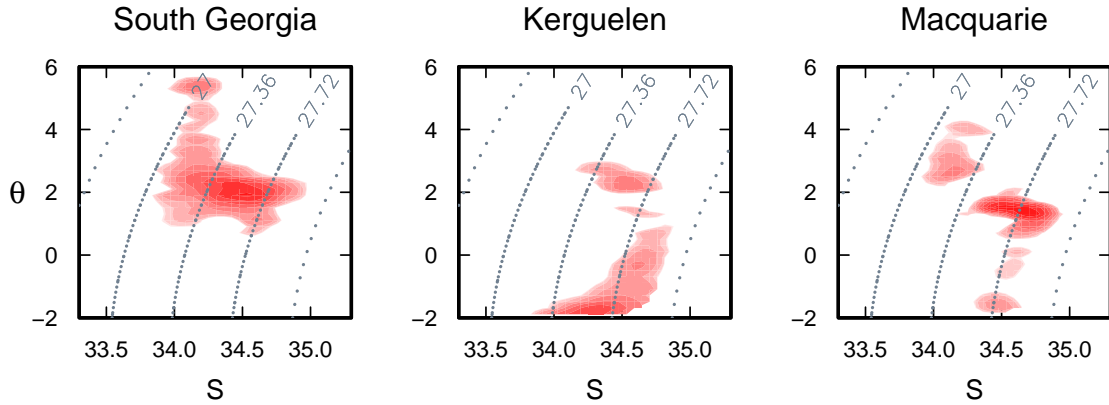


**Figure 5.5:** In situ  $\Theta$ - $S$  measurements collected by instruments deployed on Southern elephant seals at three of the main locations (South Georgia, Kerguelen, and Macquarie Island). The curved dotted lines indicate the water density corresponding to these  $\Theta$ - $S$  properties. The red surfaces represent kernel densities of  $\Theta$ - $S$  properties at the bottom of dives. Initially, two density surfaces were created for each location: one using only those dives occurring during periods of positive change in drift rate (i.e., periods of increasing relative lipid content) and the other based on dives during periods of negative change. The displayed surfaces represent the positive minus negative density surfaces, and the color intensity therefore highlights areas of predominantly increasing lipid content. Kernel surfaces were created by using a  $50 \times 50$  grid over the range of  $\Theta$  and  $S$ , yielding a resolution of  $0.056 \times 0.199$  for  $\Theta$  and  $S$ , respectively.

attempts to characterize the foraging habits of elephant seals in terms of the physical environment processes that influence nutrient availability and biological productivity. In the highly dynamic three-dimensional marine environment where geography alone is a poor descriptor, the in situ oceanographic measurements obtained by the approach presented in this paper provide a detailed description of these physical characteristics at spatial and temporal scales relevant to the animals.

The most obvious emerging pattern is the substantial basin-scale difference in habitat use by seals in the Atlantic sector in contrast with those in the Indian and Pacific sectors. The ACC frontal systems in the Atlantic are known for their comparatively high primary productivity (Holm-Hansen et al., 2004), presumably driven by a combination of iron enrichment from nearby shelf areas (Sullivan et al., 1993) and possibly

upwelling of Circumpolar Deep Water enriched in nutrients from sources in, for example, the North Atlantic. ACC frontal systems in the Atlantic sector may therefore represent an accessible and predictable resource for South Georgia seals. Although similar processes of nutrient enrichment have also been described from island shelf regions in other sectors of the SO, such as around Crozet (Pollard et al., 2002) and Kerguelen (Bucciarelli et al., 2001), these regions are substantially smaller than those in the Atlantic sector. The high upwelling and diffusivity rates reported for the Scotia Sea (Naveira Garabato et al., 2004) may also cause higher nutrient enrichment and hence support higher primary production than in other regions. These differences may explain the high usage of the ACC frontal system by South Georgian seals, whereas this strategy was much less common among seals from Macquarie and Kerguelen. During the shorter summer migrations between breeding and molt, seals from Macquarie and Kerguelen may be restricted to more northern regions closer to their colonies (Bradshaw et al., 2004), leading to migration patterns more similar to those from South Georgia. Nevertheless, it seems clear that the South Georgia population operates within different oceanographic regimes from other populations, at least during the winter migration.

Our findings are summarized schematically in Fig. 5.6, which compares hydrographic properties ( $\Theta$ -S) measured by seals with historical data along a representative SO vertical section. It is clear from this figure that areas in which elephant seals show positive changes in body condition can be characterized by specific hydrographic properties, and that these properties follow the general horizontal and vertical circulation regimes of the SO. In general, within the ACC, regions of upwelling of nutrient-rich Circumpolar Deep Water are clearly favored, whereas there is an almost total avoidance of AAIW. South of the ACC, favorable conditions are mainly found beneath the seasonally mixed layer, in waters that feature temperature and salinity maxima derived from the Lower Circumpolar Deep Water. In the subpolar gyres, this water is

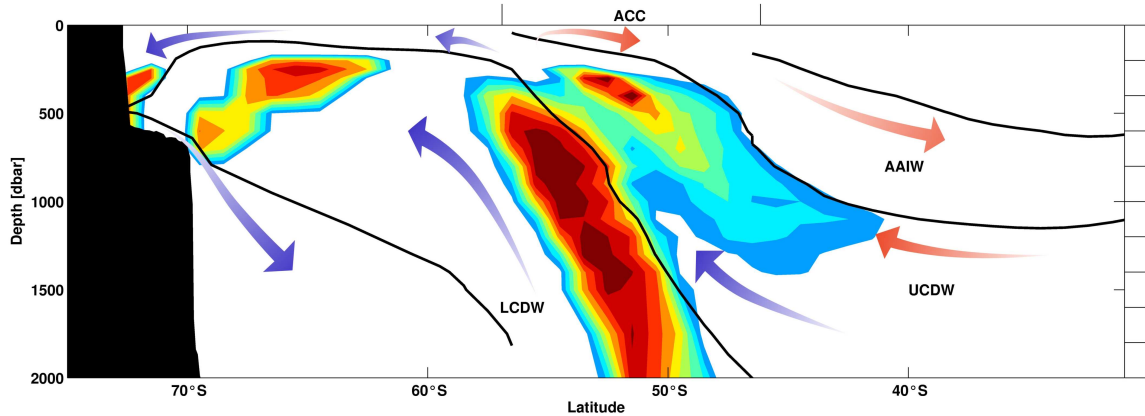


**Figure 5.6:** Generalized section of the SO, highlighting areas where Southern elephant seals are predicted to change their relative body fat stores. We used typical sections of temperature and salinity from the Levitus  $1^\circ$  dataset (Levitus et al., 1994). The derived potential density values were matched to those in table 2 in Heywood and King (2002) to highlight the main water mass boundaries between AAIW, Upper Circumpolar Deep Water (UCDW), and Lower Circumpolar Deep Water (LCDW). Colored contours represent the accumulated number of matches between temperature, salinity, and derived density values obtained from seals, and corresponding values in the schematic hydrographic section. We used only values at the deepest point of each profile, and only those profiles obtained during periods of positive change in drift rate. The arrows indicate the main circulation pathways as summarized by Toggweiler et al. (2006). Note the preference for upwelling regions of Circumpolar Deep Water and water mass transformation regions adjacent to the Antarctic continent, and the avoidance of regions of AAIW subduction. The gradual deepening of predicted regions to the north agrees well with the patterns of daytime and nighttime dive depths shown in Fig. 5.3.

often termed Warm Deep Water. Another region of positive change in body condition corresponds to the sinking and spreading of mixed waters to the south of the Antarctic Slope Front. The predicted depth ranges correspond well with those observed and presented in Fig. 5.5, including the gradual deepening to the north within the ACC.

#### 5.4.6 Ecological Implications

The observed differences in the occurrence of positive changes in drift rate between populations could have important consequences for the energy budgets of these animals. As an example, our results suggest that seals from Kerguelen and Macquarie may spend four times longer in transit compared with their South Georgia coun-

terparts before they show signs of improved body condition. Seals from Kerguelen and Macquarie may therefore spend as much as one extra month in transit during a roundtrip winter migration and travel an extra distance of >1,000 km. Using equations of the diving metabolic rate of grey seals (Sparling and Fedak, 2004) scaled up to the body size of elephant seals, we estimate that this corresponds to the expenditure of four to five times more energy, which must be recouped by a higher net energy gain while on the feeding grounds to ensure an unchanged overall net energy balance over the entire trip. Based on estimates of reproductive expenditure of female elephant seals (see, e.g., Fedak et al. (1996)), a breeding female at Kerguelen or Macquarie that is unable to recoup this additional expenditure at sea would have to reduce her reproductive expenditure on land by  $\approx 10\text{-}20\%$  compared with her South Georgia counterpart, either by reducing the energy and material transferred to her pup or by somehow reducing her metabolic overheads. This could have a negative effect on the subsequent survival of their pups, particularly in years of low or uncertain summer food abundance.

Although these estimates are relatively imprecise and do not take individual variation in energy budgets into account, they nevertheless suggest a simple mechanism that may contribute to the different population trends observed for these populations during the 1950s-1970s. There is evidence for a significant decline in Antarctic sea ice extent through this period along the coast of East Antarctica (Curran et al., 2003), whereas some other regions (notably the Weddell Sea) remained relatively unchanged (Murphy et al., 1995). The hydrographic properties we identified as key features of favorable feeding regions depend partially on sea ice dynamics. It is likely that such changes in circulation patterns and ice conditions may affect prey abundance and/or distribution and, ultimately, the net energy gain of seals while at sea. This discussion suggests possible mechanisms by which environmental variation can affect individual behavior and ability to obtain sufficient energy stores to allow them to reproduce

successfully, and exemplifies a promising approach for studying these interactions. As pointed out in Stevenson and Woods (2006), such detailed individual studies are also crucial for understanding population changes and how they are affected by environmental variability.

## 6 Discussion

The year 2007 was an exceptional one. Measurements in the Arctic showed that the extent of sea ice in August was almost a third below the long-term average, exceeding all previous records<sup>1</sup>. Torrential rain and thunderstorms spread across Asia, killing hundreds and displacing millions across Bangladesh and North India. Widespread flooding occurred throughout the United Kingdom killing at least 10 people. Corals in the Pacific ocean were dying faster than previously thought, having declined by 20%. However, the global temperature for 2007 was the same as that for 2006. All these events are linked by ocean observations, without which we wouldn't be able to predict weather, shrinking sea ice and climate.

The Global Ocean Observing System, which monitors the open ocean, is composed of a network of profiling floats, moorings and repeat hydrographic sections. The biggest gaps in this network occur in polar regions, close to and underneath the sea ice. However, observations and model simulations indicate that polar regions are particularly sensitive to climate change, with the potential for significant feedbacks involving sea ice, the ocean carbon cycle and global thermohaline circulation. The lack of observations means that our ability to detect and interpret change is poor, particularly in the Southern Ocean, where the ocean beneath the sea ice remains almost entirely unobserved. Understanding the large and small scale processes in the Southern Ocean and their effects on climate will improve our predictions of climate

---

<sup>1</sup>[http://nsidc.org/news/press/2007\\_seaiceminimum/20071001\\_pressrelease.html](http://nsidc.org/news/press/2007_seaiceminimum/20071001_pressrelease.html)

change. One hope is that the International Polar Year, which also started in 2007, will not only provide new circumpolar measurements, but will also provide the basis for long-term observations in the polar regions as part of the Southern Ocean Observing System.

The purpose of this thesis has been not only to aid better understanding of the most prominent feature of the Southern Ocean, the ACC, but also to provide the basis for animal-borne sensors to be integrated into existing ocean observing systems. Therefore this dual purpose resulted in a very broad-based thesis, ranging from technical topics regarding sensors, via physical oceanography to relating animal behaviour to their immediate physical environment. On this account, I organised the general discussion into three main topics. First, I will summarise and discuss the use of animal-borne sensors in oceanography. Then, I discuss the frontal system of the ACC in the Atlantic sector and finally, discuss the links between marine animals and their physical environment.

## **6.1 Animal-borne sensors in oceanography**

I have shown that animal platforms present a complement to the existing observing systems. CTD-SRDLs were attached to marine animals and reported vertical profiles of salinity, temperature and pressure to depth of up to 2000 m. This is not a new idea, but the Sea Mammal Research Unit together with Valeport Ltd. were the leading forces in developing a CTD sensor, small enough yet accurate enough to be integrated into existing animal tags (Ch. 2).

### 6.1.1 Sensor accuracy

Recent studies show that mid-depth Southern Ocean temperatures have warmed by as much as  $0.17^{\circ}\text{C}$  since the 1950's (Gille, 2002), but long-term changes in the ocean temperature are usually of the order of  $0.01^{\circ}\text{C}$  per decade (Zenk et al., 2003; Fukasawa et al., 2004). To incorporate ocean temperature and salinity data into oceanographic datasets the accuracy should be in the order of 0.1 and to play a role in the study of global climate change the accuracy needs to be better by at least one order (Ch. 2).

The sensor head of CTD-SRDLs is constantly evolving and, at the moment, lab calibrations of CTD-SRDLs show an accuracy of better than 0.01 in temperature and salinity (Ch. 2). Thus, the sensors are supposed to be of at least same quality as XBT data (Boyd and Linzell, 1993) and close to the accuracy demanded by the Argo project for profiling float accuracy (Wong et al., 2003; Gould et al., 2004; Boehme and Send, 2005). However, similar to the Argo floats, recalibrations are difficult to conduct. So, a remote delayed-mode quality control system needs to be set up and the algorithms used by the Argo community offer the best results (Bacon et al., 2001; Wong et al., 2003; Boehme and Send, 2005). Unfortunately, the high variability in the Southern Ocean yield high uncertainties for the estimated corrections (Ch. 2). In addition, the lack of historical reference data complicates the interpretation of an estimated correction even further. The difference between a CTD-SRDL measurement and a calculated reference (Wong et al., 2003; Boehme and Send, 2005) can be due to a sensor drift and/or a change in watermass properties since the historical reference profiles were made. One way to improve this technique is to get as many accompanying reference CTD profiles as close by in time and space as possible. Another way to improve the quality of this technique is to use data of the CTD-SRDLs themselves, when enough different CTD-SRDLs are operating in the same area as described in Boehme (2004). Other methods can be used in conjunction with these fundamental

comparisons. One possibility is, for example, to analyze the differences and complementarities between altimeter sea level anomalies based on satellite measurements and CTD-SRDL data at different time and space scales. Comparisons of CTD-SRDL derived dynamic height with altimeter sea level anomalies could be particularly instrumental in detecting systematic errors from specific CTD-SRDL sub-sets (Guinehut, pers. comm.).

Nevertheless, I have shown that the accuracy of CTD-SRDLs is in the order of other traditional oceanographic measurements techniques and are a very useful tool for ocean observations.

### **6.1.2 Spatial and temporal coverage**

I have shown that CTDs on animal platforms can deliver data from large scale, ocean basin wide observations (Ch. 3) to small scale, localized observations (Chs. 1, 2 and 4). Depending on their software configuration, CTD-SRDLs can deliver more than 4 CTD profiles a day for up to several months (Chs. 1 and 2). By getting in situ measurements on such short temporal scale in the Southern Ocean we might be able to investigate the short-term variability of the ACC for which sampling intervals very much shorter than 10 days are needed (Meredith and Hughes, 2005).

When deployed on wide ranging marine animals, CTD-SRDLs deliver also a huge spatial dataset, e.g. Southern elephant seals travel up to 12000 km during their migration between moulting and breeding (Fig. 6.1). The main advantage in this context is that they are not bound to ocean currents, but hydrographic sections across main ocean currents (e.g. ACC) are obtainable on a regular basis (Ch. 4). On the other hand, by choosing a species linked to a certain habitat (e.g. Weddell seals), data from a specific location over a long period can be obtained (see Chs. 1 and 2). The spatial resolution during such deployments can be below 10 km (Chs. 2 and 4). Here, the

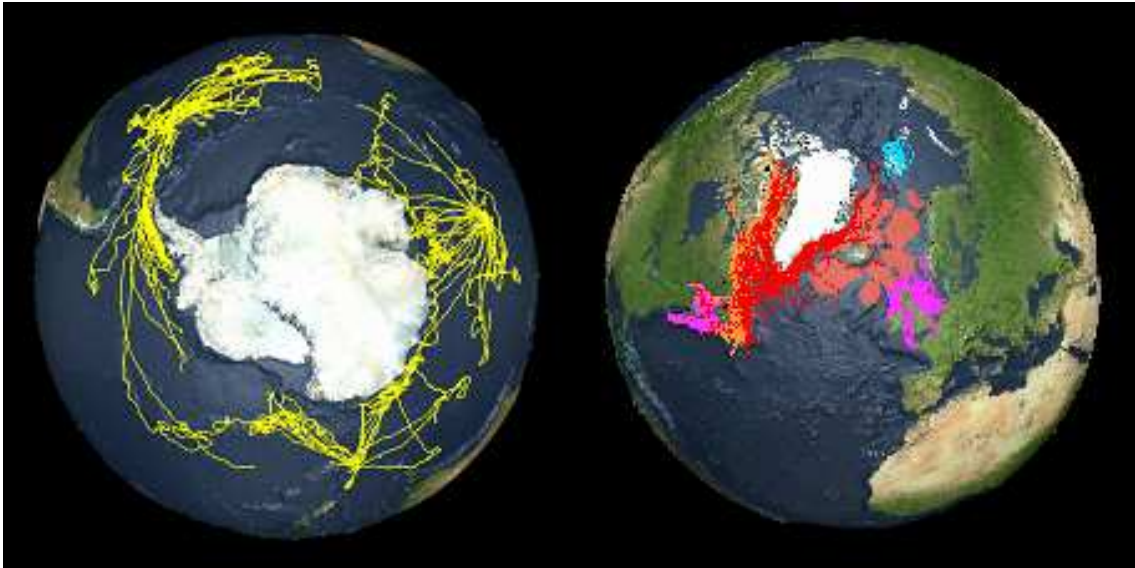


**Figure 6.1:** Animal tracks from previous studies in the Southern Ocean (on the left) and in the North Atlantic (on the right). The same coverage will be provided during the International Polar Year by joint efforts from the UK, France, Norway, Australia, USA, South Africa, Germany, Brazil and Canada.

information collected by biologist helps to find the right animal for the job. Such a temporal and spatial coverage is unmatched by any other traditional oceanographic instrument.

This thesis shows also that certain marine mammal species are ‘adaptive samplers’, directing sampling effort to particularly interesting and productive regions as they adaptively sample their environment based on previous experience (Ch. 4). CTD-SRDLs on such animals deliver a higher horizontal resolution close to such regions, e.g. ocean fronts, even when the CTD-SRDL is set up to transmit ‘only’ 2 profiles a day (Ch. 4). Marine mammals are also likely to retrace previous tracks, and can therefore provide repeat sections (Fig. 6.2).

During the International Polar Year, animal-borne sensors will be deployed on a range of species in polar regions to cover the Southern Ocean and the polar part of the North Atlantic (Fig. 6.1) as part of the MEOP (Marine Mammal Exploration of the Oceans Pole to Pole) project. MEOP is based on the success of SEaOS and started

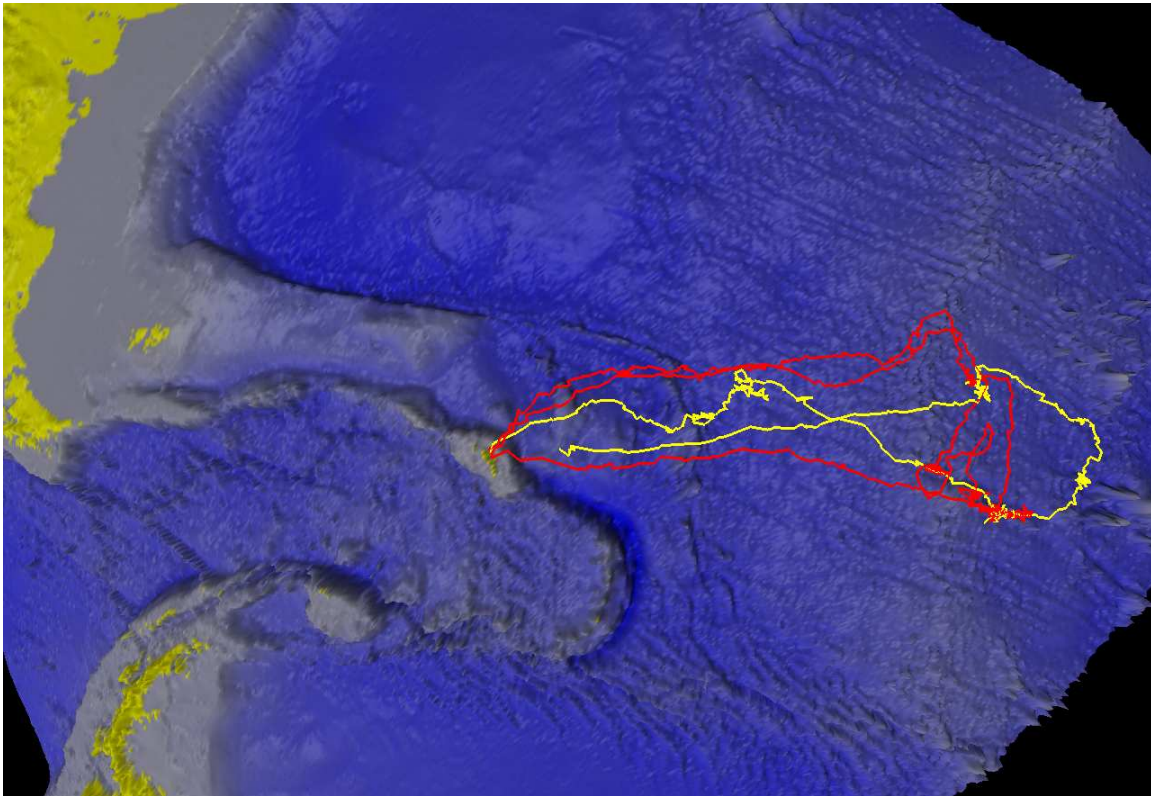


**Figure 6.2:** Migration of the Southern elephant seal *Bernt* tagged in 2005 (red and figure 6.5) and retagged in February 2008 (yellow).

in July 2007. This project will provide a unique source of fundamental physical and biological data from both polar oceans.

### 6.1.3 Ocean Observing System

In chapter 4, I show that the CTD-SRDLs have enabled us to obtain an in situ dataset with high spatial resolution even in the wintertime across Drake Passage. Weddell seals provide data from even further south (Ch. 2). By sampling the ocean during winter, CTD-SRDLs fill a ‘blind spot’ in the sampling coverage of existing ocean observing systems. Another benefit of animal-borne sensors is that some marine mammals live beneath the sea ice and can carry sensors to obtain oceanographic data from such important but undersampled regions (see Chs. 1 and 2).

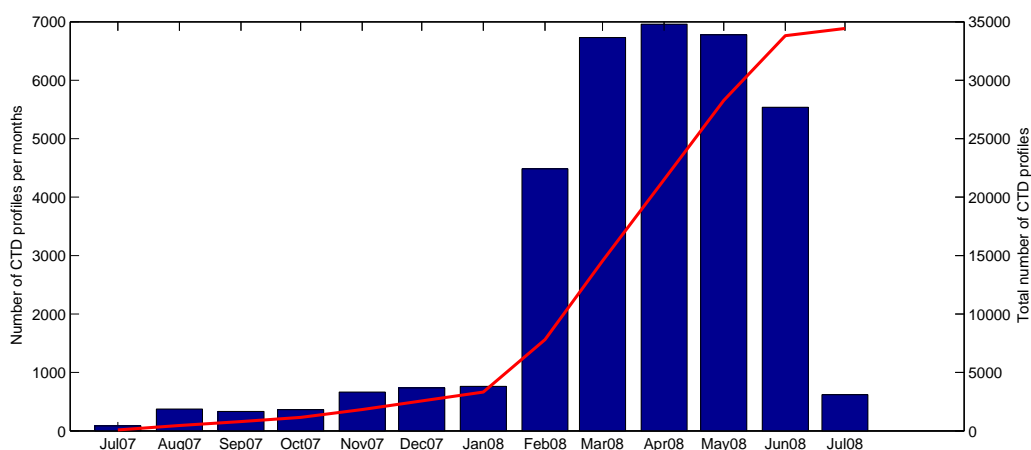


**Figure 6.3:** Number of CTD profiles collected per month during the MEOP project (bars) and cumulative sum of profiles since July 2007 (solid line).

Not only does the possible spatial and temporal coverage of animal-borne sensors make them a suitable for integration into the Global Ocean Observing System, but their real-time data transfer makes them a valuable tool for short term weather and ocean forecast systems. The data of the SEaOS project will be integrated into a new version of the World Ocean Database and is already submitted to the British Oceanographic Data Centre (BODC). Data collected within the MEOP project are not only archived for post-deployment analysis, but are also freely available in near real-time. These data are being distributed via the World Meteorological Organization (WMO) Global Telecommunication System (GTS) to operational forecasting centres where they can be assimilated into models that are run to provide ocean forecasts and long-range seasonal and climate predictions. This system started working at the beginning of July 2008 and is part of the UK project Oceans 2025. More than 33500 CTD profiles were eligible for transmission on the GTS by beginning of July 2008 with more than 150 CTD profiles forwarded per day.

Forwarding the CTD-SRDL data in near real-time onto the GTS is just one step to make such data freely available and useful for a wider audience. In the future,

CTD-SRDL data will be forwarded and processed at data centres, e.g. the BODC and Coriolis, to provide quality controlled data.

#### **6.1.4 The future of animal-borne sensors in oceanography**

Animal-borne sensors have many advantages when incorporated into ocean observing strategies. Two main issues will determine the future of animal-borne sensors during the next decade. Firstly, we have to improve the efficiency and sensor performance. The second question is how animal-borne sensors will combine with other autonomous instrumentation in a comprehensive ocean observing system.

In this thesis, I have discussed the first issue in detail showing both the limitations and the strengths of animal-borne sensors in measuring ocean data. The main constraints on the design are power consumption and size. The size limits the use of ‘off the shelf’ sensors to be incorporated into the existing CTD head (Ch. 2). Nevertheless, we are in the process of developing a miniature chlorophyll-a sensor as an add-on to the existing system, with a feasibility study by French collaborators on Kerguelen, who deployed such a system on Southern elephant seals in February 2008. These SRDLs deliver CTD and fluorescence data from the shelf region of the antarctic continent. In the future, additional sensors will be either incorporated into the CTD head or provide complete new sensor heads focussing on e.g. biochemical measurements.

I have shown that CTD-SRDLs can deliver broad- and small-scale observations. However, their accuracy is less than ship-based measurements, the vertical resolution is less than most traditional techniques and CTD-SRDL data are limited to animal habitats, e.g. cannot deliver data from below ice shelves, where e.g. gliders and AUVs can be used to obtain high-resolution data. Nevertheless, the strength is their complementary character to existing techniques. Oceanographers are not only able to extend the temporal and spatial resolution of existing datasets (Chs. 3 and 4), but they can

also fill in some ‘blind spots’ by using CTD-SRDLS. The ACES-FOCAS BAS core project deployed four tags on Weddell Seals in the southern Weddell Sea in early 2007 and, by September 2007, over 1300 profiles to depths greater than 300 m had been obtained from over the continental shelf (Ch. 2). This deployment increased the number of existing CTD profiles in this area by one order, despite the fact that most historical profiles were from the summertime. In the wintertime the profiles transmitted by the CTD-SRDLS were more than 1500 km from the ice edge deep in the pack ice. A truly unprecedented dataset in both temporal and spatial resolution. Such difficult-to-access regions are the natural niche for CTD-SRDLS in the future and other such developments are being actively pursued, including bids to the Antarctic Funding Initiative and elsewhere.

## **6.2 The frontal system of the ACC**

It is an unfortunate fact that one of the most informative parts of the ocean is also the least hospitable, the Southern Ocean around Antarctica. The ACC, which dominates the circumpolar flow in the Southern Ocean, is a critical component of the ‘Great Ocean Conveyor Belt’, but we have only just started to develop the tools to observe the variability of the ACC at high spatio-temporal resolution using in situ data.

### **6.2.1 The variability of the ACC**

Previous studies describing the Southern Ocean on a coarser scale were hampered by the lack of in situ data, cloud cover or low spatial resolution. None of these studies describe the three major fronts of the ACC (SAF, PF and SACCF) simultaneously with good spatial and temporal coverage. Orsi et al. (1995) and Belkin and Gordon (1996) were the first to map the circumpolar distribution of the Southern Ocean fronts,

but the lack of in situ data only allowed a very limited view at the average positions of the different fronts. This thesis shows that by combining data from animal-borne sensors with Argo float data, we are able to investigate the variability of the frontal system from Drake Passage to the Mid-Atlantic Ridge on short temporal scales (Ch. 4). This comprehensive dataset collected in 2004 and 2005 enabled us to map the monthly positions of the SAF, PF and SACCF. The striking feature here are the more northerly positions of the Subantarctic Front, the Polar Front and the Southern ACC Front between South Georgia and the Mid-Atlantic Ridge compared to their historical mean positions (Fig. 6.4). A recent paper (Fyfe, 2006) argued that the observed warming of the Southern Ocean (Gille, 2002) is anthropogenic in origin, and related to a southward shift of the ACC caused by an increase in zonal winds. However, this is based on coarse-resolution modeling, and whilst there has been some support for a southward shift of the ACC from satellite studies (Dong et al., 2006), it is important to note that satellites are really only effective at tracking the Polar Front or the Subantarctic Front, not the whole ACC, and there are questions concerning how well the surface features reflect deep frontal expressions. In addition, this thesis shows that even the Polar Front and Subantarctic Front are sometimes without corresponding surface expression (Ch. 3) and in situ data are necessary.

Previous work and this thesis show that the ACC shows variability on time scales from days to years. This high variability in time and space makes it difficult to monitor the transport variability with repeat hydrographic sections. Nevertheless, this thesis shows that such data might be capable on longer timescales (decadal) of monitoring changes in the ACC (Chs. 3 and 4), but there is a need to increase the amount of wintertime in situ data to minimise aliasing. This is a difficult task and only achievable by maintaining the ship-based sections and enhancing the number of CTD-SRDl deployments into the future, thus enabling us to address interannual variability (Fig. 6.5).

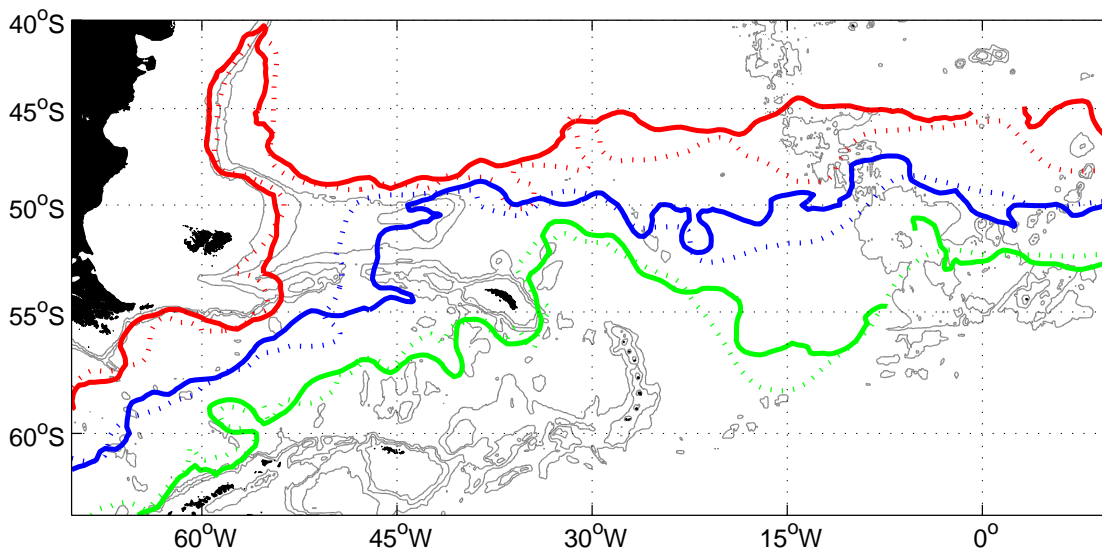


**Figure 6.4:** Comparison of the mean positions of the Subantarctic Front (red), Polar Front (blue) and Southern ACC Front (green) between previous work by Orsi et al. (1995) and Thorpe et al. (2002) (dotted) and from this thesis (solid)

By using empirical relationships between upper ocean temperatures and baroclinic mass transport we determined the transport through Drake Passage (Ch. 4). The mean total baroclinic transports in June 2004 and April 2005 are estimated to be  $124 \pm 14$  Sv and  $112 \pm 14$  Sv respectively. But CTD-SRDLs deliver also salinity and the relative geostrophic currents relative to the surface are calculated. By combining the data with the now freely available maps of absolute dynamic topography a section of absolute geostrophic currents of the upper 1000 m of Drake Passage (Fig. 4.7) was derived. At longer periods these new data may help define more robust transport means of the ACC, if sustained over several decades.

### 6.2.2 The branching of ACC fronts

Previous work and chapters 3 and 4 show that the ACC includes three major fronts (SAF, PF and SACCF), which coincide with particular water mass features. This means that simple phenomenological criteria such as the location of a particular

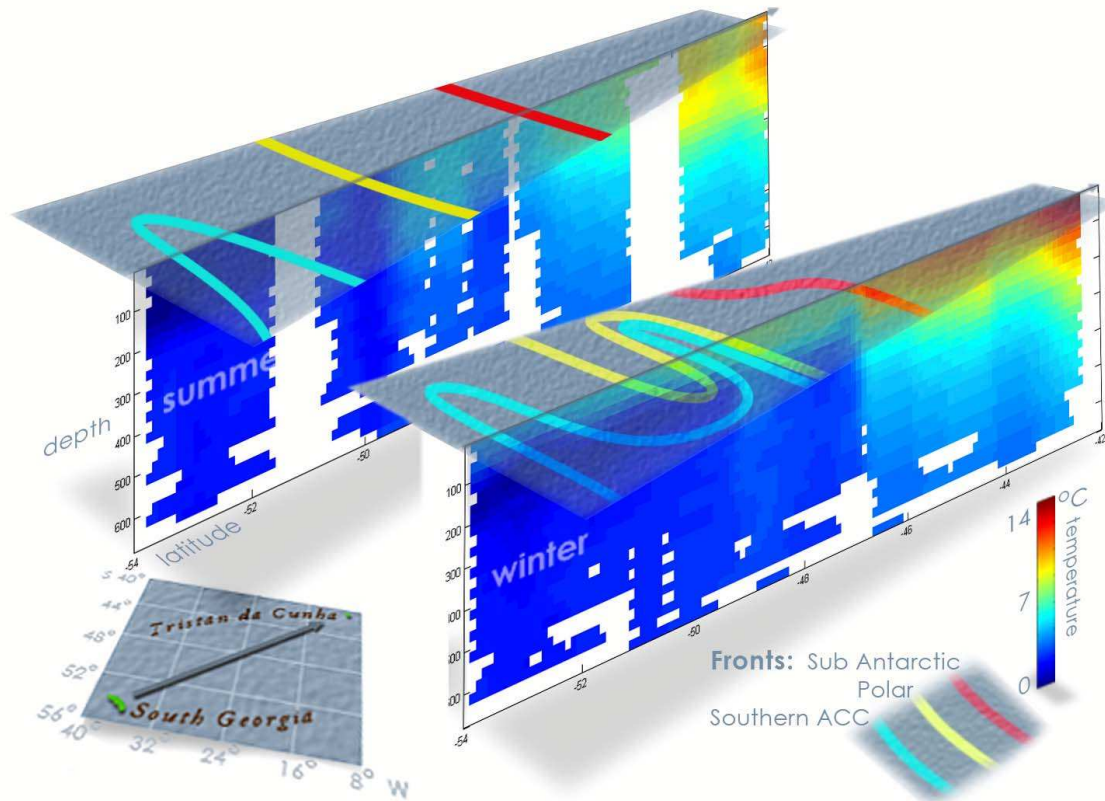


**Figure 6.5:** Two temperature sections recorded by one elephant seal (Bernt) tagged on the island of South Georgia in 2005.

isotherm at a particular depth can be used to locate these fronts (Ch. 3). These major fronts are robust features of the Southern Ocean and circumpolarly continuous. However, recent high-resolution observations from ships and satellites have made it clear that the frontal structure of the ACC is more complex than previously inferred from measurements with coarser sampling (e.g., Sokolov and Rintoul, 2007). The ‘adaptive’ sampling of animal-borne sensors enabled us to address this mismatch between the frontal positions based on surface properties (Ch. 3), and the multiple subsurface fronts and current jets which rather split and merge and re-split (Pollard et al., 2002, Ch. 4). The detailed hydrographic CTD-SRDL sections (Figs. 4.2 and 4.7) in chapter 4 indicate multiple horizontal and vertical branches and many of the

major ACC fronts consist of multiple branches or filaments, which merge and diverge along the circumpolar path (e.g., Pollard et al., 2002; Sokolov and Rintoul, 2007).

So, do we need to define new fronts or are such branches ‘only’ part of the major fronts, so that we can define a northern, middle and southern branch of each front as e.g. Sokolov and Rintoul (2007) did? Sokolov and Rintoul (2007) find that the multiple jets of the ACC fronts are consistently aligned with particular streamlines based on Sea Surface Height (SSH). This alignment between the jets and streamlines (and hence water mass properties) is remarkably robust and this result helps to bridge between the two disparate views of the ACC fronts (Sokolov and Rintoul, 2007). This existence of multiple jets might help to explain why previous studies and this thesis have not agreed on the location of the Subantarctic and Polar Fronts. Although very similar or even identical hydrographic criteria are used in these studies different branches of the primary fronts are picked out. The temporal separation of the studies can also result in different intensity and water mass properties of the branches and the horizontal separation of the frontal locations.

Newer high-resolution observations will resolve the complex current structure of the ACC in even more detail and might highlight even more branches than shown in Sokolov and Rintoul (2007). However, this complex structure is only existing in the surface layer, while the three major fronts, as defined and used in this thesis, are deep reaching to depths of more than 2000 m. When looking at changes in the ACC on time scales longer than inter-annual, I propose to look at these deep reaching hydrographic fronts, which are not effected as much by the short term variability and multiple branching in the surface layer.

### 6.2.3 The future of monitoring the ACC

I have shown above that a combination of Argo and CTD-SRDLs has been uniquely effective at tracking the actual positions of fronts (Ch. 3), and seek to implement this technique further. We therefore set up the South Atlantic Variability Experiment (SAVEX) as part of MEOP, which successfully obtained funding from the Natural Environment Research Council (NERC) and started in December 2007. Within the project we will extend the data obtained by SEaOS and will investigate further the latitudinal shifts of the ACC in response to wind forcing and other changes in driving mechanisms. Many issues remain unresolved, particularly: does the position of the ACC change in a systematic way in response to changes in winds? By extending the data obtained by SEaOS we will determine if a northward shift of the ACC has occurred in recent years. The data available to Fyfe and Saenko (2006) suggested the opposite but they did not have available the fine resolution in-situ data provided by the combination of Argo and SEaOS data. If what we observed is not merely a transient seasonal variation, the implications of it for ocean circulation are substantial.

To address this question, we deployed 10 CTD-Satellite Relay Data Loggers on Southern elephant seals at South Georgia in February 2008. 30 more CTD-SRDLs will be deployed in October 2008, February 2009 and October 2009, which will provide high-resolution ocean data from an area spanning the ACC from the Antarctic Continent to the Subtropical Convergence. I have shown already that a combination of Argo and CTD-SRDLs is most effective at tracking the actual positions of fronts (Ch. 3), and I will implement this technique further in the SAVEX project.

Some results of this thesis are already in use. The post-processed data and the monthly positions of the ACC fronts are incorporated into work at the Bullard Labs in Cambridge University. Here, a method is developed to use seismic data to image ocean currents, focussing specifically on the Southern Ocean around the Falklands.

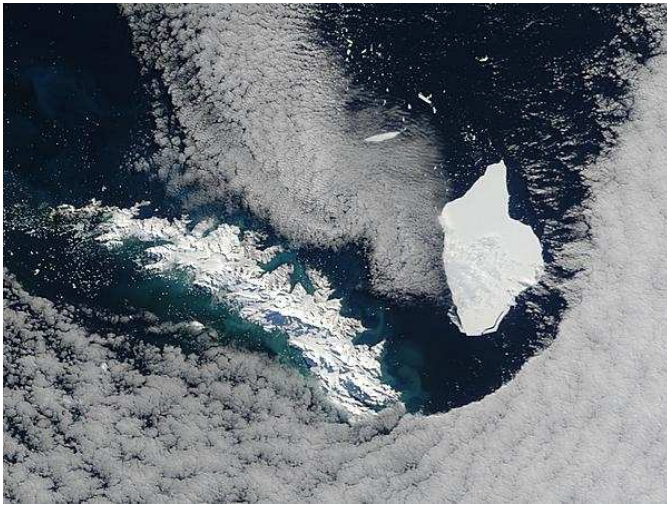


**Figure 6.6:** Huge iceberg east of South Georgia in 2005.

Another beneficiary is the German Alfred-Wegener-Institute, which is using the data to improve their investigations of a melting iceberg and its influence on the regional oceanography east of South Georgia (Fig. 6.6).

### **6.3 Behaviour of marine animals in relation to their immediate environment**

It is often difficult or impossible to observe directly how marine predators interact with their environment and the prey within it. Even relating movement and behavioral data from animal tracking to specific local environmental features is challenging. Either data are often not available at relevant spatial and temporal scales (esp. in the Southern Ocean) or data on ocean surface properties may not be good indicators of environmental conditions relevant to deep-diving species. The hydrographic data collected by CTD-SRDLs are therefore of particular interest to biologists. The vast amount of data collected during the SEaOS project enabled us to study the behavioral and physiological responses of Southern elephant seals to spatial environmental variability throughout their circumpolar range (Ch. 5).

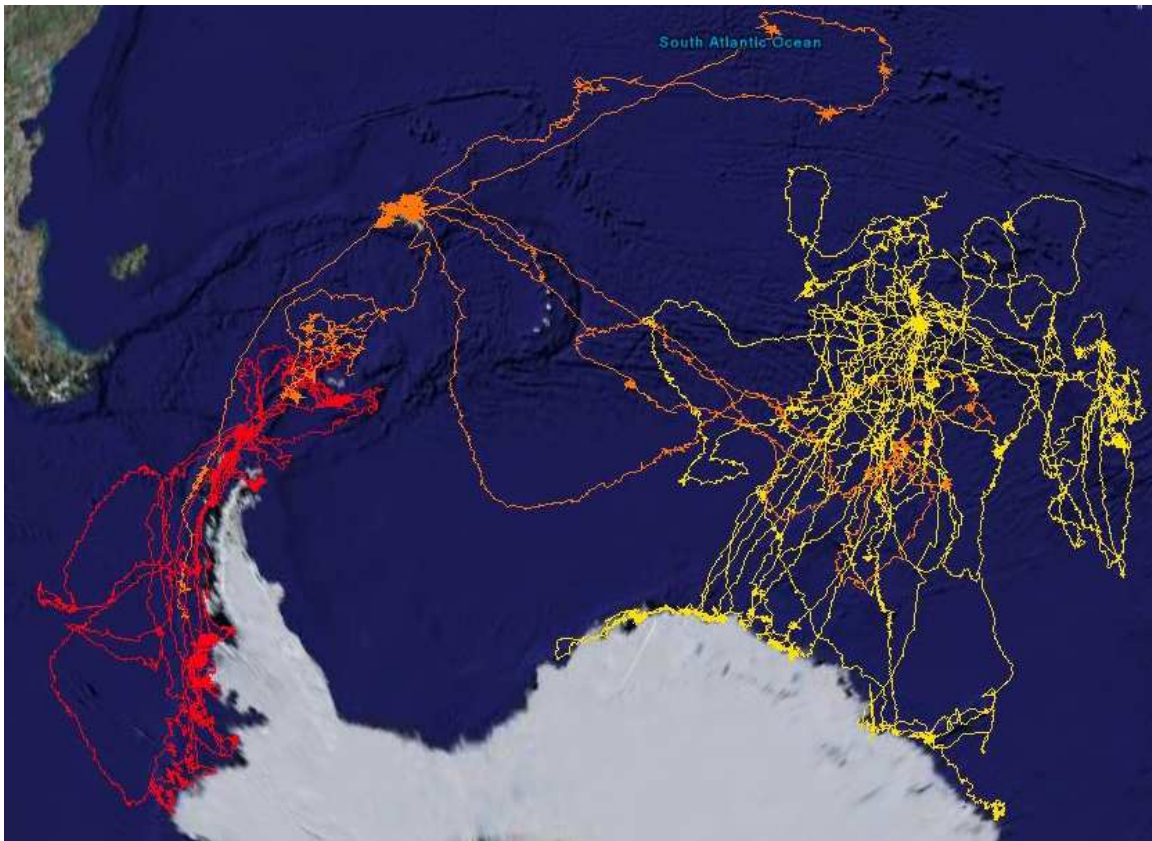


**Figure 6.7:** Migration of the Southern elephant seals tagged with CTD-SRDLs in the 2007/2008 season on South Georgia, UK (orange), Bouvet Island, Norway/South Africa (yellow) and King George Island, Brazil (red).

For this study, I investigated data obtained by CTD-SRDLs on 85 Southern elephant seals from South Georgia, Kerguelen Islands, Macquarie Island and Livingston Island. The movements of the 85 seals extended the documented range of the species, and demonstrated the circumpolar coverage of their migrations, from subtropical waters in the north to continental polar waters in the south. This overlapping coverage can also be seen in the actual deployments from South Georgia, Bouvet Island and King George Island (Fig. 6.7). While seals in the Atlantic sector did not cross the Weddell/Scotia Confluence into Antarctic waters during the SEaOS project in 2004 and 2005, one seal ventured into the Weddell Sea in March 2008. This shows that we still don't know the whole range of Southern elephant seals.

The CTD-SRDL data collected during SEaOS enabled us to study the behavioural

responses to their physical environment. While elephant seals from all colonies displayed strong diurnal patterns in their diving behaviour, day and night dive depths were not uniform across the Southern Ocean. This was especially evident for night-time dives, which were substantially deeper ( $>500$  m) north of the Polar Front than further south ( $\approx 200$ - $400$  m). The greatest diurnal differences were found between the SAF and the SACCF, where seals typically dived to  $\approx 200$ - $300$  m at night and  $400$ - $600$  m or more during daylight hours. Small-scale variations in dive depth were observed in some areas, such as within the main ACC system in the Atlantic sector. Elephant seals obviously dive to find food and the variations in diving behaviour possibly indicate association with high eddy activity and increased vertical mixing processes at these frontal regions.

Changes in animal buoyancy (i.e., relative fat content) were mapped across the Southern Ocean. The largest positive changes occurred within the ACC, especially between the SAF and the SACCF, for seals tagged on South Georgia, while seals from Kerguelen and Macquarie showed strong negative changes while migrating across the ACC, especially between the PF and SACCF. For these two populations, positive changes in drift rate were observed mainly south of the SACCF, either along the continental margin and shelf break along East Antarctica or within the marginal ice zone in the Ross Sea. Improved body condition of seals in the Atlantic sector was associated with Circumpolar Deep Water upwelling regions within the Antarctic Circumpolar Current, whereas High-Salinity Shelf Waters or temperature/salinity gradients under winter pack ice were important in the Indian and Pacific sectors.

The observed differences in the occurrence of positive changes in drift rate between populations could have important consequences for the energy budgets of these animals and although these estimates are relatively imprecise and do not take individual variation in energy budgets into account, they nevertheless suggest a simple

mechanism that may contribute to the different population trends observed for these populations during the 1950s-1970s.

### 6.3.1 Marine mammal habitats in a changing environment

The biggest challenge facing marine mammal ecologists in the 21st century will be understanding, predicting and where possible, ameliorating the effects of climate change. Predicting how marine mammal populations respond to habitat changes will be essential for developing conservation management strategies. Responses to previous environmental change may be informative in the development of predictive models. During the work for this thesis, I realized that not only the behaviour of marine animals might change in relation to their immediate environment, but that their habitat can very often be described by very simple proxies of their physical environment. Here I describe the likely effects of the last ice age on Grey seal population size and distribution. This work is still in progress and I will give only a short overview.

I used satellite telemetry data to define Grey seal foraging habitat in terms of the temperature and depth ranges exploited by the contemporary populations. More than 50000 dive and temperature profiles from Grey seals in the eastern and western North Atlantic were analysed including the annual sea surface temperature (SST) at the dive locations. The results show that the Grey seals inhabit a SST range from  $3^{\circ}\text{C}$  to  $13^{\circ}\text{C}$ , with 95% of all seals within  $4.5^{\circ}\text{C}$  to  $11^{\circ}\text{C}$  and that they spend 95% of their time in areas with a water depth of less than 126 m depth. These results agree with the general knowledge that Grey seals spend their time solely on the shelf and dive most of the time to the sea floor for foraging. To test these results, I estimated today's Grey seal habitat based on bathymetry data and SST data of the World Ocean Database 2005 (Fig. 6.8).

Then, I estimated the available extent of such habitat in the North Atlantic at the

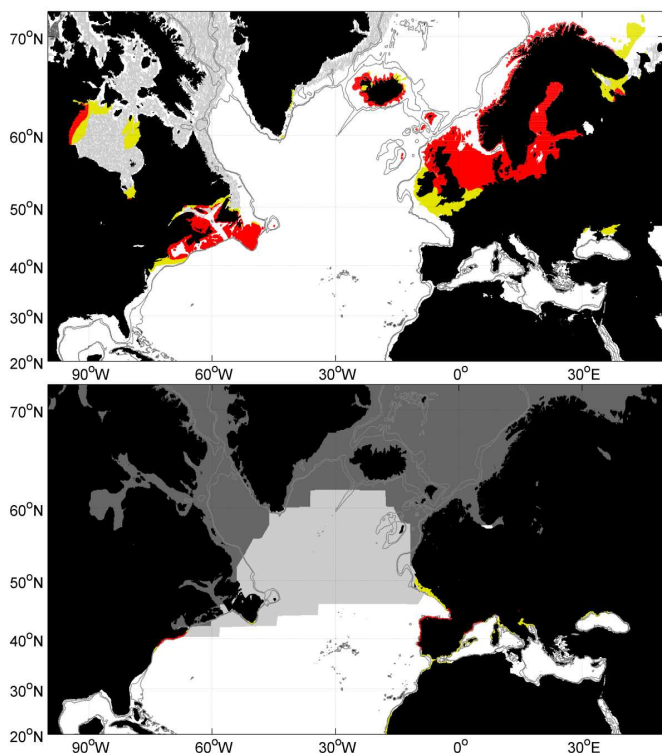


**Figure 6.8:** Estimates of today's Grey seal habitat (top) and at the last glacial maximum (bottom). Grey seal habitat based on waterdepth and a temperature range of  $4.5 - 11^{\circ}\text{C}$  is shown in red and habitat based on waterdepth and a temperature range of  $3 - 13^{\circ}\text{C}$  is shown in red and yellow. Iso-baths are 500m, 1000m and land is shaded black. Winter sea ice cover is shown in light grey and summer sea ice cover in dark grey.

last glacial maximum (LGM); taking account of glacial and seasonal sea-ice coverage, estimated reductions of sea-level (120-160 m) and seawater temperature hind-casts from GLAMAP-2000 (Fig. 6.8). Most of the extensive continental shelf waters (North Sea, Baltic Sea and Scotian Shelf), currently supporting  $> 95\%$  of Grey seals, were unavailable at the LGM. A combination of lower sea-level and extensive ice-sheets, massively increased seasonal sea-ice coverage and southerly extent of cold water would have pushed Grey seals into areas with no significant shelf waters. Grey seal populations may have fallen to  $< 5\%$  of current levels. An alternative scenario involving a major change to a pelagic/bathy-pelagic foraging niche cannot be discounted. However, that niche is currently dominated by hooded seals that appear to out-compete and effectively exclude Grey seals from such habitat. If as seems likely, the Grey seal population fell to very low levels and it would have remained low for several thousand years before expanding into current habitats over the last 12000 years or so.

Another example of the immediate uptake of findings from this thesis is the use of the positions of the ACC fronts (Ch. 3) by the British Antarctic Survey to look into the gene-flow between populations of deep-water benthopelagic fish over large geographic distances. In particular, they are investigating possible pathways for toothfish (*Dissostichus eleginoides*) from South Georgia to migrate to the Patagonian Shelf or the South Sandwich Islands.

This shows that, by implementing animal-borne sensors into ocean observing strategies, we not only gain information about the global ocean circulation and enhance our understanding of climate and the corresponding heat and salt transports, but at the same time we increase our knowledge about the oceans top predators, their life history and their sensitivity to climate change.

# List of Figures

1.1	Fronts in the Southern Ocean. . . . .	15
1.2	Block diagram of the Southern Ocean. . . . .	16
1.3	Southern elephant seal tagged with miniature SRDL-CTD. . . . .	18
1.4	All temperature sections along seals' migration obtained during the SEaOS project. . . . .	21
1.5	Accumulated number of CTD profiles per degree latitude in the Southern Ocean (Southern Ocean Database in green with 10513 profiles, 547 Argo floats in blue with 19463 profiles and 64 SEaOS animal tags in red with 22230 profiles) and positions of SEaOS operations (little insert at top right). . . . .	22
1.6	8 hydrographic sections recorded simultaneously by Southern elephant seals in 2004. . . . .	23
2.1	Picture of a CTD-Satellite Relay Data Logger (CTD-SRDL). . . . .	33
2.2	Calibration of SRDLs in the calibration lab at the Naval Postgraduate School in Monterey . . . . .	36
2.3	Comparison between the controlled temperature and conductivity baths and the CTD-SRDL measurements. . . . .	37

*List of Figures*

---

2.4	External field effect on salinity . . . . .	39
2.5	Differences in temperature (left) and salinity (right) of a CTD-SRDL and a ship-based CTD. The CTD-SRDL was attached to the frame of the ship-based instrument. Only measurements taken in a homogeneous water mass are used. . . . .	39
2.6	Percentage of numbers of Argos messages received for each surfacing (left) and the Argos location class for each calculated position (right). The position accuracy is: 3 (< 250m), 2 (< 500m), 1 (< 1500m), 0 (> 1500m), A (three messages received), B (two messages received), Z (no position fix). Data are from 69 CTD-SRDLs south of 40° S . . . .	44
2.7	Positions ( <i>top</i> ) and temperature profiles ( <i>middle</i> ) of a CTD-SRDL ( <i>Rudolph</i> ) and Argo floats. CTD-SRDL profiles between 1 and 2 October 2004 (black), Argo float 3900084 profile at 24 October 2004 (red) and Argo profiles of float 3800085 from 22 May to 21 June 2005 (blue). Standard deviation of temperature on different depth levels as derived from these five Argo temperature profiles in red ( <i>bottom</i> ). Differences between the calculated mean temperatures and the CTD-SRDL measurements in black. . . . .	46
2.8	Positions ( <i>top</i> ) and estimated correction of the recorded salinity ( <i>bottom</i> ) of a CTD-SRDL ( <i>28494</i> ) between February and November 2005.	47
2.9	Temperature vs. salinity diagram. Data collected by Argo floats in black and data from a CTD-SRDL in red. Uncorrected CTD-SRDL data are shown in the left panel, while CTD-SRDL data in the right panel are corrected by a constant offset of $-0.1406$ in salinity. . . . .	49

*List of Figures*

---

2.10	Spatial coverage of the two studies discussed in the text. The large map shows the locations of CTD profiles gathered during the SEaOS project (red) and the Weddell Sea project (blue). The inset is a magnification of this particular study area. . . . .	52
2.11	Picture of a CTD-Satellite Relay Data Logger (CTD-SRDL). . . . .	52
2.12	Distance between two successive CTD profiles. The top panel shows data from the SEaOS project, while the lower panel shows the data obtained by the Weddell Seals. . . . .	53
2.13	CTD-SRDL attached to the fur of a Weddell Seal after their moult (January/February) in 2007. Photo by R. Stevens. . . . .	54
3.1	Schematic of the southern South Atlantic (top) and the Scotia Sea (b). . . . .	64
3.2	Spatial distribution of Argo float data (top) and CTD-SRDL data (bottom) in the years 2004 (red) and 2005 (blue). . . . .	66
3.3	Monthly number of hydrographic profiles (bars) and mean distance to the neighbouring profile (line) from the combined Argo/SRDL dataset. . . . .	67
3.4	Spatial and cross-isobath scales of the Southern Ocean in the South Atlantic. . . . .	71
3.5	Time scale of the Southern Ocean in the South Atlantic. . . . .	72
3.6	Data from a CTD-SRDL between 7 June 2004 and 24 June 2004. . . . .	75
3.7	Data from a CTD-SRDL between 14 January 2005 and 26 February 2005. . . . .	77
3.8	Data from a CTD-SRDL between 13 April 2004 and 4 May 2004. . . . .	78
3.9	Position of the Subantarctic Front during 2004 and 2005. . . . .	81
3.10	Position of the Polar Front during 2004 and 2005. . . . .	83
3.11	Position of the Southern ACC Front during 2004 and 2005. . . . .	85

*List of Figures*

---

3.12 SST ( <i>top</i> ) and SST gradient ( <i>bottom</i> ) at frontal positions with mean as solid line and standard deviation as patch from monthly data for the period 2004 - 2005, inclusive. The SAF is in red, the PF in blue and the SACCF in black. The horizontal dotted black line in the bottom panel shows the mean meridional increase in SST to the north. . . . .	88
3.13 Standard deviation of daily SST data for the period 2004 - 2005, inclusive and the mean frontal positions of SAF, PF and SACCF as derived by this study (solid black lines). Isobaths are 1000 m, 2000 m and 3000 m and land is shaded black. . . . .	89
3.14 Variance of sea level anomaly based on weekly gridded altimeter data for the period 08/2001-06/2006, inclusive. Mean frontal positions of SAF, PF and SACCF as derived by this study. Isobaths are 1000 m, 2000 m and 3000 m and land is shaded black. . . . .	90
4.1 The positions of the CTD-SRDL hydrographic profiles from <i>Rudolph</i> and <i>Jason</i> sampled between 7-20 June 2004 and 1-15 April 2005 respectively. . . . .	108
4.2 In situ temperature section sampled by <i>Rudolph</i> . . . . .	109
4.3 In situ temperature ( <i>top</i> ) and salinity ( <i>bottom</i> ) sections made by <i>Jason</i> . . . . .	109
4.4 Potential temperature versus salinity for the stations made by <i>Jason</i> . . . . .	112
4.5 The transport per unit width ( $10^6 \text{ m}^3 \text{ s}^{-1}$ ) above 2500 m depth derived from mass transport function $Q_{2500}$ , $U_Q$ (solid line) and the baroclinic transport stream function $\chi_{2500}$ , $U_\chi$ (dotted line) for the Drake Passage transects of ( <i>a</i> ) <i>Rudolph</i> in June 2004, and ( <i>b</i> ) <i>Jason</i> in April 2005. . . . .	115

*List of Figures*

---

4.6	Cumulative transport ( $10^6 \text{ m}^3 \text{ s}^{-1}$ ) above 2500 m depth derived from mass transport function $Q_{2500}$ , $U_Q$ (solid line) and the baroclinic transport stream function $\chi_{2500}$ , $U_\chi$ (dotted line) for the Drake Passage transects of (a) <i>Rudolph</i> in June 2004, and (b) <i>Jason</i> in April 2005. The data are integrated from south to north, starting at the first profile with a water depth of more than 2500 m. . . . .	116
4.7	(a) Cumulative transport ( $10^6 \text{ m}^3 \text{ s}^{-1}$ ) (top) above 250 m depth (dotted line) derived from (b) absolute geostrophic velocities across the Drake Passage ( $\text{m s}^{-1}$ ) at the beginning of April 2005. . . . .	118
5.1	Orthographic view of the Southern Ocean. . . . .	135
5.2	Histograms of (a) the maximum pressures of all T-S profiles and (b) the distance between consecutive T-S profiles obtained from the Southern elephant seals during the Southern Elephant Seals as Oceanographic Samplers (SEaOS) program. . . . .	136
5.3	Circumpolar interpolated surface map of weighted mean nighttime dive depths of Southern elephant seals. . . . .	138
5.4	Circumpolar map of physiological changes during winter migrations of elephant seals. . . . .	139
5.5	In situ $\Theta$ -S measurements collected by instruments deployed on Southern elephant seals at three of the main locations. . . . .	142
5.6	Generalized section of the SO, highlighting areas where Southern elephant seals are predicted to change their relative body fat stores. . .	144

*List of Figures*

---

6.1	Animal tracks from previous studies in the Southern Ocean (on the left) and in the North Atlantic (on the right). The same coverage will be provided during the International Polar Year by joint efforts from the UK, France, Norway, Australia, USA, South Africa, Germany, Brazil and Canada. . . . .	151
6.2	Migration of the Southern elephant seal <i>Bernt</i> tagged in 2005 (red and figure 6.5) and retagged in February 2008 (yellow). . . . .	152
6.3	Number of CTD profiles collected per month during the MEOP project (bars) and cumulative sum of profiles since July 2007 (solid line). . .	153
6.4	Comparison of the mean positions of the Subantarctic Front (red), Polar Front (blue) and Southern ACC Front (green) between previous work by Orsi et al. (1995) and Thorpe et al. (2002) (dotted) and from this thesis (solid) . . . . .	157
6.5	Two temperature sections recorded by one elephant seal ( <i>Bernt</i> ) tagged on the island of South Georgia in 2005. . . . .	158
6.6	Huge iceberg east of South Georgia in 2005. . . . .	161
6.7	Migration of the Southern elephant seals tagged with CTD-SRDs in the 2007/2008 season on South Georgia, UK (orange), Bouvet Island, Norway/South Africa (yellow) and King George Island, Brazil (red). . . . .	162
6.8	Estimates of today's Grey seal habitat (top) and at the last glacial maximum (bottom). Grey seal habitat based on waterdepth and a temperature range of 4.5 – 11 °C is shown in red and habitat based on waterdepth and a temperature range of 3 – 13 °C is shown in red and yellow. Isobaths are 500m, 1000m and land is shaded black. Winter sea ice cover is shown in light grey and summer sea ice cover in dark grey. . . . .	165

# List of Tables

2.1	Summary of calibration checks done at Valeport Ltd, Devon, UK. 10 CTD-SRDLs were calibrated and then re-tested against one known temperature and salinity and against a range of pressure from 0 dbar to 2000 dbar in December 2007. . . . .	35
2.2	CTD-SRDL depths look-up table . . . . .	42
2.3	CTD-SRDL costs . . . . .	50
3.1	Summary of front indicators of the ACC in the South Atlantic used in this chapter. The last column indicates whether a SST gradient can be utilised to locate a front. . . . .	80

# Bibliography

- Aldrige, H. D. J. N. and R. M. Brigham, 1988: Load carrying and maneuverability in an insectivorous bat: a test of the 5% 'rule' of radio-telemetry. *Journal of Mammalogy*, **69**, 379–382.
- Argos, 1989: Guide to the argos system. Technical report, Collecte Localisation Satellites (CLS), Toulouse, France.
- Argos, 1996: *Argos User's manual*. Collecte Localisation Satellites (CLS).
- Arhan, M., A. C. Naveira Garabato, K. J. Heywood, and D. P. Stevens, 2002: The antarctic circumpolar current between the falkland islands and south georgia. *Journal of Physical Oceanography*, **32**, 1914–1931.
- Bacon, S., L. R. Centurioni, and W. J. Gould, 2001: The Evaluation of Salinity Measurements from PALACE Floats. *Journal of Atmospheric and Oceanic Technology*, **18**, 1258–1266.
- Bailleul, F., J.-B. Charrassin, P. Monestiez, F. Roquet, M. Biuw, and C. Guinet, 2007: Successful foraging zones of southern elephant seals from the Kerguelen Islands in relation to oceanographic conditions. *Phil. Trans. R. Soc. B.*

- Belkin, I. M. and A. L. Gordon, 1996: Southern Ocean fronts from the Greenwich meridian to Tasmania. *Journal of Geophysical Research*, **101**, 3675–3696.
- Bell, M., A. Hines, and J. Turton, 2005: Forecasting ocean assimilation model.
- Biuw, M., B. McConnell, C. J. A. Bradshaw, H. Burton, and M. A. Fedak, 2003: Blubber and buoyancy: monitoring the body condition of free-ranging seals using simple dive characteristics. *Journal of Experimental Biology*, **206**, 3405–3423.
- Boehme, L., 2004: Argo Quality Control in Highly Variable Environments. *Argonautics*, **5**, 2–3.
- Boehme, L. and U. Send, 2005: Objective analyses of hydrographic data for referencing profiling float salinities in highly variable environments. *Deep Sea Research II*, **52**, 651–664.
- Botnikov, V. N., 1963: Geographical position of the antarctic convergence zone in the southern ocean (in russian). *Sov. Antarct. Exped. Inf. Bull.*, **4**, 324–327, engl. Trans.
- Boyd, I. L. and T. R. Walker and J. Poncet, 1996: Status of southern elephant seals at South Georgia. *Antarct. Sci.*, **8(3)**, 237–244.
- Boyd, J. D. and R. Linzell, 1993: The Temperature and Depth Accuracy of Sippican T-5 XBTs. *Journal of Atmospheric and Oceanic Technology*, **10**, 128–136.
- Bradshaw, C. J. A., J. Higgins, K. J. Michael, S. J. Wotherspoon, and M. A. Hindell, 2004: At-sea distribution of female southern elephant seals relative to variation in ocean surface properties. *ICES J. Mar. Sci.*, **61**, 1014–1027.
- Bradshaw, C. J. A., M. A. Hindell, M. D. Sumner, and K.J. Michael, 2004: Loyalty pays: potential life history consequences of fidelity to marine foraging regions by southern elephant seals. *Anim. Behav.*, **68(6)**, 1349–1360.

- Bradshaw, C. J. A., M. A. Hindell, N. J. Best, K. L. Phillips, G. Wilson, and P. D. Nichols, 2003: You are what you eat: describing the foraging ecology of southern elephant seals (*Mirounga leonina*) using blubber fatty acids. *Proceedings of the Royal Society of London Series B-Biological Sciences*, **270(1521)**, 1283–1292.
- Brierley, A. S. and D. N. Thomas, 2002: Ecology of southern ocean pack ice. *Advances in Marine Biology*, **43**, 171–276.
- Broecker, W. S., 1991: The great ocean conveyor. *Oceanography*, **4**, 79–89.
- Bucciarelli E, S. Blain, and P. Treguer, 2001: Iron and manganese in the wake of the Kerguelen Islands (Southern Ocean). *Mar. Chem.*, **73(1)**, 21–36.
- Campagna, C., M. A. Fedak, and B. J. McConnell, 1999: Post-breeding distribution and diving behavior of adult male southern elephant seals from patagonia. *Journal of Mammalogy*, **80**, 1341–1352.
- Charrassin, J.-B., Y.-H. Park, Y. Le Maho, and C.-A. Bost, 2004: Fine resolution 3d temperature fields off kerguelen from instrumented penguins. *Deep Sea Research I*, **51**, 2091–2103.
- Clarke, M. R. and N. MacLeod, 1982: Cephalopods in the diet of elephant seals at Signy Island, South Orkney Islands. *British Antarctic Survey Bulletin*, **57**, 27–31.
- CLS, 2007: *SSALTO/DUACS User Handbook: (M)SLA and (M)ADT Near-Real Time and Delayed Time Products*.
- Cochran, W. W., 1980: Wildlife telemetry. *Wildlife management techniques manual*, S. D. Schemnitz, ed., The Wildl. Soc., Washington, D.C., Vol. Fourth ed., 507–520.
- Cunningham, S. A., S. G. Alderson, B. A. King, and M. A. Brandon, 2003: Transport and variability of the antarctic circumpolar current in drake passage. *Journal of Geophysical Research*, **108**, 8084.

- Curran, M. A. J., T. D. van Ommen, V. I. Morgan, K. L. Phillips, and A. S. Palmer, 2003: Ice core evidence for Antarctic sea ice decline since the 1950s. *Science*, **302(5648)**, 1203–1206.
- Davis, R. E., 1998: Preliminary results from directly measured middepth circulation in the tropical and South Pacific. *Journal of Geophysical Research*, **103**, 24619–24639.
- Deacon, G. E. R., 1984: *The Antarctic circumpolar ocean*. Cambridge University Press, 180pp.
- Dong, S., J. Sprintall, and S. T. Gille, 2006: Location of the Antarctic Polar Front from AMSR-E Satellite Sea Surface Temperature Measurements. *Journal of Physical Oceanography*, **36**, 2075–2089.
- Ducet, N., P. Y. L. Traon, and G. Reverdin, 2000: Global high-resolution mapping of ocean circulation from TOPEX/Poseidon and ERS-1 and -2. *Journal of Geophysical Research*, **105**, 19477–19498.
- Evans, W. E., 1970: Uses of Advanced Space Technology and Upgrading the Future of Oceanography. *AIAA Paper*, **7-01273**, 3pp.
- Fedak, M., S. S. Anderson, and M. G. Curry, 1983: Attachment of a radio tag to the fur of seals. *Journal of Zoology*, **200**, 298–300.
- Fedak, M. A., T. Arnbohm, and I. L. Boyd, 1996: The relation between the size of southern elephant seal mothers, the growth of their pups, and the use of maternal energy, fat and protein during lactation. *Physiol. Zool.*, **69(4)**, 887–911.
- Fedak, M., P. Lovell, B. McConnell, and C. Hunter, 2002: Overcoming the Constraints of Long Range Radio Telemetry from Animals: Getting More Useful Data from Smaller Packages. *INTEG. AND COMP. BIOL.*, **42**, 3–10.

- Foster, L. A., 1972: *Current measurements in the Drake Passage*. Master's thesis, Dalhousie University, 61pp.
- Fu, L.-L., B. Cheng, and B. Qiu, 2001: 25-day period large-scale oscillations in the argentine basin revealed by the topex/poseidon altimeter. *Journal of Physical Oceanography*, **31**, 506–517.
- Fukasawa, M., H. Freeland, R. Perkin, T. Watanabe, H. Uchida, and A. Nishina, 2004: Bottom water warming in the North Pacific Ocean. *Nature*, **427**, 825–827.
- Fyfe, J. C., 2006: Southern ocean warming due to human influence. *Geophysical Research Letters*, **33**, L19701.
- Fyfe, J. C. and O. A. Saenko, 2006: Simulated changes in the extratropical southern hemisphere winds and currents. *Geophysical Research Letters*, **33**, L06701.
- Ganachaud, A. and C. Wunsch, 2000: Improved estimates of global ocean circulation, heat transport and mixing from hydrographic data. *Nature*, **408**, 453–457.
- Gille, S. T., 1994: Mean sea surface height of the antarctic circumpolar current from geosat data: methods and application. *Journal of Geophysical Research*, **99**, 18255–18273.
- Gille, S. T., 2002: Warming of the southern ocean since the 1950s. *Science*, **295**, 1275–1277.
- Gille, S. T. and C. W. Hughes, 2001: Aliasing of high-frequency variability by altimetry: Evaluation from bottom pressure recorders. *Geophysical Research Letters*, **28**, 1755–1758.
- Goni, G. J. and I. Wainer, 2001: Investigation of the brazil current front variability from altimeter data. *Journal of Geophysical Research*, **106**, 31117–3128.

- Gordon, A. L., 1971: Antarctic polar frontal zone. *Antarctic Oceanology I, Antarct. Res. Ser.*, J. L. Reid, ed., AGU, Washington, D.C., Vol. 15, 205–221.
- Gould, J., D. Roemmich, S. Wijffels, H. Freeland, M. Ignaszewsky, X. Jianping, S. Pouliquen, Y. Desaubies, U. Send, K. Radhakrishnan, K. Takeuchi, K. Kim, M. Danchenkov, P. Suttom, B. King, B. Owens, and S. Riser, 2004: Argo Profiling Floats Bring New Era of In Situ Ocean Observations. *EoS*, **85**, 179, 190–191.
- Guinehut, S., P. Y. Le Traon, G. Larnicol, and S. Philipps, 2004: Combining Argo and remote-sensing data to estimate the ocean three-dimensional temperature fields - A first approach based on simulated observations. *Journal of Marine Systems*, **46**, 85–98.
- Guinet, C., L. Dubroca, M. Lea, S. Goldsworthy, Y. Cherel, G. Duhamel, F. Bonadonna, and J.-P. Donnay, 2001: Spatial distribution of foraging in female Antarctic fur seals *Arctocephalus gazella* in relation to oceanographic variables: a scale-dependent approach using geographic information systems. *Marine Ecology Progress Series*, **219**, 251–264.
- Guinet, C., P. Jouventin, and H. Weimerskirch, 1999: Recent population change of the southern elephant seal at Iles Crozet and Iles Kerguelen: the end of the decrease?. *Antartct. Sci.*, **11(2)**, 193–197.
- Heywood, K. J. and B. A. King, 2002: Water masses and baroclinic transports in the South Atlantic and Southern oceans. *Journal of Marine Research*, **60**, 639–676.
- Hindell, M. A., C. J. A. Bradshaw, M. D. Sumner, K. J. Michael, and H. R. Burton, 2003: Dispersal of female southern elephant seals and their prey consumption during the austral summer: relevance to management and oceanographic zones. *journal of Applied Ecology*, **40**, 703–715.

- Hindell, M. A. and H. R. Burton, 1987: Past and Present Status of the Southern Elephant Seal (*Mirounga-Leonina*) at Macquarie Island. *J. Zool.*, **213**, 365–380.
- Hindell, M. A., H. R. Burton, and D. J. Slip, 1991: Foraging Areas of Southern Elephant Seals, *Mirounga-Leonina*, As Inferred From Water Temperature Data. *Austr. J. Mar. Fresh. Res.*, **42(2)**, 115–128.
- Hindell, M. A., D. J. Slip, and H. R. Burton, 1991: The Diving Behavior of Adult Male and Female Southern Elephant Seals, *Mirounga-Leonina* (Pinnipedia, Phocidae). *Austr. J. Zool.*, **39(5)**, 595–619.
- Hindell, M. A., D. J. Slip, H. R. Burton, and M. M. Bryden, 1992: Physiological implications of continuous, prolonged, and deep dives of the southern elephant seal (*mirounga-leonina*). *Can. J. Zool.*, **70**, 370–379.
- Holm-Hansen, O., M. Naganobu, S. Kawaguchi, T. Kameda, I. Krasovsik, P. Tchernyshkov, J. Priddle, R. Korb, M. Brandon, and D. Demer, 2004: Factors influencing the distribution, biomass, and productivity of phytoplankton in the Scotia Sea and adjoining waters. *Deep-Sea Res. II*, **51(12-13)**, 1333–1350.
- Hooker, S. K. and I. L. Boyd, 2003: Salinity sensors on seals: use of marine predators to carry ctd data loggers. *Deep Sea Research I*, **50**, 927–939.
- Hughes, C. W., P. L. Woodworth, M. P. Meredith, V. Stepanov, T. Whitworth, and A. R. Pyne, 2003: Coherence of Antarctic sea levels, Southern Hemisphere Annular Mode, and flow through Drake Passage. *Geophysical Research Letters*, **30**, 1464.
- Klatt, O., O. Boebel, and E. Fahrbach, 2007: A profiling float's sense of ice. *Journal of Atmospheric and Oceanic Technology*, **24**, 1301–1308.
- Kostianoy, A. G., A. I. Ginzburg, S. A. Lebedev, M. Frankignoulle, and B. Delille, 2003: Fronts and Mesoscale Variability in the Southern Indian Ocean as Inferred

- from the TOPEX/POSEIDON and ERS-2 Altimetry Data. *Oceanology*, **43**, 632–642.
- Laws, R. M., 1994: History and present status of southern elephant seals populations. *Elephant Seals*, B. J. LeBoeuf and R. M. Laws, eds., Los Angeles, University of California Press, 49–65.
- Lawson, G. L., P. H. Wiebe, C. J. Ashjian, S. M. Gallagher, 2004: Acoustically-inferred zooplankton distribution in relation to hydrography west of the Antarctic Peninsula. *Deep-Sea Res. II*, **51(17-19)**, 2041–2072.
- Le Traon, P.-Y. and G. Dibarboure, 1999: Mesoscale mapping capabilities of multi-satellite altimeter missions. *Journal of Atmospheric and Oceanic Technology*, **16**, 1208–1223.
- Le Traon, P.-Y., G. Dibarboure, and N. Ducet, 2001: Use of a high-resolution model to analyze the mapping capabilities of multiple-altimeter missions. *Journal of Atmospheric and Oceanic Technology*, **18**, 1208–1223.
- Lea, M. A. and L. Dubroca, 2003: Fine-scale linkages between the diving behaviour of Antarctic fur seals and oceanographic features in the southern Indian Ocean. *ICES Journal of Marine Science*, **60**, 990–1002.
- Lenn, Y.-D., T. K. Chereskin, J. Sprintall, and E. Firing, 2007: Mean jets, mesoscale variability and eddy momentum fluxes in the surface layer of the Antarctic Circumpolar Current in Drake Passage. *Journal of Marine Research*, **65**, 27–58.
- Levitus, S., R. Burgett, and T. Boyer, 1994: World Ocean Atlas 1994 Vol. 3: Salinity. Washington DC., U.S. Gov. Printing Office.
- Lockheed Martin Sippican, Inc., 2005: XBT: Expendable Bathythermograph. internet

publication.

URL <http://www.sippican.com/>

- Lydersen, C., O. A. Nøst, K. M. Kovacs, and M. A. Fedak, 2004: Temperature data from Norwegian and Russian waters of the northern Barents Sea collected by free-living ringed seals. *Journal of Marine Systems*, **46**, 99–108.
- Lydersen, C., O. A. Nøst, P. Lovell, B. J. McConnell, T. Gammelsrød, C. Hunter, M. A. Fedak, and K. M. Kovacs, 2002: Salinity and temperature structure of a freezing Arctic fjord monitored by white whales (*Delphinapterus leucas*). *Geophysical Research Letters*, **29(23)**, 2119.
- McCann, T. S., 1985: in *Studies of Sea Mammals in South Latitudes*, J. K. Ling and M. M. Bryden, eds., Sydney: South Australia Museum, 1–17.
- McCarthy, M., L. D. Talley, and D. Roemmich, 2000: Seasonal to interannual variability from XBT and TOPEX/Poseidon data in the South Pacific subtropical gyre. *Journal of Geophysical Research*, **105**, 19535–19550.
- McClain, E. P., W. G. Pichel, and C. Walton, 1985: Comparative performance of AVHRR based multi-channel sea surface temperatures. *Journal of Geophysical Research*, **90**, 11587–11601.
- McConnell, B. J., C. Chambers, and M. A. Fedak, 1992: Foraging ecology of southern elephant seals in relation to the bathymetry and productivity of the Southern ocean. *Antarctic Science*, **4**, 393–398.
- McIntosh, P. C., 1990: Oceanographic Data Interpolation: Objective Analysis and Splines. *Journal of Geophysical Research*, **95**, 13529–13541.
- McMahon, C. R., M. N. Bester, H. R. Burton, and M. A. Hindell, 2005: Population

- status, trends and a re-examination of the hypotheses explaining the recent declines of the southern elephant seal *Mirounga leonina*. *Mamm. Rev.*, **35**(1), 82–100.
- Meredith, M. P., M. A. Brandon, E. J. Murphy, P. N. Trathan, S. E. Thorpe, D. G. Bone, P. P. Chernyshkov, and V. A. Sushin, 2005: Variability in hydrographic conditions to the east and northwest of South Georgia, 1996-2001. *Journal of Marine Systems*, **53**, 143–167.
- Meredith, M. P. and A. M. Hogg, 2006: Circumpolar response of southern ocean eddy activity to a change in the southern annular mode. *Geophysical Research Letters*, **33**.
- Meredith, M. P. and C. Hughes, 2005: On the sampling timescale required to reliably monitor interannual variability in the antarctic circumpolar transport. *Geophysical Research Letters*, **32**, L16608.
- Meredith, M. P., K. E. Grose, E. L. McDonagh, K. J. Heywood, R. D. Frew, and P. F. Dennis, 1999: Distribution of oxygen isotopes in the water masses of Drake Passage and the South Atlantic. *Journal of Geophysical Research*, **104**, 20949–20962.
- Meredith, M. P., J. L. Watkins, E. J. Murphy, N. J. Cunningham, A. G. Wood, R. Korb, M. J. Whitehouse, S. E. Thorpe, and F. Vivier, 2003a: An anticyclonic circulation above the Northwest Georgia Rise, Southern Ocean. *Geophysical Research Letters*, **30**, 2061.
- Meredith, M. P., J. L. Watkins, E. J. Murphy, P. Ward, D. G. Bone, S. E. Thorpe, and S. A. Grant, 2003b: The southern ACC front to the northeast of South Georgia: Part I. Pathways, characteristics and fluxes. *Journal of Geophysical Research*, **108**, 3162.

- Meredith, M. P., P. L. Woodworth, C. W. Hughes, and V. Stepanov, 2004: Changes in the ocean transport through drake passage during the 1980s and 1990s, forced by changes in the southern annular mode. *Geophysical Research Letters*, **31**.
- MERSEA, 2004: Mersea ocean systems and partners model overview. internet publication.  
URL <http://strand1.mersea.eu.org/html/strand1/model.html>
- Moore, J. K. and M. R. Abbott, 2000: Phytoplankton chlorophyll distributions and primary production in the Southern Ocean. *Journal of Geophysical Research*, **105**, 28709–28722.
- Moore, J. K., M. R. Abbott, and J. G. Richman, 1999: Location and dynamics of the Antarctic Polar Front from satellite sea surface temperature data. *Journal of Geophysical Research*, **104**, 3059–3074.
- Murphy, E. J., A. Clark, C. Symon, and J. Priddle, 1995: Temporal variation in Antarctic sea-ice: analysis of a long term fast-ice record from the South Orkney Islands. *Deep Sea Research I*, **42**, 1045–1062.
- Naveira Garabato, A. C., K. J. Heywood, and D. P. Stevens, 2002: Modification and pathways of southern ocean deep waters in the scotia sea. *Deep-Sea Research I*, **49**, 681–705.
- Naveira Garabato, A. C., K.L. Polzin, B. King, K. J. Heywood, and M. Visbeck, 2004: Widespread Intense Turbulent Mixing in the Southern Ocean. *Science*, **303**, 210–213.
- Nowlin, W. D. and M. Clifford, 1982: The kinematic and thermohaline zonation of the antarctic circumpolar current at drake passage. *Journal of Marine Research*, **40**, 481–507.

- Nowlin, W. D. and J. M. Klinck, 1986: The physics of the antarctic circumpolar current. *Rev. Geophys.*, **24**, 469–491.
- Nowlin, W. D., T. Whitworth III, and R. D. Pillsbury, 1977: Structure and transport of the antarctic circumpolar current at drake passage from short-term measurements. *Journal of Physical Oceanography*, **7**, 778–802.
- Orsi, A. H., W. D. Nowlin, and T. Whitworth III, 1993: On the circulation and stratification of the Weddell Gyre. *Deep Sea Research I*, **40**, 169–203.
- Orsi, A. H., T. Whitworth III, and W. D. Nowlin, 1995: On the meridional extent and fronts of the Antarctic Circumpolar Current. *Deep Sea Research I*, **42**, 641–673.
- Peterson, R. G. and T. Whitworth III, 1989: The subantarctic and polar fronts in relation to deep water masses through the southwestern atlantic. *Journal of Geophysical Research*, **94**, 10817–10838.
- Pickard, G. L. and W. J. Emery, 1990: *Descriptive Physical Oceanography, An Introduction*. Permagon Press, 5th edition.
- Pinaud, D. and H. Weimerskirch, 2005: Scale-dependent habitat use in a long-ranging central place predator . *Journal of Animal Ecology*, **74**, 852–863.
- Piola, A. R. and A. L. Gordon, 1989: Intermediate waters in the southwest South Atlantic. *Deep Sea Research, Part A*, **36**, 1–16.
- Pollard, R., M. Lucas, and J. Read, 2002: Physical controls on biogeochemical zonation in the Southern Ocean. *Deep Sea Research II*, **49**, 3289–3305.
- Pollard, R., J. F. Read, J. T. Allen, G. Griffiths, and A. I. Morrison, 1995: On the physical structure of a front in the Bellingshausen Sea. *Deep Sea Research II*, **42**, 955–982.

- Prezelin, B. B., E. E. Hofmann, C. Mengelt, and J. M. Klinck, 2000: The linkage between Upper Circumpolar Deep Water (UCDW) and phytoplankton assemblages on the west Antarctic Peninsula continental shelf. *Journal of Marine Research*, **58**, 165–202.
- Reid, J. L. and W. D. Nowlin, 1971: Transport of water through the drake passage. *Deep Sea Research*, **18**, 51–64.
- Reynolds, R. W., H.-M. Zhang, T. M. Smith, C. L. Gentemann, and F. Wentz, 2005: Impacts of in situ and additional satellite data on the accuracy of a sea-surface temperature analysis for climate. *International Journal of Climatology*, **25**, 857864.
- Ridgway, K. and J. S. Godfrey, 1994: Mass and heat budgets in the East Australian Currenta direct approach. *Journal of Geophysical Research*, **99**, 3231–3248.
- Rintoul, S. R., J. R. Donguy, and D. H. Roemmich, 1997: Seasonal evolution of upper ocean thermal structure between Tasmania and Antarctica. *Deep Sea Research I*, **44**, 1185–1202.
- Rintoul, S. R., C. W. Hughes, and D. Olbers, 2001: The Antarctic circumpolar current system. *Ocean Circulation and Climate: Observing and Modelling the Global Ocean*, G. Siedler, J. Church, and J. Gould, eds., Academic Press, San Diego, CA, 271–302.
- Rintoul, S. R., S. Sokolov, and J. A. Church, 2002: A 6 year record of baroclinic transport variability of the Antarctic Circumpolar Current at 140E derived from XBT and altimeter measurements. *Journal of Geophysical Research*, **107**, 3155.
- Rio, M.-H. and F. Hernandez, 2004: A mean dynamic topography computed over the world ocean from altimetry, in situ measurements, and a geoid model. *Journal of Geophysical Research (Oceans)*, **109**, C12032.

- Rodhouse, P. G., T. R. Arnbom, M. A. Fedak, and A. W. A. Murray, 1992: Cephalopod prey of the southern elephant seal, *Mirounga leonina*. *Canadian Journal of Zoology*, **70**(5), 1007–1015.
- Roemmich, D., S. Riser, R. Davis, and Y. Desaubis, 2004: Autonomous Profiling Floats: Workhorse for Broad-scale Ocean Observations. *Marine Technology Society Journal*, **38**, 31–39.
- Rual, P., 1996: Onboard quality control of XBT bathy messages. *Summary of Ship-of-Opportunity programmes and technical reports*, Paris, Intergovern. Oceanograph. Commn (of UNESCO) & World Meteorol. Org., 142–152.
- Smetacek, V. and S. Nicol, 2005: Polar ocean ecosystems in a changing world. *Nature*, **437**, 362–368.
- Sokolov, S., B. A. King, S. R. Rintoul, and R. L. Rojas, 2004: Upper ocean temperature and the baroclinic transport stream function relationship in Drake Passage. *Journal of Geophysical Research*, **109**.
- Sokolov, S. and S. R. Rintoul, 2002: Structure of Southern Ocean fronts at 140°E. *Journal of Marine Systems*, **37**, 151–184.
- Sokolov, S., and S. R. Rintoul, 2007: Multiple Jets of the Antarctic Circumpolar Current South of Australia. *Journal of Physical Oceanography*, **37**(5), 1394–1412, doi:10.1175/JPO3111.1.
- Sokolov, S., S. R. Rintoul, and B. Wienecke, 2006: Tracking the Polar Front south of New Zealand using penguin dive data. *Deep-Sea Research I*, **53**, 591–607.
- Sparling, C. E. and M. A. Fedak, 2004: Metabolic rates of captive grey seals during voluntary diving. *J. Exp. Biol.*, **207**(10), 1615–1624.

- Sprintall, J., 2003: Seasonal to interannual upper-ocean variability in the Drake Passage. *Journal of Marine Research*, **61**, 25–57.
- Stevenson, R. D. and W. A. Woods, 2006: Condition indices for conservation: new uses for evolving tools. *Integrative and Comparative Biology*, **46(6)**, 1169–1190.
- Sullivan, C. W., K. R. Arrigo, C. R. McClain, J. C. Comiso, and J. Firestone, 1993: Distributions of Phytoplankton Blooms in the Southern Ocean. *Science*, **262**, 1832–1837.
- Sun, C. and D. R. Watts, 2002: Heat flux carried by the antarctic circumpolar current mean flow. *Journal of Geophysical Research*, **6107**, 3119.
- Talley, L. D., 1996: Antarctic intermediate water in the south atlantic. *The South Atlantic: Present and Past Circulation*, G. Wefer et al., ed., Springer-Verlag, New York, 219–238.
- Thompson, D. W. J. and S. Solomon, 2002: Interpretation of recent Southern Hemisphere climate change. *Science*, **296**, 895–899.
- Thompson, D. W. J. and J. M. Wallace, 2000: Annular modes in the extratropical circulation. Part I: Month-to-month variability. *Journal of Climate*, **13**, 1000–1016.
- Thorpe, S. E., K. J. Heywood, M. A. Brandon, and D. P. Stevens, 2002: Variability of the Southern Antarctic Circumpolar Current Front north of South Georgia. *Journal of Marine Systems*, **37**, 85–105.
- Toggweiler, J. R., J. L. Russell, and S. R. Carson, 2006: Midlatitude westerlies, atmospheric CO<sub>2</sub>, and climate change during the ice ages. *Paleoceanography*, **21(2)**, PA2005.
- Tomczak, M. and J. S. Godfrey, 1994: *Regional Oceanography: An Introduction*. Pergamon, 422pp.

- Tsuchiya, M. and L. D. Talley, 1998: A Pacific hydrographic section at 88° W: Water-property distribution. *Journal of Geophysical Research*, **103**, 12899–12918.
- van den Hoff, J., H. Burton, R. Davies, 2003: Diet of male southern elephant seals (*Mirounga leonina* L.) hauled out at Vincennes Bay, East Antarctica. *Polar Biology*, **26**(1), 27-31.
- Vivier, F., C. Provost, and M. P. Meredith, 2001: Remote and local forcing in the brazil/malvinas region. *Journal of Physical Oceanography*, **31**, 892–913.
- Whitworth, T., 1980: Zonation and geostrophic flow of the antarctic circumpolar current at drake passage. *Deep-Sea Research*, **21**, 497–507.
- Whitworth, T., 1983: Monitoring the transport of the antarctic circumpolar current at drake passage. *Journal of Physical Oceanography*, **13**, 2045–2057.
- Whitworth, T. and R. G. Peterson, 1985: Volume transport of the antarctic circumpolar current from bottom pressure measurements. *Journal of Physical Oceanography*, **15**, 810816.
- Wong, A. P. S., G. C. Johnson, and W. B. Owens, 2003: Delayed-Mode Calibration of Autonomous CTD Profiling Float Salinity Data by  $\Theta$ -S Climatology. *Journal of Atmospheric and Oceanic Technology*, **20**, 308–318.
- Zenk, W., E. Morozov, A. Sokov, and T. J. Müller, 2003: Vema Channel: Antarctic bottom water temperatures continue to rise. *CLIVAR Exchanges*, **8**, 24–26.